The Investigation of the Kinin-Kallikrein Pathway in Prion Pathogenicity

by

Kamilla Kosciuczyk

A Thesis submitted to the Faculty of Graduate Studies of

The University of Manitoba

in partial fulfilment of the requirements of the degree of

MASTER OF SCIENCE

Department of Medical Microbiology and Infectious Diseases

University of Manitoba

Winnipeg

Table of Contents

Abstract 6

Acknowledgements 8

List of Tables 9

List of Figures 10

List of Abbreviations 13

A. Introduction 15

1. Transmissible Spongiform Encephalopathy 15
   i) Prion History 15
2. Human Prion Diseases 17
   i) Sporadic Prion Disease 17
   ii) Inherited Prion Diseases 18
   iii) Acquired Prion Diseases 20
3. Protein Only Hypothesis 22
4. Prion Biochemistry 23
   i) Cellular Prion Protein Function 25
      a) Copper Binding Activity 25
      b) Promotes Synapse Function 26
      c) Promotes Neuronal Plasticity 26
      d) Anti-Apoptotic Function 27
      e) Antioxidant Function 27
      f) Transmembrane Signalling 28
5. Prion Pathology 29
   i) Histopathological Changes 29
   ii) Gliosis 30
   iii) Oxidative Stress 31
6. Therapeutic Treatments 34
   i) Small Molecules 35
   ii) Monoclonal Antibodies 35
7. Diagnostics 36
8. Our Laboratory 38
9. Kinin-Kallirein System 39
   i) History 39
10. Components of the Kinin Kallirein System 40
    i) Kinins 40
    ii) Kininases 40

iii) Kininogen 42
iv) Kallikreins 43
a) Plasma Kallikrein 43
b) Tissue Kallikrein 43
v) Kinin Receptors 44
a) B2 Receptor 45
b) B1 Receptor 45
11. Signal Transduction 46
12. Inducible Nitric Oxide Synthase 48
13. Kinin-Kallikrein System and its Role in the Nervous System 49
i) Traumatic Brain Injury 50
ii) Brain Ischemia 50
iii) Multiple Sclerosis 51
iv) Alzheimer's Disease 51
14. Alzheimer's Versus Prion Disease 51
15. Hypothesis and Project Goals 52
16. The Selection of the Animal Model 53

B. Materials and Methods 55

1. Animal Model 55
2. Whole Brain Tissue Extraction 57
3. Total RNA Extraction 59
4. Total RNA Purification 60
5. Determining Total RNA Integrity 60
6. Synthesis of cDNA 61
7. Development of Standard Curve Calibrator for qRT-PCR 64
i) Generating Target Gene Fragment 64
ii) Gel Extraction of Target Gene Fragment 65
iii) The Synthesis and Propagation of Plasmid with Target Gene Fragment 66
iv) Plasmid Isolation 67
v) Development of the Standard Curve 68
8. qRT-PCR for Genes of Interest 69
i) RT-PCR of Whole Brain Homogenate 69
ii) Analysis of Gene Expression 69
9. Total Protein Purification 70
10. Protein Quantification 71
11. Western Blot Analysis 72
i) Gel Electrophoresis and Transfer 72
ii) Total Protein Quantification 73
iii) Target Protein Detection 73
iv) Re-probing for Loading Control 74
v) Analysis of Protein Expression 74
12. 8OH-dG Urine Assay 75

13. Immunohistochemistry 76
i) Histological Analysis 78

C. Results 79

1. Defining Stages of Disease Relative to Days Post Infection 79
2. qRT-PCR 79
i) Inducible Nitric Oxide Synthase 81
ii) B1 Receptor 81
3. Western Blot Analysis 88
i) High Molecular Weight Kininogen 89
ii) Low Molecular Weight Kininogen 89
iii) Inducible Nitric Oxide Synthase 94
iv) Glial Fibrillary Acidic Protein 94
4. ELISA 100
5. Immunohistochemistry 100
i) Inducible Nitric Oxide Synthase Expression Levels 103
a) CA1 Region of the Hippocampus 103
b) CA3 Region of the Hippocampus 106
c) DG Region of the Hippocampus 106
d) Thalamus Region of the Brain 109
ii) B1 Receptor Expression Levels 109
a) CA1 and DG Regions of the Hippocampus 109
b) CA3 Region of the Hippocampus and Thalamus 112

D. Discussion 116

1. Glial Cell Activation and Oxidative Stress 116
i) Levels of 8-OHdG 116
ii) Levels of Glial Fibrillary Acidic Protein 117
iii) The Correlation between Gliosis and Oxidative Stress 118
2. The Detection of Kininogens in Brain Tissue 119
i) High Molecular Weight Kininogen 119
ii) Low Molecular Weight Kininogen 120
iii) Literature Validity of our Kininogen Findings 121
3. The Detection of the B1 Receptor in Brain Tissue 121
i) Transcriptional Levels of the B1 Receptor 122
ii) Literature Validity of our B1 Receptor Findings 123
iii) Translational Levels of the B1 Receptor 124
4. Inducible Nitric Oxide Synthase 126
i) Transcriptional Levels of iNOS 126
ii) Literature Validity of our iNOS Findings 127
iii) Translational Levels of iNOS 127

E. Conclusions 131

F. Future Directions 132

Appendix 1 134

Appendix 2 135

Appendix 3 136

Appendix 4 137

Appendix 5 139

Appendix 6 151

References 154

Abstract

It has been suggested that the conversion of the host-encoded prion protein (PrP^{C}) to the misfolded disease-associated isoform (PrP^{Sc}) results in the loss of the putative superoxide dismutase enzyme activity of PrP. Another hallmark of prion diseased brains is atypical inflammation represented by presence of activated microglia capable of generating prodigious amounts of reactive oxygen species (ROS). Increased oxidative stress susceptibility combined with increased exposure to ROS is thought to explain the neurodegeneration observed.

Previously, 2D-DIGE analysis of the urine of mice infected with the scrapie strain, ME7, and aged matched controls demonstrated differential abundance of the proteins kininogen, kallikrein and prostaglandin H-isomerase. These proteins are all members of the kinin-kallikrein pathway suggesting its modulation in response to prion disease. Downstream effects of the pathway produce metabolites; prostaglandins, ROS, and nitric oxide which initiate inflammation and contribute to oxidative stress, characteristics that have been demonstrated to be associated with prion diseases. It has not yet been demonstrated whether or not the presence of these proteins in the urine, reflect disease process occurring in the primary site of prion pathology, the brain.

Our hypothesis is that the activation of the kinin-kallikrein pathway may be in part responsible for the atypical inflammation and oxidative stress observed in the prion infected brain. Levels of pathway-specific proteins including kininogen as well as the inducible nitric oxide synthase (iNOS) and the B1 receptor in whole brains of ME7

infected C57BL/6 mice were determined. Western blotting has demonstrated that the levels of kininogen statistically fluctuate at the onset of clinical disease. In addition, statistically significant iNOS levels were detected just prior to clinical stages of disease. Real-time PCR and immunohistochemistry staining further support increasing levels of iNOS through disease progression and the activation of the B1 receptor at the terminal stage of disease. To determine whether this is a cause or consequence of the disease the levels of 8-OHdG, a marker of oxidative stress, and glial fibrillary acidic protein (GFAP), a marker of inflammation, were measured at corresponding time points. These studies suggest that the kinin-kallikrein pathway is activated in prion disease and may be involved in the atypical inflammation and oxidative stress observed in the brain.

Acknowledgements

I would like to extend my sincerest gratitude to my supervisor Dr. David Knox for his patience, guidance and understanding during the course of my research and thesis preparation.

I would also like to thank my committee members Dr. Keith Fowke and Dr. Leigh Murphy for their comments and expertise.

Thank you to Angela Nelson for keeping me on track with all the administrative requirements involved to obtaining a Master`s degree in the department of Medical Microbiology at the University of Manitoba.

Thank you to the Public Health Agency of Canada for funding my degree. With a special thanks for the opportunity to travel to NeuroPrion 2013.

Thank you to all members in the department of the Prion Laboratory Services for making my experience in the lab a memorable one. With a special thank you to all the students in the department for your comments and questions, encouraging me to become a better public speaker.

An enormous thank you goes to Sharon Simon whose endless support, guidance and encouragement always kept me pushing forward.

I would also like to thank my family for their unwavering support and love. Without them, none of this would have been possible.

A final thank you goes to my dearest husband Derek Gale. He not once lost faith in me even when I thought I did.

List of Tables

Table 1: Transmissible spongiform encephalopathies in humans and animals

Table 2: Experimental design of the in vivo model system: collection time points, number of mice collected and intended use of the brain tissue

Table 3: Experimental design of the in vivo model system: collection time points, number of mice collected and intended use of the urine sample

List of Figures

Figure 1: All definite and suspected mutations of the human prion protein gene thought to cause prion disease

Figure 2: The primary structure and posttranslational modifications of the prion protein

Figure 3: General overview of prion pathogenicity

Figure 4: General overview of kinin production

Figure 5: General overview of the signalling pathway involved in the kinin-kallikrein system

Figure 6: An example of the electropherogram, gel image and overall results obtained by using the Agilent 2100 Bioanalyzer

Figure 7: An overlap schematic of 8-OHdG levels versus GFAP levels through the course of prion disease

Figure 8: iNOS mRNA levels relative to GAPDH in whole mouse brain at DPI 70, 90, 100, 110, 120, 130 and term

Figure 9: iNOS mRNA levels relative to HRPT1 in whole mouse brain at DPI 70, 90, 100, 110, 120, 130 and term

Figure 10: iNOS mRNA levels relative to PGK1 in whole mouse brain at DPI 70, 90, 100, 110, 120, 130 and term

Figure 11: B1 receptor mRNA levels relative to GAPDH in whole mouse brain at DPI 70, 90, 100, 110, 120, 130 and term

Figure 12: B1 receptor mRNA levels relative to HRPT1 in whole mouse brain at DPI 70, 90, 100, 110, 120, 130 and term

Figure 13: B1 receptor mRNA levels relative to PGK1 in whole mouse brain at DPI 70, 90, 100, 110, 120, 130 and term

Figure 14: HMWK protein levels in whole mouse brain at DPI 60, 90, 100, 110, 120, 130 and term

Figure 15: DPI 130 Western blot image comparing HMWK protein expression between scrapie infected and age-matched control mice

Figure 16: LMWK protein levels in whole mouse brain at DPI 60, 90, 100, 110, 120, 130 and term

Figure 17: DPI 120 Western blot image comparing LMWK protein expression between scrapie infected and age-matched control mice

Figure 18: iNOS protein levels in whole brain at DPI 60, 90, 100, 110, 120, 130 and term

Figure 19: DPI 90 Western blot image comparing iNOS protein expression between scrapie infected and age-matched control mice

Figure 20: DPI 130 Western blot image comparing iNOS protein expression between scrapie infected and age-matched control mice

Figure 21: Term Western blot image comparing iNOS protein expression between scrapie infected and age-matched control mice

Figure 22: GFAP protein levels in whole brain at DPI 60, 70, 90, 100, 110, 120, 130 and term

Figure 23: Term Western blot image comparing GFAP protein expression between scrapie infected and age-matched control mice

Figure 24: 8-OHdG levels in urine at DPI 7, 21, 35, 49, 77, 91, 105 and 119

Figure 25: Total iNOS protein levels in the hippocampus and thalamus regions of the brain at DPI 70, 100 and term

Figure 26: Immunohistological staining for iNOS protein levels in the CA1 region of the hippocampus through the course of prion disease

Figure 27: Immunohistological staining for iNOS protein levels in the CA3 region of the hippocampus through the course of prion disease

Figure 28: Immunohistological staining for iNOS protein levels in the DG region of the hippocampus through the course of prion disease

Figure 29: Immunohistological staining for iNOS protein levels in the thalamus through the course of prion disease

Figure 30: Total B1 receptor protein levels in the CA3 region of the hippocampus and thalamus regions of the brain at term stages of disease

Figure 31: Immunohistological staining for B1 receptor protein levels in the DG region of the hippocampus through the course of prion disease

Figure 32: Immunohistological staining for B1 receptor protein levels in the CA3 region of the hippocampus through the course of prion disease

Figure 33: Immunohistological staining for B1 receptor protein levels in the thalamus through the course of prion disease

List of Abbreviations

8-OHdG	8-hydroxy-2'-deoxyguanosine
ACE	angiotensin I converting enzyme
B1R	B1 receptor
B2R	B2 receptor
BBB	blood brain barrier
BK	bradykinin
BSA	bovine serum albumin
BSE	bovine spongiform encephalopathy
Ca^{2+}	calcium
cAMP	cyclic adenosine monophosphate
cDNA	complementary DNA
cGMP	cyclic guanosine monophosphate
CJD	Creutzfeldt-Jakob disease
CNS	central nervous system
Cu^{2+}	copper
Cu-Zn SOD	copper zinc superoxide dismutase
DAG	diaglycerol
DPI	days post infection
EAE	experimental autoimmune encephalomyelitis
eNOS	endothelial nitric oxide synthase
ERK	extracellular signal-regulated kinase
fCJD	familial Creutzfeldt-Jakob disease
FFI	fatal familial insomnia
FXII	Hageman factor
FXIIa	activated Hageman factor
GFAP	glial fibrillary acidic protein
GPI	glycosylphosphatidylinositol
GSS	Gerstmann–Sträussler–Scheinker syndrome
H_2O_2	hydrogen peroxide
HMWK	high molecular weight kininogen
IL1-β	interleukin 1 beta
iNOS	inducible nitric oxide synthase
IP3	1, 2, 5-triphosphate
KD	kallidan
kDa	kilodalton
KKS	kinin-kallikrein system
LMWK	low molecular weight kininogen
MAPK	mitogen-activated protein kinase
NaDOC	sodium deoxycholate
NCAM	neural cell adhesion molecule
NMDA	N-methyl-D-aspartate

nNOS	neuronal nitric oxide synthase
NO	nitric oxide
$O2^-$	super oxide
$ONOO^-$	peroxynitrite
PBS	phosphate buffered saline
PCR	polymerase chain reaction
PK	prekallikrein
PKC	protein kinase C
PLC	phospholipase C
PRCP-1	prolylcarboxypeptidase isoform 1
PrP	prion protein
PrP^c	cellular prion protein
PrP^{sc}	scrapie prion protein
PrP^{res}	protease resistant prion protein
qRT-PCR	quantitative real-time polymerase chain reaction
RANTES	regulated on activation, normal T cell expressed and secreted
RCF	relative centrifugal force
RNS	reactive nitrogen species
ROS	reactive oxygen species
sCJD	sporadic Creutzfeldt-Jakob disease
TBS	tris buffered saline
TBST	tris-buffered saline with tween 20
TCA	trichloroacetic acid
TSE	transmissible spongiform encephalopathy
vCJD	variant Creutzfeldt-Jakob disease

A. Introduction

1. Transmissible Spongiform Encephalopathy

Transmissible Spongiform Encephalopathies (TSEs), also known as prion diseases, consist of a range of invariably fatal neurodegenerative disorders of the central nervous system. These disorders are characterized by a quiescent incubation period, followed by rapid neurodegeneration resulting in loss of motor control, dementia, paralysis, and eventual death [1,2]. TSEs affect both humans and animals (**Table 1**).

i) Prion History

TSEs have been described for more than 250 years. It was around 1732 where scrapie, a prion disease of sheep, was first identified by shepherds in the United Kingdom [1]. The name scrapie originated from the observation that affected animals would nibble at their claws and feet and scratch their backs against fence posts [3]. It was in 1936 when Cuille and Chelle from France scientifically confirmed scrapie transmissibility by intraocular inoculation of healthy sheep with a preparation of spinal cord from an affected sheep [4].

The first human TSE disease, coined Kuru by the native inhabitants, was identified in 1957 in the eastern highlands of Papua New Guinea by Carleton Gajdusek and Vincent Zigas [5]. The malady was observed primarily in children and elderly women, always ending in fatality typically within 3-6 months of symptom onset. Victims began with involuntary tremors which progressed into severe cerebellar ataxia. Mobility and speech were lost, behavioural changes occurred such as aggressiveness or compulsive,

Table 1: Transmissible spongiform encephalopathies in humans and animals [2,6].

Prion Disease	Host	Transmission
Kuru	Human	Ritualistic cannibalism
Sporadic CJD	Human	Unknown (genetic component possible)
Familial CJD	Human	Mutations in *PRNP* gene
Variant CJD	Human	Consumption of infected cattle
Iatrogenic CJD	Human	Acquired through infected organs or surgical tools
Gerstmann-Sträussler-Scheinker Syndrome	Human	Mutations in *PRNP* gene
Familial Fatal Insomnia	Human	Mutations in *PRNP* gene
Bovine spongiform encephalopathy	Cow	BSE-agent contamination in meat-and-bone meal fed to calves
Scrapie	Sheep, Goat	Pasture contamination, lamb exposure to infected sheep
Chronic Wasting Disease	Deer, Elk	Pasture contamination
Transmissible mink encephalopathy	Mink	Either scrapie or BSE-agent contamination of feed, possibly cannibalism
Feline spongiform encephalopathy	Domestic Cat, Puma, Cheetah, Ocelot, Tiger, Lion	BSE-agent contaminated feed
Transmissible spongiform encephalopathy of captive wild ruminants	Nyala, Gemsbok, Arabian Oryx, Eland Kudu, Scimitar-horned Oryx, Ankole, Bison	BSE-agent contaminated feed

inappropriate laughter. Finally the victim lost the ability to chew or swallow and succumbed to starvation, muscle contracture and spasms. Comprehension remained intact until advanced stages of disease [5,7].

Gajdusek later won the Nobel Prize for determining the source of transmission, ritualistic eating of the brains of deceased relatives. He confirmed this hypothesis through intracerebral inoculation of homogenate from Kuru infected brains into chimpanzees [7,8]. However, credit should be given to Hadlow who initially observed the parallel likeness of scrapie and kuru [9]. Thus, a new class of diseases were identified, together known as TSEs. Today, human TSEs can be further divided into three categories; sporadic, inherited and infectious or acquired disorders.

2. Human Prion Diseases

i) Sporadic Prion Disease

Sporadic Creutzfeld-Jakob disease (sCJD) is the most common type of human TSE consisting 85-90% of all cases. It occurs at an incidence of approximately 1 to 1.5 per million per year, specifically affecting middle and old age populations. The peak onset is 60 – 65 years with a mean duration of disease being 7 months. Death typically occurs within 1 year of the disease [1, 2]. There is no evidence suggesting a bias in gender although one study indicates an incidence 2.7 times higher in Caucasians compared to African Americans [10]. Initial symptoms can range from fatigue, appetite loss, behavioural and cognitive changes to vision loss, ataxia including myoclonus in later stages, aphasia and motor deficits, all rapidly declining by late stages of disease [1,2].

Although the etiology of sCJD is still unknown, scientists believe genetic makeup plays a large role in an individual's susceptibility to develop disease. Popular belief indicates that polymorphisms in the prion protein (PrP) gene, *PRNP,* can encourage the spontaneous misfolding of normal prion protein into the pathogenic form [1]. There are three genetic subgroups, codon 129 can have either valine (V) or methionine (M) as alleles, generating three possible combinations, MM, MV and VV. Approximately 37% of the general population are MM, 51% are MV and 12% are VV [11]. There is a strong correlation between homozygous alleles (MM or VV) and sCJD [1, 12]. In fact, in all sCJD cases, 70% carry either MM or VV [13].

ii) Inherited Prion Diseases

Inherited TSEs such as familial CJD, familial fatal insomnia (FFI) and Gerstmann–Sträussler–Scheinker syndrome (GSS) make up 10-15% of all cases. Inheritance is autosomal dominant with high, age-dependant penetrance. This means, it is very common to be an asymptomatic mutation carrier at a young age with disease onset beginning later in life, anywhere from 30-55 years of age [13]. GSS progression is slower than sCJD and may take several years. FFI receives its name for specifically spreading lesions in the thalamus, the area responsible for sleep regulation. Thus, victims succumb to progressive insomnia [1].

There are currently 63 mutations thought to cause genetic prion disease **(Figure 1)**. However, new evidence has arisen revealing that some of these mutations are not more common in people with CJD than the general population. In addition, many of these

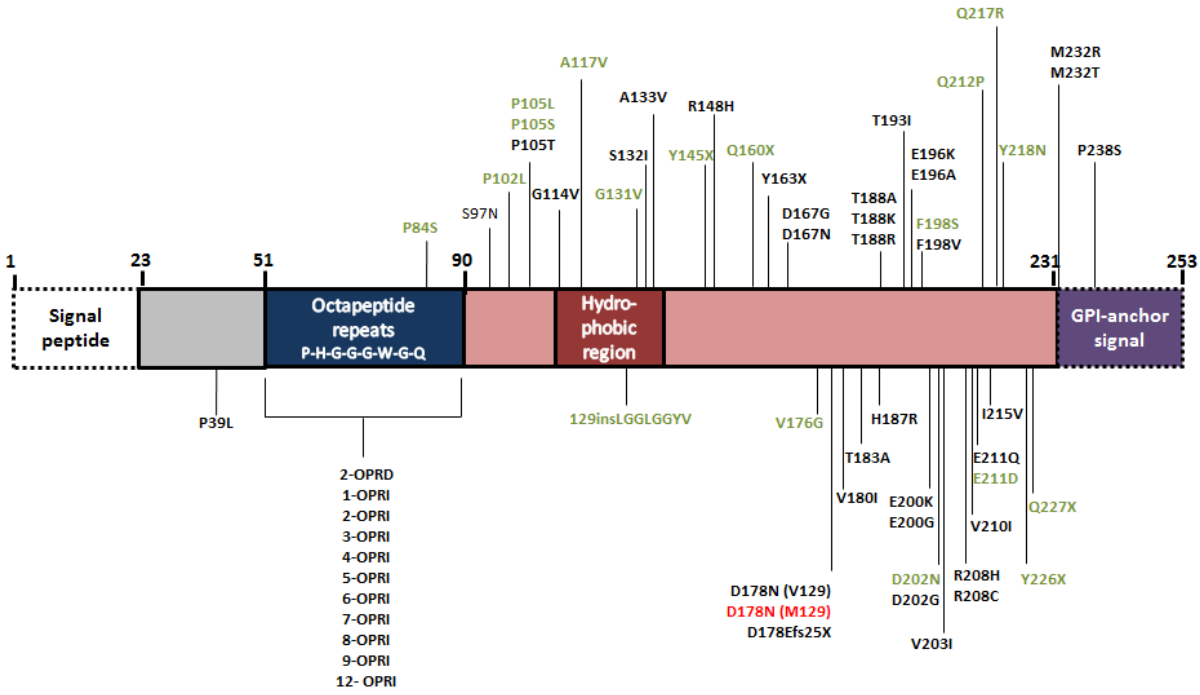

Figure 1: The human prion protein gene (PRNP) with all definite and suspected gene variants reported to cause prion disease [13, 14]. Familial CJD is indicated in the black, Gerstmann-Sträussler-Scheinker Syndrome is indicated in the green and familial fatal insomnia is indicated in the red. OPRD denotes octapeptide repeat deletion whereas OPRI denotes octapeptide repeat insertion.

mutated variants demonstrate incomplete penetrance. Thus, it is possible to be an asymptomatic carrier with varying estimates of lifetime risk [14]. Mutations can range from missense, stop codons, deletions and insertions such as the infamous octapeptide repeat [1, 13]. However, the most common *PRNP* mutation is E200K followed by D178N, P102L and V210I. These four point mutations along with five or six insertions of the octapeptide repeat make up 95% of all familial cases [2]. E200K is most prevalent in Libyan and Tunisian Jewish heritage and is associated with familial CJD [15]. D178N in combination with V homozygosity at codon 129 is also linked to familial CJD. However, D178N in combination with M homozygosity at codon 129 interestingly appears to be linked to FFI [16]. Mutation V210I has also been linked to familial CJD while P102L along with at least 15 other mutations are associated with GSS [17].

iii) Acquired Prion Diseases

The least common category of human TSEs is infectious or acquired disorders, making up the last 1-3% of total cases [1, 2]. These cases received much attention in recent years due to the realization that animal prion diseases could cross the human species barrier [18]. In 1994 a new form of CJD emerged called variant CJD (vCJD). vCJD is distinctly different from sCJD, resulting in earlier on set of disease with an average mortality age of 29. It involves psychiatric and sensory symptoms not typically seen in sCJD patients and prolonged disease duration after initial clinical signs [2]. As of April 2016, 228 cases have been reported worldwide. The majority of victims were in the UK and all cases were homozygous at codon 129 for methionine except for most recently one heterozygous individual [19]. Heterozygosity at codon 129 appears to be associated with a

longer incubation period suggesting that new, asymptomatic cases may emerge in the future [11, 20].

The source responsible for vCJD is a prion strain found in BSE-affected cows. Common practice at the time was to use ruminant tissues for feed supplement, more specifically meat-and-bone meal, now believed to have been contaminated with the BSE prion strain [1, 21]. Consequently, over 180 000 cattle in Great Britain alone succumbed to disease, creating an enormous loss in livestock and immensely exposing the general public to contamination. vCJD has an average, quiescent incubation period of 10 years, making it very likely that a large portion of the UK population was exposed to the BSE strain. Fortunately, factors such as infectious dose exposure through the gastric route play an important role in the efficiency of transmissibility [1, 2]. Nevertheless, there is some evidence that asymptomatic carriers of vCJD are infectious. Several individuals were reported to have been infected through contaminated blood taken from donors at a time when they were asymptomatic [11]. Interestingly, a study conducted on the U.K. population, looked for the presence of prion protein in appendices and revealed an estimated 237 per million rate of infection as opposed to the current global rate of 1-1.5 per million [22].

Another form of acquired prion disease is termed iatrogenic CJD (iCJD). These cases involve the accidental transmission of infectious biological extracts or tissues into individuals during medical procedures [2, 23]. iCJD can be acquired through human growth hormone and gonadotrophin injections, cornea transplants, dura mater grafts and blood transfusions if the donor is positive for prion disease [2, 23, 24]. Historically there have also

been a few cases where contaminated surgical tools used previously on a sCJD patient transferred the infectious agent. Interestingly, homozygosity at codon 129 also appears to contribute to a patient's susceptibility to iCJD [2, 23]. Fortunately, with research moving forward we are now more vigilant with screening processes and have also turned to alternative materials such as synthetic material for dura mater grafts and recombinant hormones [23, 25].

3. Protein Only Hypothesis

The protein-only hypothesis consists of two premises: (i) The pathogenic, misfolded prion protein denoted by PrP^{sc}, is the sole component of the infectious agent involved in TSEs and (ii) Although the mechanism remains unknown, PrP^{sc} converts normal cellular prion protein (PrP^{c}) into the misfolded pathogenic conformation [1].

The idea of a non-viral, non-bacterial infection, devoid of nucleic material began to unravel as early as 1966 by Alper and colleagues. Observations and estimations in size, $2x10^5$ Da being the minimum molecular weight to maintain infectivity, interestingly in range with todays sophisticated measurements, indicate a size far too small to be a micro-organism or the simplest virus [26, 27, 28]. In 1967, it was proposed that the transmissible scrapie agent was of protein nature capable of self-replication [29] and soon after, three models were proposed explaining how a protein could possibly self-replicate in the absence of nucleic acid [30]. Fifteen years later, 1982 unleashed controversy among fanatics and sceptics alike when Prusiner and colleagues isolated "small proteinaceous infectious particles" from scrapie infected hamster brains and coined the term 'prion' [31].

After over three decades of research, we know that PrP^c is required to initiate an infection because PrP deficient mice are not susceptible to disease [32]. An in vitro assay called Protein Misfolding Cyclic Amplification (PMCA) was developed in 2001 allowing for efficient and rapid propagation of PrP^{Sc}. This milestone demonstrated that prions can replicate indefinitely and that newly generated PrP^{Sc} further triggers misfolding, creating this auto-catalytic reaction of replication [28, 33]. However, the most convincing piece of evidence for the protein-only hypothesis was obtained in 2010 when infectious material was successfully generated in vivo from recombinant PrP [34].

4. Prion Biochemistry

Cellular prion protein (PrP^c) is a cell surface-associated sialoglycoprotein that contains a glycosyl phosphatidyl inositol (GPI) moiety at the C terminus, anchoring the protein on the cell surface (**Figure 2**) [1, 35, 36]. It is predominantly found at high levels in neurons of the brain and spinal cord [37]. More specifically, PrP^c is preferentially concentrated along axons and in pre-synaptic terminals of the neuron [38]. Lower levels are found in glial cells of the CNS and various peripheral cell types [39, 40]. Its synthesis is similar to that of other membrane and secreted proteins. Translation begins in the rough endoplasmic reticulum, followed by post translational modifications, translocation to the Golgi and finally delivery and attachment to the cell surface among cholesterol-rich lipid rafts [1, 42]. From the cell surface, PrP^c is internalized and mostly recycled where a small percentage is degraded [43].

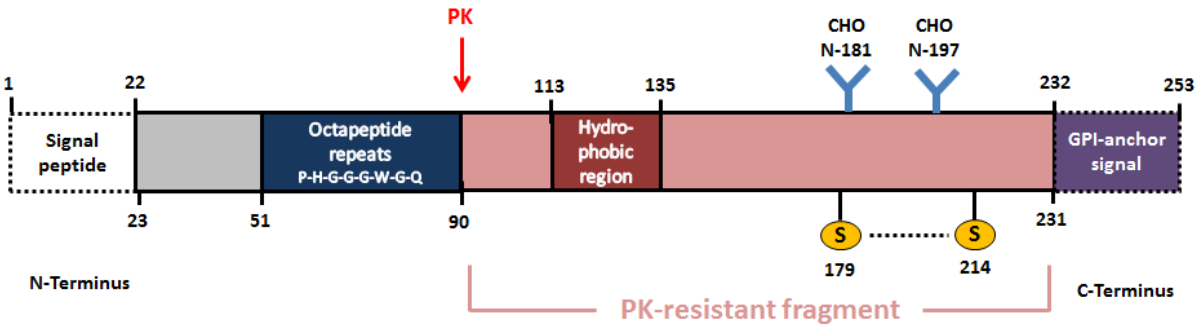

Figure 2: The primary structure and posttranslational modifications of the prion protein. The sequence is cleaved at the N-terminus at residue 23 to generate a signal peptide for prion trafficking into the ER. The octapeptide repeat region consists of four sequential repeats serving as the major copper ion binding domain. The hydrophobic region is believed to play a role in the conversion of PrP^{C} into PrP^{SC}. N-linked glycosylation occurs at residues 181 and 197 and one disulphide bond is created between cysteine residues 179 and 214. The C-terminus is cleaved at residue 231, allowing for the attachment of the GPI-anchor. Digestion with proteinase K (PK) results in cleavage of the protein at residue 90 and generates a PK-resistant fragment (90-231) approximately 27-30 kDa that retains its infectivity [32, 41].

Structurally, the mature cellular prion protein consists of 3 α-helices and an anti-parallel β-sheet, yielding 42% α -helix structure and 3% β-sheet. The protein is soluble in detergents and sensitive to heat and proteinase K digestion. In contrast, the misfolded prion protein is identical in amino acid sequence but favouring β-sheet conformation. PrP^{sc} contains 30% α -helix and 43% β-sheet. This change in conformation drastically alters the protein's physical properties. Under physiological conditions, PrP^{sc} is highly insoluble in detergents, aggregates, becomes heat resistant and is proteinase K resistant. Digestion with proteinase K yields prion protein fragments, denoted as PrP^{res}, with molecular weights of 27-30 kDa that maintain full infectivity [44, 45, 46].

i) Cellular Prion Protein Function

An explosion of studies have emerged targeting PrP^{c} function in the hopes to understand the pathogenesis of prion diseases. After all, it is fair to say that its alteration in function may play a role in the disease process. Historically, prion pathogenicity was hypothesized to involve one of two mechanisms: 1) toxic gain of function through the generation of novel properties associated with PrP^{sc} or 2) loss of function in any of the several putative functions associated with PrP^{c} below. Today it is quite clear that the molecular mechanism driving the disease is a lot more complex than initially thought [47].

a) Copper Binding Activity

To this day, the precise function of PrP^{c} is unknown. However, as research continues to progress, we in turn unveil more properties about the mysterious PrP^{c}. Compelling

evidence suggests that it functions as a copper-binding protein through its octarepeat domain on the N-terminus [48]. During electrical depolarization of neurons, copper ions are released into the synaptic cleft from their storage vesicles [49, 50]. It has been proposed that PrP^c may serve as a copper buffer in the synaptic cleft or may be involved in the re-uptake of copper into the presynapse. Alternatively, it may be of structural importance for the N-terminus, influencing PrP^c binding to other protein [51, 52].

b) **Promotes Synapse Function**

Given the preferential localization of PrP^c along axons and in pre-synaptic terminals, more recent experimental observations have further supported a role for PrP^c at the synapses of neurons [53]. Neurons incubated with recombinant PrP induced rapid elaboration of axons and dendrites, and increased the number of synaptic contacts [54]. Other groups were able to use PrP^c deficient mice to demonstrate impaired long-term potentiation [55], abnormal circadian rhythm [56], decreased overall strength of glutamatergic transmission [57] and alteration in dopaminergic transmission [58]. A neuroprotective function was also observed, suggesting PrP^c modulates excitotoxicity by inhibiting NMDA receptors [59] and prevents degeneration of perkinje cells and demyelination of peripheral nerves [60, 61].

c) Promotes Neuronal Plasticity

Some studies have been able to show that PrP^c plays a role in nervous system development by promoting neurite outgrowth. PrP^c directly binds with neural cell adhesion molecule (NCAM) and together they act as a signal receptor initiating neurite outgrowth. Consequently, in NCAM deficient or PrP^c deficient neurons, outgrowth is

abolished [62]. Another important protein PrP^c has been found to directly and with great affinity bind to is Laminin [63]. Laminin is a major structural component in basement membranes, involved with neuronal differentiation, migration and regeneration. Its interaction with PrP^c has been shown to be important for neuritogenesis. When PrP^c undergoes laser inactivation, hippocampal neurons cease to differentiate and retract their mature neurites [64].

d) Anti-Apoptotic Function

Other authors have proposed an anti-apoptotic function for PrP^c. Bax is a pro-apoptotic protein of the Bcl-2 family. Neurons in the presence of Bax resulted in 90% apoptosis but co-injection of Bax with PrP^c reduced apoptosis to 10%. Furthermore, deletion of the octapeptide repeat abolished PrP^c protection from Bax but deletion of the C-terminus did not impair protection, indicating that PrP^c was not required to be anchored to the cell surface [65]. Complementary findings were produced by Kuwahara and colleagues where Bax expression was stimulated through serum deprivation of neuronal cells [66].

e) Antioxidant Function

PrP^c has also been proposed to play a role in oxidative stress protection. Neurons null of PrP^c were more susceptible to induced stress by hydrogen peroxide (H_2O_2), xanthine oxidase and copper ions [67, 68]. In addition, brain tissue of PrP^c deficient mice showed increased biomarkers, including protein carbonyls and lipid peroxidation products, indicative of oxidative stress [69].

The mechanism involved for this protection is not yet known but is hypothesized to be direct and/or indirect. PrP^c may directly detoxify reactive oxygen species (ROS) by mimicking copper-dependent superoxide dismutase (SOD) activity [70, 71]. ROS, such as O_2^- radicals, are highly reactive molecules that if not appropriately broken down by natural host defence mechanisms, such as through Cu-Zn SOD enzyme activity, will damage surrounding tissue [72].

Conversely, PrP^c may promote oxidative stress protection by up-regulating this enzyme`s activities, thereby indirectly detoxifying surrounding ROS. Evidence indicates a 10-50% reduction in copper loading volumes for the Cu-Zn SOD enzyme, in the brains of PrP^c deficient mice. Correspondingly, mice over expressing PrP^c were shown to have increased activity and copper loading of Cu-Zn SOD [67, 73].

Additionally, PrP^c may act either upstream or downstream of ROS accumulation. Oxidative stress within a cell stimulates apoptotic pathways and thus, the anti-apoptotic properties of PrP^c described above may be responsible for the protection of cells against oxidative stress [53, 74].

f) Transmembrane Signalling

Many investigators are also studying PrP^c as a transmembrane signalling candidate seeing that it is localized on the cell surface [1]. Experimental evidence involving antibody-induced cross-linking of PrP^c indicates possible association with a non-receptor tyrosine kinase (Fyn) [75] as well as casein kinase 2 [76] and growth factor receptor-bound protein-2 [77].

5. Prion Pathology

In all human and animal TSE cases, the only organ system demonstrating severe damage as a consequence of prion infection is the brain [78]. However, it is clear that a silent reservoir is required to house PrP^{sc} during its incubation period where it can slowly multiply. Studies have proposed the lymphoid organs to be the culprit followed by delivery to the CNS via the periphery nervous system [79, 80]. Nevertheless, a large gap in knowledge is still present regarding the mechanistic details of this hypothesis [78].

i) Histopathological Changes

What we do know is that prion infection presents itself in a classical triad of morphological features; spongiform change, characterized by small circular vacuoles in the neuropil, gliosis, both microglial and astroglial, and neuronal loss [81]. This is further accompanied with occasional amyloid plaques and more commonly, various sizes of PrP^{sc} deposits throughout the brain [82]. However, the presence and arrangement of these histopathological changes greatly vary between disease subtypes, prion strains characterized by slight differences in how the protein misfolds [47]. For example, in sCJD, studies have shown that the physical properties of PrP^{sc} plus genetic background of the patient have the most influence on the morphological and clinical phenotypes [83]. Microscopically, brains tend to show severe spongiform vacuolation and accumulation of only a few amyloid plaques [84]. In contrast, vCJD reveals many large plaques surrounded by a halo of spongiform change, distinctly different from sCJD [85]. FFI is strongly characterised by thalamic degeneration with extensive astrogliosis but little or

no spongiform change [47, 86]. And in some instances, lesions may develop in both FFI and GSS patients without PrP^{sc} accumulation [47, 87, 88].

Historically, it was believed that PrP^{sc} deposition correlated with the histopathological changes in the brain but the evidence is controversial [47, 89]. What is interesting is that PrP^{sc} deposits require intact neuronal components and will not aggregate in pre-existing brain lesions such as scarred infarctions with extensive gliosis [81]. It is becoming clearer that host factors such as genotype, individual and selective vulnerability of neuronal subsets along with PrP^{sc} properties such as type of strain, have a large influence on PrP^{sc} deposition [47]. These insights may provide some explanation as to why some individuals may be asymptomatic carriers while other family members succumb to disease [14].

ii) Gliosis

Animal studies indicate that gliosis often occurs prior to clinical illness and well before neuronal degeneration [90]. Gliosis is the rapid stimulation and proliferation of glial cells in response to injury of the CNS [91]. Although initially intended as a host defence system, it's early, chronic activation and positive correlation with PrP^{sc} deposition has led many to believe that it may actually contribute and accelerate disease progression rather than protect [92, 93, 94].

Activated glial cells secrete cytokines including chemokines as well as neurotrophic and neurotoxic factors, demonstrating a neuroinflammatory component to prion disease [95]. An array of elevated, proinflammatory mediators have been identified in both human and animal cases [95, 96, 97]. However, scientists have observed a very atypical inflammatory response. Although cytokine production is statistically significant in the

diseased, fewer cytokines are elevated and at much lower levels when compared to other bacterial or viral infections of the CNS [97, 98]. The significance of this observation is unknown but chronic exposure to such mediators even at lower concentrations can make the environment neurotoxic.

The gliosis process is believed to begin with resting microglial cells detecting abnormal PrP^{sc} deposition (**Figure 3**) [99]. Upon stimulation, they secrete interleukin-1 and interleukin-6 cytokines both of which synergistically stimulate surrounding astrocytes that have been specifically exposed to the infectious agent [100]. This is not a farfetched hypothesis as studies have shown astrocytes may also be involved in prion propagation, transferring infectivity to surrounding neurons. A strong astrocyte response is elicited, marked by increased expression of an astrocyte-specific intermediate filament, GFAP [101]. More cytokines are released and in combination with surrounding neurons, cytokines such as RANTES stimulate the migration of more microglial cells into the area [102]. Due to continuous PrP^{sc} propagation, this process is chronically activated until terminal stages of disease.

iii) Oxidative Stress

Under normal conditions, microglial cells remain inactive. However, they are readily alert for any surrounding cues indicative of injury, infection or any immunological stimuli present in the brain. Activated microglial cells are important for promoting neuronal survival by; cleaning up pathogens and toxic cellular debris including damaged or unnecessary neurons and synapses, cytokine secretions both pro and anti-

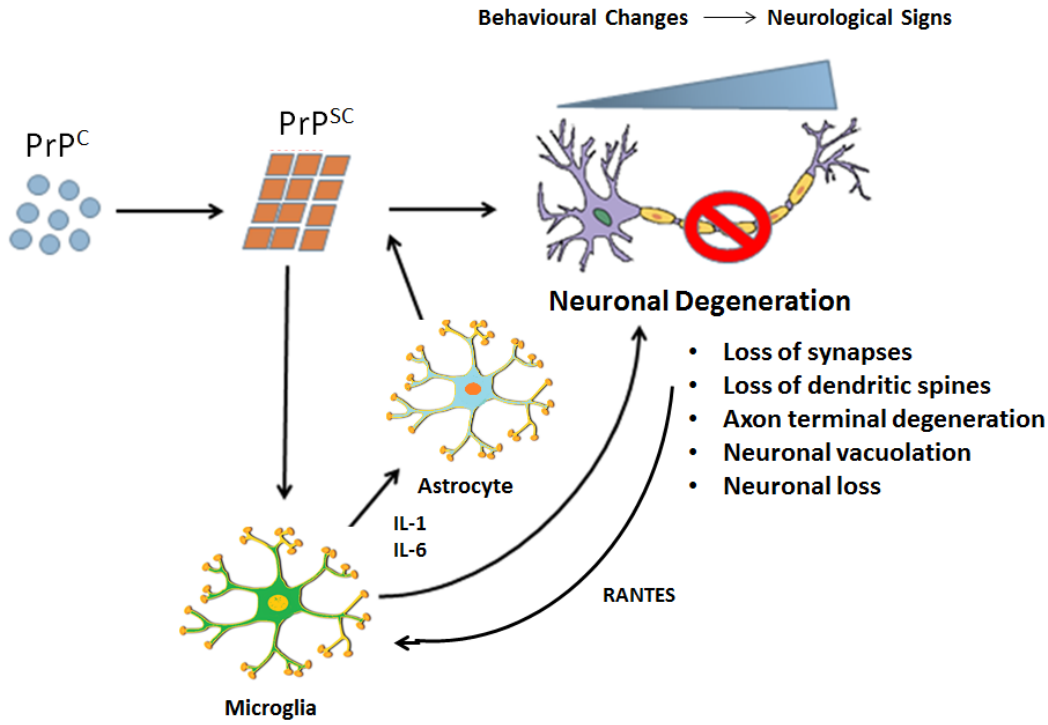

Figure 3: General overview of prion pathogenicity. PrP^{C} misfolds into PrP^{SC} through an unknown mechanism and deposits into the extracellular space. PrP^{SC} deposits stimulate microglia in the area and induce cytokine secretions. Specifically IL-1 and IL-6 induce astrocyte activation. Astrocytes contribute to prion pathogenicity through the induction of a chronic inflammatory response and most recently, contribute by the spread of the misfolded PrP^{SC} to neurons through direct contact. Over activated microglia contribute to neuronal degeneration through the generation of oxidative stress. Excessive ROS production directly damages surrounding cells and can initiate apoptotic pathways. Distressed neurons secrete cytokines such as RANTES which recruit more microglial cells to the area, creating a perpetual negative feedback loop. Neuronal degeneration phenotypically begins with behavioural changes before clear neurological deficits occur, a consequence of the damage to the synapses, dendritic spines and axon terminals of neurons. As the disease progresses, the severity of the damage increases, neuronal populations die and the central nervous system can no longer sustain the body [99, 100, 101, 102, 168].

inflammatory, guiding the migration of stem cells to site of injury and contributing to neurogenesis [103].

Microglial function is directly linked to redox homeostasis. Microglia, internally generate ROS and reactive nitrogen species (RNS) which act as secondary messengers to transition between resting, pro-inflammatory and anti-inflammatory states or phenotypes. When the balance between ROS/RNS production and antioxidant activity falters, microglial cells can enter an over-activated state and produce detrimental levels of ROS/RNS that weaken the permeability of the blood brain barrier (BBB) and harm surrounding cells [104]. ROS/RNS, are highly reactive molecules that induce irreversible oxidative modifications to lipids, proteins and DNA, inhibiting their function. Depending on the degree of damage, it can induce cellular apoptosis [72].

Microgliosis has been well documented in various neurodegenerative diseases including prion disease [103]. Without a doubt, it is a contributor to oxidative stress but another source is believed to be due to the loss of function of PrP^{c}. ROS production is also generated in the synaptic cleft. During neuronal depolarization, Cu^{2+} ions are released and can undergo the Cu^{2+}-based Fenton reaction [105]. If PrP^{c} indeed physiologically binds up to a possible six Cu^{2+} ions, this buffering mechanism is lost when PrP^{c} misfolds into PrP^{sc} [106]. As previously mentioned, PrP^{c} is preferentially localized in the synaptic terminals and the evidence demonstrating accelerated endocytosis of Cu^{2+}-PrP^{c} complexes, further supports the hypothesis that PrP^{c} binds toxic free Cu^{2+} ions and eliminates them from the synaptic cleft [107].

Numerous studies have revealed the presence of oxidative stress markers including 8-OHdG, an oxidized nucleoside that is indicative of DNA damage, in TSE infected brains of both humans and animals [108, 109, 110]. In fact, markers have been detected as early as preclinical stages of disease, prior to synaptic loss in neurons, suggesting a pivotal role for oxidative stress and its contribution to neurodegeneration [111]. It is reasonable to hypothesize that gliosis induced oxidative stress in combination with the loss of the anti-oxidant function of PrP^{c}, is what triggers neuronal cell death. However, the direct evidence for this phenomenon is still missing and the search for the molecular mechanisms driving prion pathogenicity remains.

6. Therapeutic Treatments

To put it simply, TSEs are incurable and there are no therapeutic treatments available for these diseases. In some cases, patients may be treated for certain symptoms such as the jerking of limbs, behavioural changes and sleep disturbances to temporarily relieve their discomfort, but ultimately their health still rapidly deteriorates [112]. Research for treatment is ongoing with the most recent clinical trials exploring the efficacy of two pre-approved drugs quinocrine [113] and doxycycline [114]. Although these compounds appeared to have anti-prion properties in preliminary studies, both double blind studies had no significant change in patient survival. It is becoming evident that researchers will need to develop novel compounds and at this time, two broad stream therapeutic approaches are being explored, 1) generation of small molecule compounds and 2) development of monoclonal antibodies.

i) Small Molecules

The beauty of small molecules is that they are the most effective approach when it comes to crossing the blood brain barrier (BBB), the first obstacle to overcome in any neurodegenerative disease. Most laboratories are taking a shot gun approach screening through chemical libraries of small molecules that inhibit prion replication, for example, reduce expression of cell surface PrP [115]. Mice devoid of PrP^{c} do not develop prion disease and although we cannot abolish its expression in humans, we can certainly reduce it as studies have shown that disease progression depends on PrP availability in a concentration-dependent manner [116].

A few novel compounds have been identified to work very well against mouse prion strains, compdB [117, 118] and IND24 [119] but only Anle138b showed promise against human PrP^{Sc} strains as well. Authors believe Anle138b interferes with protein aggregation and not only with PrP^{Sc} but also with alpha-synuclein in Parkinson's disease. Preliminary toxicity studies look promising and with a bit more tweaking as stated by the authors, hopefully they can push for a first clinical trial in the near future [120]. Although Anle138b is not a cure as mice do eventually succumb to disease, it would be the first therapeutic treatment available to slow prion disease progression.

ii) Monoclonal Antibodies

Another avenue for treatment that is being explored is anti-PrP monoclonal antibodies. In vitro studies show that antibodies inhibit prion propagation and are capable of eliminating all prion infectivity [121]. When testing these antibodies in vivo, researchers found a substantial decrease in peripheral PrP^{Sc} levels and infectivity. Unfortunately,

administration had to be given before the infection reached the brain [122]. The next challenge to overcome is to be able to deliver enough antibodies to cross the BBB. Some studies do indicate that fractional amounts of antibodies can cross the BBB [123]. This in combination with an overall weakened BBB simply due to disease progression [124] has fuelled institutes such as The Medical Research Council Prion Unit in the United Kingdom to push forward with a novel, future clinical study. They have developed a monoclonal antibody coined PRN100 which strongly binds to PrP^{c} and stabilizes its native conformation. They have reported to be manufacturing antibodies in preparation for their first clinical trial [112].

7. Diagnostics

Diagnostic tests for prion diseases are still in dire need. At this time, complete confirmation of disease is still obtained through invasive biopsies of brain tissue administered typically late into disease or post mortem. The challenge is that PrP^{sc} is not uniformly distributed throughout the body with highest concentrations in the brain and trace levels in bodily fluids such as blood and urine [125]. Thus, much research has gone into the search of biomarkers that may be deregulated exclusively in CJD patients, indicating a positive infection.

The current methods available for sCJD patients, on top of established neurological signs, include the detection of a biomarker called protein 14-3-3 in the cerebrospinal fluid. High levels tend to be indicative of a positive infection but it is not a definitive diagnosis [125]. This in combination with high levels of another biomarker, tau protein, has assisted in making diagnoses but this protein has not officially made the international

diagnostic criteria [126, 127]. In some cases an electroencephalogram (EEG) may be performed to detect any abnormal electrical activity produced by the brain. Spike and wave complexes about once every second could suggest prion infection but this is only evident in patients 65% of the time. Another tool that could be useful and support a diagnosis is magnetic resonance imaging (MRI). People with CJD may display abnormalities in the cerebral cortex, striatum and/or thalamus of the brain in which case this could be sufficient for a diagnosis and eliminate the need for a brain biopsy [127, 128].

Unfortunately, the above techniques do not work for patients with vCJD. vCJD is the result of an infection by the BSE strain through the consumption of infected beef. Unsurprisingly, PrP^{Sc} propagation begins in organs other than the brain and thus alternative approaches are needed for detection. Some studies have shown that a tonsil biopsy helps to differentiate between vCJD and other prion diseases [127, 128]. Also in the pipeline, is an ultra-sensitive ELISA with a steel powder capture technique allowing the detection of very low concentrations of PrP^{Sc} in blood. This technique however, is only effective with vCJD patients and still only displays a sensitivity of 71% with 100% specificity [129].

Nevertheless, any diagnostic approach available today, follows pre-established neurological signs. Given the rapid neurological decline in patients, a reliable ante mortem test capable of detection in the early stages of disease is required if we are to administer future therapeutics and be successful. Scientists have been able to show that if treated early on by depleting endogenous neuronal PrP^{C} in an established prion

infection, mice can experience a reverse in early spongiform change and no longer progress to clinical stages of disease [130]. These results are hopeful and with a new exciting technique in the works called RT-QuIC, the future may become brighter in the diagnostic world [127].

RT-QuIC or real-time quaking-induced conversion is an evolved PMCA seeding assay that uses recombinant PrP^{c} as a substrate, fluorescence of thioflavin T and uniform shaking to generate real-time amplification of PrP^{sc}. The concept being, if PrP^{sc} is present in the sample, it will convert recombinant PrP^{c} into PrP^{sc}, amplifying exponentially until reaching a detectable fluorescent level indicative of a positive infection [127]. Due to its incredible sensitivity, researchers are using various bodily fluids for testing including olfactory mucosa which revealed 97.5% sensitivity and 100% specificity [131]. Many groups are exploring this technique on various TSEs and on multiple prion strains which all looks very promising [127, 132].

8. Our Laboratory

The focus of our research is on prion diagnostics. Our goal is to identify possible biomarkers indicative of a prion infection in easily accessible fluids such as urine. We have demonstrated through two-dimensional differential gel electrophoresis that several urinary proteins are differentially expressed in prion infected mice when compared to age matched healthy controls and Alzheimer's prone transgenic mice. Among the 20 disease discriminant classifiers, eleven gel spots were selected and submitted for mass spectrometry analysis revealing 22 proteins as putative biomarkers. Three of these proteins were of particular interest for us: kinninogen 2 isoform,

kallikrein-1 and prostaglandin-H2-isomerase [133]. These three protein candidates are involved in the kinin-kallirein pathway, a complex inflammatory system that has been particularly well studied in Alzheimer's disease both in humans and animals.

9. Kinin-Kallikrein System

i) History

The kinin-kallikrein system (KKS) is an endogenous system that is responsible for multiple biological processes in the human body. Although it has been identified to play many direct and indirect roles with other pathways, it is most known for its role in blood pressure control and inflammation [134]. It was first described in 1909 by Abelou and Bardier. After intravenously injecting dogs with human urinary extract, a substantial decrease in blood pressure was observed. Priban and Hernheiser demonstrated a similar reduction in blood pressure in rabbits eleven years later. However, the fundamental system that we refer to today was established by Emil-Karl Frey, Heinrich Kraut and Eugen Werle. It was not until 1928 when Frey confirmed the detection of a hypotensive substance in human urine. Kraut coined the mystery substance kallikrein in 1930 which was then further characterized by Werle as a proteolytic enzyme in the pancreas, which cleaves kininogen into kallidin in blood plasma [134, 135].

Bradykinin, another component of the KKS, was identified independently in 1949 by Rocha e Silva and coworkers. Venom of *Bothrops Jararaca* and blood were added into a perfusion bath containing isolated guinea pig gut. The result was a slow and delayed contraction of the ileum. This hypotensive and smooth muscle stimulating effect was repeatable with other proteolytic, coagulating snake venoms and by trypsin. This

discovery allowed Eugen Werle to make the connection between kallidin, bradykinin and an origin from a common precursor. This led to the discovery of structure for both substances in the 60's and in 1964, Melville Schachter coined the term "Kinin" describing all polypeptides originating from their precursor kininogen. Today, we know that the KKS consists of a complex network of proteins and peptides [134, 135].

10. Components of the KKS

i) Kinins

Kinins are the key physiological effectors of the KKS. They are short-lived but extremely potent, bioactive peptides, displaying a wide range of function. Kinins are vasodilators and smooth muscle stimulators, thus, play an important role in the regulation of blood pressure. They regulate sodium homeostasis, implicating their involvement in the renin-angiotensin system. They also partake in vascular permeability, neutrophil chemotaxis, pain and in our case, promote inflammation [134, 136, 137, 138, 139].

Bradykinin and Lys-bradykinin or Kallidan are the two main kinins in mammals (**Figure 4**). They are very short peptides (Arg^1-Pro^2-Pro^3-Gly^4-Phe^5-Ser^6-Pro^7-Phe^8-Arg^9), 9 and 10 amino acids long respectively, differing in sequence only by an additional lysine at the N-terminus. Both kinins are released from the hydrolysis of a larger protein precursor called kininogen [136, 137, 138].

ii) Kininases

Kinins are short-lived, half-life of about 15-20 seconds, because they are rapidly degraded by various kininases. Among these, Aminopeptidase converts kallidan into

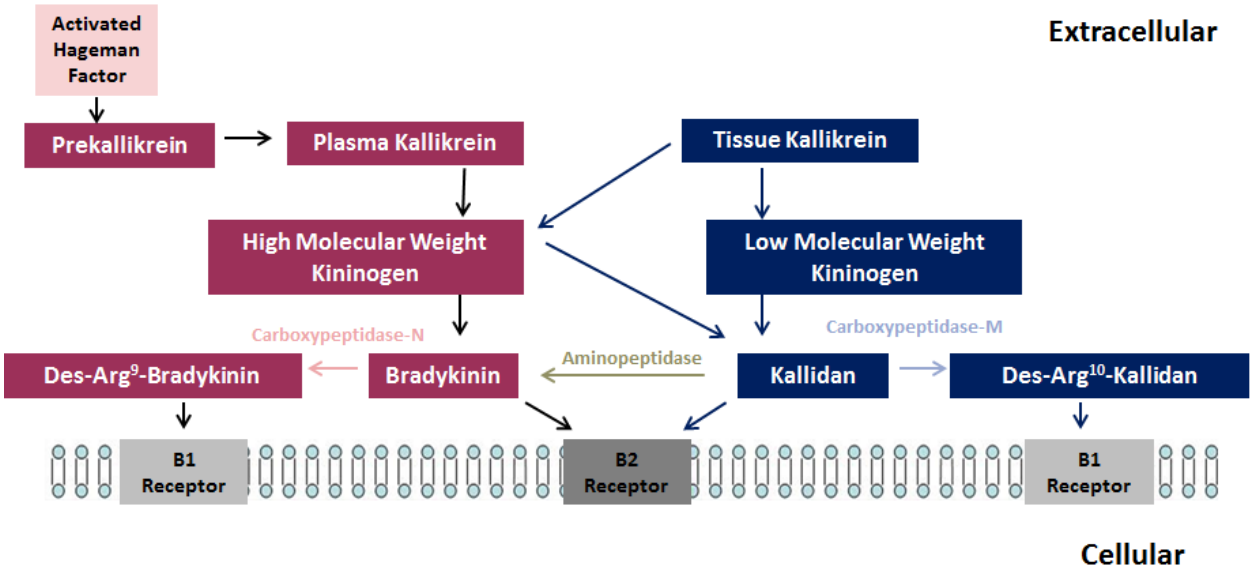

Figure 4: General overview of kinin production. Upon injury, the Hageman factor is activated and in turn activates prekallikrein into plasma kallikrein. Plasma kallikrein cleaves high molecular weight kininogen, releasing a short nonapeptide known as bradykinin. Bradykinin is an agonist for the B2 receptor. However, it can also be broken down into smaller metabolites such as des-arg^{9}-bradykinin by a kininase known as carboxypeptidase-N. This alters the agonist's affinity to the B1 receptor. Tissue kallikrein is also stimulated through injury or an inflammatory response but the exact mechanisms remain unclear. Activated tissue kallikrein can act on both high and low molecular weight kininogen but most evidence reveals a preference for low molecular weight kininogen. In both cases, tissue kallikrein releases a decapeptide known as kallidan. Kallidan is an agonist for the B2 receptor. However, Kallidan can be broken down further by various kininases. In the presence of aminopeptidase, kallidan is cleaved to become bradykinin. In the presence of carboxypeptidase-M, kallidan is broken down into des-arg^{10}-kallidan. This alters the agonist's affinity to the B1 receptor [136,137,138,139].

bradykinin by cleaving the lysine at the N-terminus. Kininase I, also known as carboxypeptidase N (from plasma) and carboxypeptidase M (from cell membrane) remove the carboxy-terminal arginine at the end of the kinin peptide. This results in active metabolites des-Arg^{9}-BK and des-Arg^{10}-KD. These metabolites can be further cleaved by Kininase II, also known as angiotensin I converting enzyme (ACE). ACE is a dipeptidyl carboxypeptidase which removes the dipeptide Phe^{8}-Arg^{9} from the carboxy terminus end of bradykinin or kallidan. ACE can further degrade the inactive bradykinin 1-7 metabolite into a bradykinin 1-5 fragment by the removal of Ser^{6}-Pro^{7}. Other important kininases include aminopeptidase P and neutral endopeptidases which appear to have similar cleavage specificities as ACE [134, 136, 140].

iii) Kininogen

Kininogen is a multifunctional and multi domain glycoprotein. Aside from being a kinin precursor, it is involved with fibrinolysis and thrombosis, an inhibitor of endothelial migration, proliferation and angiogenesis as well as an inhibitor of cysteine proteases such as cathepsins [136, 141, 142]. In most mammals such as humans or mice, it occurs in two forms, high-molecular weight (90-120 kDa) kininogen (HMWK) and low molecular weight (50-68 kDa) kininogen (LMWK). Both forms are coded by a single gene on chromosome 3 and are a result of alternative splicing of the gene transcript. They are predominantly synthesized in the liver but have also been found in the kidney and in the brain, specifically in select neuronal and glial cell types [136].

iv) Kallikreins

Kallikreins are serine proteases and kininogenases. Kallikreins directly cleave kininogen to release bradykinin or kallidan [136]. Two types of kallikreins are involved in the kinin-kallikrein system, plasma kallikrein and tissue kallikrein.

a) Plasma Kallikrein

In humans, plasma kallikrein is encoded by one gene on chromosome 4 and is expressed predominantly in the liver. It is initially released into the blood in its inactive form, prekallikrein (PK). Prekallikrein readily and preferentially binds to the C terminal domain of HMWK in a 1:1 ratio, remaining catalytically inactive as a complex. Prekallikrein activates when Hageman factor (FXII) binds to negatively charged surfaces such as damaged basement membranes or endothelial cells. Upon activation, activated Hagemen factor (FXIIa) cleaves PK into activated kallikrein which in turn reciprocally triggers further FXII activation and cleaves HMWK, liberating bradykinin into the surrounding environment [136, 137, 138]. More recently, studies have also shown that prolylcarboxypeptidase isoform 1 (PRCP1), a member of the peptidase S28 family of serine exopeptidases, is also capable of directly activating prekallikrein while simultaneously enhancing FXIIa activation of PK. Plasma kallikrein is regulated by the C1 esterase inhibitor and any deficiencies of the inhibitor result in kinin induced angioedema [136].

b) Tissue Kallikrein

Tissue kallikrein comes from a large family of glandular kallikrein genes that are tightly clustered on one chromosome. Currently there are 15 kallikrein and kallikrein-related

genes in this cluster, 20 in rats and at least 24 in mice, about 10 being pseudogenes. However, only one gene, KLK1, contains both the catalytic triad (histidine, aspartic acid and serine) and the extended active site to be able to properly contact and cleave kininogen in a physiologically relevant environment [136]. Thus, moving forward, focus will be directed towards KLK1, the kinin liberating kallikrein in mammals.

In humans, KLK1 is located on chromosome 19 and has the highest expression in the pancreas, kidney, salivary gland and large intestine. However, it is also expressed in the reproductive system, arteries and of course the brain [136]. Tissue kallikrein activity is evident even in post mortem human brain tissue from individuals demonstrating no evidence of brain injury or disease. More specifically, it is observed on neurons of the hypothalamus, thalamus, cerebral grey matter, reticular areas of the brain stem as well as cells of the anterior pituitary and epithelial cells of the choroid plexus [143]. It is synthesized and released in its inactive form, prokallikrein. Prokallikrein is activated into tissue kallikrein by the cleavage of a 17 amino acid fragment on the N terminus. However, the enzyme responsible for this in vivo cleavage is still unknown. Once activated, tissue kallikrein readily cleaves both HMWK and LMWK, releaseing kallidan in humans and bradykinin in rodents [138, 144]. Tissue kallikrein is mainly regulated by kallistatin, forming a covalent complex to inhibit the release of kinins [136].

v) Kinin Receptors

There are two receptors mediating the effects of kinins, B1 and B2 receptors (B1R and B2R) [136]. B1R and B2R are G protein-coupled receptors that couple specifically to Gαq and Gαi G protein families [145]. They have been reported to be expressed throughout the

central nervous system, more specifically, in neurons, astrocytes, microglia, endothelial cells and oligodendrocytes [146]. Bradykinin and kallidan are agonists for the B2R whereas the kinin metabolites, des-Arg^{9}-BK and des-Arg^{10}-KD, have a preferential affinity for the B1R [136, 145].

a) B2 Receptor

The B2R is constitutively expressed in normal tissue. Upon stimulation by its agonists, bradykinin and kallidan, the receptor becomes rapidly desensitized [145]. It undergoes phosphorylation and then recruitment of β-arrestin 2 to disassemble the receptor from the G protein. It is then internalized in a clathrin-dependent manner and recycled back to the cell surface [147]. This immediate and rapid recycling process describes why B2R activation is generally considered an acute and transient response [140, 147].

b) B1 Receptor

In comparison, the B1R is an inducible receptor typically induced by the presence of proinflammatory cytokines such as IL1-β [140]. It may be present in normal tissue at low levels but is strongly up-regulated during tissue injury and inflammation [136, 145]. It is considered to be constitutively internalized during agonist absence via a clathrin-dependent pathway. Once stimulated by des-Arg^{9}-BK and/or des-Arg^{10}-KD, its constitutive internalization is inhibited and the receptor remains activated on the cell surface. B1R does not undergo phosphorylation and is only marginally desensitized during agonist stimulation. B1R does not recruit β-arrestin 2 but rather binds to a G-protein coupled receptor-associated sorting protein where it is eventually directed to a lysosome for degradation. This delay allows for the high number of receptors on the cell

surface and is also the reason why B1R activation is involved in a constitutive or chronic response [140, 147]. Interestingly, it has been demonstrated that only B1Rs mediate bradykinin induced microglia migration [148].

11. Signal Transduction

Both receptors have been shown to bind predominantly to the Gαq G protein with the B2R characterized as the prototypical Gαq/11 receptor [140, 145]. Physiological effects mediated through the Gαq G protein result in the activation of phospholipase C (PLC). PLC hydrolyses phosphotidylinositol-4-5-biphosphate into two metabolites, inositol-1,2,5-triphosphate (IP3) and diaglycerol (DAG). IP3 is soluble and is released into the cytosol of the cell where it travels to the endoplasmic reticulum. IP3 binds to calcium channels causing them to open and release calcium ions (Ca^{2+}) into the cytosol. This increase in Ca^{2+} concentration triggers secondary messenger systems within the cell such as activation of protein kinase C (PKC), protein kinase A through cyclic adenosine monophosphate (cAMP) stimulation, protein kinase G through cyclic guanosine monophosphate (cGMP) stimulation and the release of neurotransmitters such as nitric oxide (NO) by nitric oxide synthases (NOS) (**Figure 5**) [145, 146].

Additionally, DAG further undergoes hydrolysis to produce arachidonic acid via DAG lipase. This buildup of arachidonic acid leads to the production of inflammatory prostaglandins. In addition to this increase in inflammation, a by-product of this arachidonic acid oxidative metabolism is the formation of reactive oxygen species (ROS) [145, 146]. ROS, such as O_2^- radicals, are highly reactive molecules. If not appropriately controlled by natural host defence mechanisms, they can alone damage surrounding

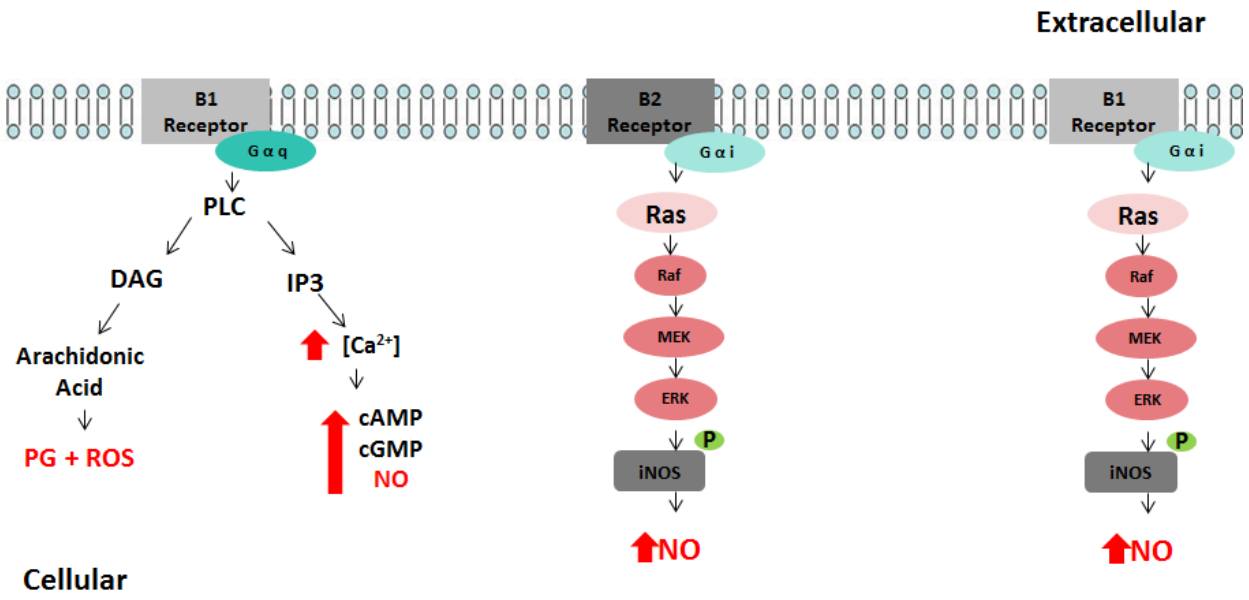

Figure 5: General overview of the signaling pathway involved in the kinin-kallikrein system. B1 and B2 receptors are G-protein coupled receptors that have both been identified to bind to Gαq and Gαi subunits. Binding of Gαq initiates phospholipase C (PLC) to cleave phophotidylinositol-4-5-bisphosphate into inositol-1,2,5-triphosphate (IP3) and diaglycerol (DAG). DAG is used to produce arachidonic acid which is used to generate prostaglandins (PG) and ROS, thereby inititating inflammation and contributing to oxidative stress. IP3 stimulates the immediate increase of intracellular calcium (Ca^{2+}) which activates multiple secondary messenger systems including production of cyclic adenosine monophosphate (cAMP), cyclic guanosine monophosphate (cGMP) and nitric oxide (NO). All metabolites are involved in neuronal activity. However, high levels of cAMP and NO have been shown to be associated with increased BBB permeability and dysfunction. Binding of Gαi initiates the Ras-Raf-MEK-ERK pathway which results in the phosphorylation of inducible nitric oxide synthase (iNOS). iNOS is an enzyme that generates uncontrolled and prolonged levels of NO. NO is also a contributor to cellular oxidative stress through its ability to readily react with surrounding ROS and generate highly reactive nitrogen species (RNS) such as perioxynityrite (ONOO) [145, 146].

tissue or further react with excess NO molecules forming even more potent reactive nitrogen species (RNS) such as perioxynityrite (ONOO) [72]. Given the NO rich environment of the brain, these reactive molecules can directly damage brain tissue by targeting lipids, proteins and DNA of neuronal cells. ROS and RNS are responsible for the oxidative stress induced injury to the CNS [146].

Many studies do indicate receptor coupling to alternative G protein families such as the Gαi G protein [145]. In some cases, the B2R has been shown to couple to Gαi and also result in similar activity as if bound to Gαq. This was demonstrated in bovine aortic endothelial cells, rat-1 cells and HEK293 cells, suggesting cell type may have an effect on which G protein binds [149, 150, 151]. However, in vascular smooth muscle cells, B2R coupled to Gαi resulted in the downstream activation of the mitogen-activated protein kinase (MAPK) cascade [152]. MAPKs are a family of Ser/Thr –specific signalling kinases that undergo a phosphorylation series induced by an intracellular stimulus. A more recent study revealed the direct activation of the extracellular signal-regulated kinase (ERK) MAPK pathway via coupling of the B1R to a Gαi G protein. Agonist stimulation of the receptor resulted in the Src-dependent activation of Ras, Raf, MEK and ERK kinases which led to the activation of inducible nitric oxide synthase (iNOS) via phosphorylation at Ser745 [145, 153].

12. Inducible Nitric Oxide Synthase

iNOS is one of three isoforms of nitric oxide synthase. Mammals express all three isoforms, NOS1 or neuronal NOS (nNOS), NOS2 or inducible NOS (iNOS) and NOS3 or endothelial NOS (eNOS) [145, 153, 154]. nNOS and eNOS are constitutively expressed, have

low basal activity due to a low affinity for calmodulin and are controlled by a receptor-ligand mechanism to initiate a calcium ion influx. During an acute response, bradykinin stimulating a Gαq coupled B2R in brain tissue would yield NO production via nNOS [145]. In contrast, iNOS is inducible and believed to be predominantly regulated at the transcriptional and post-translational levels through cytokine and inflammatory mediators [145, 154]. Once iNOS undergoes phosphorylation, it remains activated, tightly bound to calmodulin even at basal Ca^{2+} concentrations, until the protein is degraded. This property of iNOS allows for a high and protracted NO generation [145, 153]. iNOS coupled with B1R's chronic response could yield a detrimental concentration of NO in the surrounding environment under inflammatory conditions.

13. KKS and its Role in the Nervous System

As previously mentioned, all components of the KKS are expressed in the CNS and thus have been observed to play a role in various neurological disorders including traumatic brain injury, brain ischemia, multiple sclerosis and Alzheimer's disease [155, 156, 157, 158]. Appreciation for the involvement of the KKS in the CNS has been recognized since the late 80's but the extent and importance of its contribution exploded with the introduction of the KO mouse models in the 21st century [134]. We know that both bradykinin receptors are active in these disorders as it is the host's natural response to a distressed environment. However, more and more research is indicating a neuroprotective role for B2R and a pathological role for B1R [155, 157, 158, 159].

i) Traumatic Brain Injury

Early studies using knockout models and receptor inhibitors pin pointed the B2R as the mediator of detrimental effects in a murine model of diffuse brain injury [160]. This was further supported by other studies using a controlled cortical impact model, where only B2-knockout mice had less brain edema, smaller lesion volumes, and a better functional outcome when compared with wild-type mice [161]. However, controversial findings exist, especially if using an alternative brain injury model. In a cold lesion model, only B1 knockout mice displayed smaller lesion volumes, less blood–brain barrier disruption, and less inflammation in the injured brain area. This was further validated by using receptor inhibitors, which complemented the initial findings [155]. Furthermore, a weight-drop-induced brain trauma murine model also revealed a decrease in functional deficits, reduced axonal injury, astrogliosis and neuronal apoptosis in B1 knockout mice [162].

ii) Brain Ischemia

In an ischemic brain injury model, it was demonstrated that B2 deficiency increased mortality rate, infarcted areas and neurological deficit scores after 2 weeks of injury. This suggests that B2R is neuroprotective and required for stimulating survival [159]. B1 deficient mice expressed smaller brain infarctions and less neurological deficits with reduced postischemic inflammation. Using a B1 receptor inhibitor reversed the effect and recovered ischemic tissue in a dose dependent manner [156]. These observations are evidence of support for both Raslan and Weissenberger's findings with respect to benefits of B1R inhibition. The evidence of B1R and its association with neurotoxic effects continue to grow suggesting that it may be a promising therapeutic target.

iii) Multiple Sclerosis

Experimental autoimmune encephalomyelitis (EAE), an animal model for multiple sclerosis, also reveals induction of B1R. B1 knockouts revealed a significant decrease in disease severity whereas B2 knockouts demonstrated no change. B1 knockout mice had significantly lower inflammatory plaques, decreased areas of demyelination and decreased axonal damage in the spinal cord. Furthermore, administration of a B1R inhibitor significantly lowered disease maximum. Their findings also pointed to a reduction in leukocyte trafficking across the BBB [157].

iv) Alzheimer's Disease

Components of the KKS such as cleaved high molecular weight kininogen and bradykinin have been identified in the cerebrospinal fluid of Alzheimer's patients [163, 164]. Studies using knockout mouse models for B1 and B2 receptors revealed improved cognitive function in mice [165]. Inhibitors targeting components of this inflammatory pathway also revealed neuroprotective responses, attenuating the overall progression of disease [166, 167]. Moreover, inhibition of the B1 receptor specifically seemed to be associated not only with lower levels of activated glial cells and cytokines/chemokines but also lower levels of amyloid-B deposition in the brain [158].

14. Alzheimer's Versus Prion Disease

The KKS is associated with various neurodegenerative diseases but its presence specifically in Alzheimer's disease allows us to hypothesize if it could also be activated in prion disease. To the best of our knowledge, the kinin-kallikrein pathway has never been explored in prion disease. However, the similarities between Alzheimer's and prion

disease have been evident to researchers for decades. For instance, both neurodegenerative diseases involve extracellular deposits of aggregated misfolded protein. In addition, development of amyloid plaques, over-activation of microglial cells and an inflammatory response are other common pathological overlaps [168]. Given the similarities between these two diseases and our preliminary findings of several kinin-kallikrein pathway proteins in the urine of prion infected mice, has made us question whether this pathway could also contribute to prion pathogenicity [133].

15. Hypothesis and Project Goals

The excretion of several kinin-kallikrein pathway proteins through the urinary system indicates that they are being produced in abundance from somewhere in the body. Furthermore, the KKS is an inflammatory pathway that generates inflammation and oxidative stress both of which describe prion pathology. Therefore, our hypothesis was that the activation of the kinin-kallikrein pathway is in part responsible for the atypical inflammation and oxidative stress observed in prion disease progression.

To test our hypothesis we had two objectives. The first objective was to demonstrate differential abundance of kinin-kallikrein pathway proteins in the brains of scrapie infected mice. We selected to test kininogen as well as inducible targets iNOS and the B1 receptor. Our second objective was to determine if the expression of our candidate proteins precede or coincide with the onset of oxidative stress and inflammation in our scrapie mouse model. An inflammatory and oxidative stress timeline was generated as disease progressed to determine where the expression of our candidate proteins began

during the course of the disease. We used GFAP, the marker for gliosis and inflammation as well as 8-OHdG, the marker for oxidative stress.

16. The Selection of the Animal Model

Hamsters and mice are the two most common animal models used to study prion disease[169]. The Syrian hamster has been widely used due to its short incubation time[170]. However, today, mice in general are preferred due to their ease of maintenance, access to multiple tools involved in genome manipulation and ultimately their overall similarity to the human genome[169, 171].

The "gold standard" model most frequently used to study prion disease involves the intracerebral inoculation of wild type mice, typically using the C57BL/6, inbred, mouse strain because of its wide use in biomedical research[169, 172]. There is a 4-5 month incubation period, which will vary on the prion strain used, followed by a 100% mortality rate where all mice die within a few weeks or less of one another if a high prion titre was used for infectivity. It is a highly robust assay far superior to any other neurodegenerative model available today. Prion challenged mice recapitulate all neuropathological and biochemical hallmarks of human and animal diseases[169]. Nevertheless, as is with all models, there are drawbacks including the time consuming incubation phase and expense involved to maintain the mice. Thus, much research has been focused into transgenic mice model development where the PrP gene is over expressed, cutting down on the length of the incubation phase[169, 171].

As alluded to earlier, the mouse model can further be subdivided into multiple branches due to the numerous prion strains that have been identified by serially passaging

scrapie, BSE or CJD[173]. Transmissibility of the infection may not always be successful due to the interspecies barrier. Thus, transgenic mice carrying PrP genes of various animals including sheep, cattle, humans and deer have been generated to mitegate these effects[173]. Scrapie alone can be subdivided into ME7, 139A, RML and 79A prion strains contributing to the differences observed in the length of incubation and patterns in the neuropathological changes that occur in the brain[171, 173].

Although transgenic mouse models may be appealing in many prion studies, particularly in testing therapeutic compounds for humans[169], we opted for the most natural way possible to stimulate a prion infection in normal, healthy mice. A natural progression of disease was vital as our goal was to chronologically map the progression of disease and potential stimulation of the kinin-kallikrein pathway. We specifically selected the ME7 prion strain because of the ample amount of literature that is presently available, allowing us to directly compare our findings with those of others in the field.

B. Materials and Methods

All procedures involving infectious materials were carried out in a level 2+ containment unless otherwise stated.

1. Animal Model

The Canadian Science Centre for Human and Animal Health Animal Care Committee approved all procedures.

A 1% w/v brain homogenate in PBS (pH7) was prepared from either healthy control or ME7 scrapie infected, female mice that had reached the clinical stages of disease. The brains were homogenized with a tissue homogenizer (Omni International, cat. # TH115) using 7mm x 110mm tips (Omni International, cat. # 3050), diluted to 1% w/v and stored at -80^{o}C until use. The homogenate was thawed, sonicated for 3 x 30 seconds at amp40 and centrifuged at 500g for 10 minutes before injection. Female, C57BL/6 mice between 4-6 weeks of age were anaesthetized with isofluorane prior to the procedure. Then, 20uL of the prepared inoculum carrying approximately 10, 000,000 particles of infectious agent was introduced into the left side of the brain by intracerebral injection using a Tri-Dek stepper equipped with a 26G biomedical needle of 4mm in length (Pepper and Sons Inc., cat # 7400). Control animals were injected with inoculum prepared from healthy mice in the same fashion. On scheduled collection dates and terminal stage mice were euthanized by cervical dislocation (**Table 2**). Terminal stage was defined by presence of skin ulceration of any size due to overflow incontinence. Brains for gene and protein expression were placed in RNAlater stabilization

Table 2: Experimental design of the in vivo model system: collection time points, number of mice collected and intended use of the brain tissue.

	Experimental Groups	
Time of Sacrifice (Days Post Infection)	**Group 1: Healthy Control**	**Group 2: ME7 Infected**
60 dpi	6 mice – Protein Expression	6 mice – Protein Expression
70 dpi	6 mice – Gene Expression 6 mice- Protein Expression 2 mice- Immunohistochemistry	6 mice – Gene Expression 6 mice- Protein Expression 2 mice - Immunohistochemistry
90 dpi	6 mice – Gene Expression 6 mice- Protein Expression	6 mice – Gene Expression 6 mice- Protein Expression
100 dpi	6 mice – Gene Expression 6 mice- Protein Expression 2 mice - Immunohistochemistry	6 mice – Gene Expression 6 mice- Protein Expression 2 mice – Immunohistochemistry
110 dpi	6 mice – Gene Expression 6 mice- Protein Expression	6 mice – Gene Expression 6 mice- Protein Expression
120 dpi	6 mice – Gene Expression 6 mice- Protein Expression	6 mice – Gene Expression 6 mice- Protein Expression
130 dpi	6 mice – Gene Expression 6 mice- Protein Expression	6 mice – Gene Expression 6 mice- Protein Expression
Terminal	6 mice – Gene Expression 6 mice- Protein Expression 2 mice - Immunohistochemistry	6 mice – Gene Expression 6 mice- Protein Expression 2 mice - Immunohistochemistry

solution (ThermoFisher, cat. # AM7021) and stored at -80^{o}C. Brains for immunohistology were stored in formalin. Lastly, urine was collected by placing mice in metabolic cages (ThermoFisher, cat. # 012882D) overnight with free access to water but no food to prevent contamination (**Table 3**) [133, 174].

2. Whole Brain Tissue Extraction

Total RNA and total protein was isolated from whole brain homogenate by the PARIS KIT (Ambion, cat. # AM1921). Supplied kit components, including Cell Disruption Buffer, 2x Lysis/Binding Solution containing 1.4% 2-mercaptoethanol, Wash Solution 1 and Wash Solution 2/3 Concentrate, were brought to room temperature for 1 hour. Kit cell disruption buffer was combined with a homemade stock buffer (1M Tris 50mM pH 8.0, 0.5M EDTA 2mM pH 8.0, 1M NaCl 6mM, 2% Triton X-100) to provide enough buffer from the same "lot" for the entire experiment. A 10mL aliquot of the disruption buffer was used to dissolve 1 cOmplete, Mini, EDTA-free, protease inhibitor cocktail tablet (Roche, cat. # 11836170001). Working on ice, whole brain was cubed and immediately added to a gentleMACS M tube (Miltenyl Biotec, cat. # 130-096-335) containing 3mL of the cold, protease inhibited cell disruption buffer. Next, the tissue was homogenized for 45 seconds using a MACs homogenizer. Once allowed to de-foam on ice, for 8 minutes, the sample was centrifuged at 4^{o}C for 8 minutes at 5000 RCF. 1 mL of the supernatant was added to 1 mL of 2x Lysis/Binding Solution and immediately mixed by inversion. The remaining amount of supernatant was transferred to a 15mL Falcon tube, homogenized by passing through a 20 gauge needle 5x using a 3mL syringe and distributed into

Table 3: Experimental design of the in vivo model system: collection time points, number of mice collected and intended use of the urine sample.

	Experimental Groups	
Time of Sacrifice (Days Post Infection)	**Group 1: Healthy Control**	**Group 2: ME7 Infected**
7 dpi	6 mice – 8-OHdG ELISA	6 mice – 8-OHdG ELISA
21 dpi	6 mice – 8-OHdG ELISA	6 mice – 8-OHdG ELISA
35 dpi	6 mice – 8-OHdG ELISA	6 mice – 8-OHdG ELISA
49 dpi	6 mice – 8-OHdG ELISA	6 mice – 8-OHdG ELISA
77 dpi	4 mice – 8-OHdG ELISA	4 mice – 8-OHdG ELISA
91 dpi	4 mice – 8-OHdG ELISA	4 mice – 8-OHdG ELISA
105 dpi	4 mice – 8-OHdG ELISA	4 mice – 8-OHdG ELISA
119 dpi	4 mice – 8-OHdG ELISA	4 mice – 8-OHdG ELISA

three, 1.5mL Eppendorf tubes in approximately 500uL volumes to store in the -80^{o}C freezer until further processed for protein isolation (see section 9).

3. Total RNA Extraction

1mL of 100% ethanol was added to the lysate mixture and inverted several times to mix. Then the solution was divided into two PARIS filter cartridges, 700uL at a time. Samples were spun at 16000 RCF for 30 seconds. All centrifugation steps were carried out at 16000 RCF here forth. Flow through was discarded and the remaining amount of lysate/ethanol mixture was applied to the filter cartridge. Samples were spun for another 30 seconds and flow through was discarded. Next, 700uL of Wash Solution 1 was applied to each cartridge, spun for 30 seconds and flow through discarded. Then, 500uL of Wash Solution 2/3 was applied, spun for 30 seconds and flow through discarded, twice. A final 1 minute spin was done before transferring the dried filter cartridges to fresh collection tubes. Then 50uL of preheated nuclease free water (Ambion, cat. # AM9937), approximately 95^{o}C, was applied to the filter and allowed to sit at room temperature for 2 min before a 30 second centrifugation. The elution step was repeated and elute was combined into one tube per sample. RNA concentration was determined using the NanoDrop ND-1000 spectrophotometer for density readings at 260nm and 280nm and then stored in the -80^{o}C freezer until further processed for maximum purification.

4. Total RNA Purification

Raw RNA was further purified by the removal of trace DNA levels with the Turbo DNA-free Kit (Ambion, cat. # AM1907) as provided by the manufacturer. Kit components, 10x TURBO DNase Buffer, TURBO DNase and DNase Inactivation Reagent were thawed on ice. Then, a 0.1 volume of 10x TURBO DNase Buffer and 1uL of TURBO DNase was added to the RNA and mixed gently. Samples were incubated at 37^{o}C for 30 minutes and then the enzyme was inactivated with 0.1 +1 uL volume of DNase Inactivation Reagent by occasional mixing for 2 minutes at room temperature. Finally, the suspension was centrifuged at 10 000 RCF for 1.5 minutes to pellet the enzyme and the supernatant containing the RNA was transferred to a fresh tube. Purified RNA concentration was determined with the NanoDrop as described above and then the RNA was stored in the -80^{o}C freezer until further tested for integrity quality.

5. Determining Total RNA Integrity

Total RNA integrity was determined by the Agilent RNA 6000 Nano Kit (Agilent, cat. # 5067-1511). Reagents were brought to room temperature for 30 minutes. The kit supplied RNA ladder that was transferred to an RNase-free vial and heat denatured for 2 minutes at 70^{o}C. Then, it was immediately cooled down on ice to maintain single stranded structure. Aliquots of RNA ladder were stored at -20 ^{o}C in RNase-free vials. The Agilent RNA gel matrix was prepared by adding 550uL to a provided spin filter and centrifuged at 1500 RCF for 10 minutes at room temperature. Then the gel was divided into provided 0.5 mL RNase-free microcentrifuge tubes in 65uL aliquots. 1uL of RNA dye

concentrate was added to a gel aliquot just prior to use, mixed well and spun at 13000 RCF for 10 minutes at room temperature. 2uL aliquots of sample and ladder were heated for 2 minutes at 70^{o}C using a Thermo Cycler PCR machine. During heating of samples, 9uL of gel-dye mix was added to the ©marked well on the RNA chip. The chip was placed onto the open chip priming station, the plunger was positioned at 1mL and then the lid of the station was closed. The plunger was gently pressed until held by the clip for 30 seconds and then released. After 5 seconds, the plunger was slowly pulled back to the 1 mL position. The chip priming station was opened and then an additional 9uL of the gel-dye mix was added to the two remaining ©marked wells. Next, 5uL of RNA marker was added to all 12 sample wells and the ladder well. Next, 1uL of ladder or sample was added to the ladder or sample wells. The chip was placed in the IKA vortex mixer and mixed for 1 minute at 2400 rpm. Agilent Bioanalyzer 2100 electrodes were decontaminated with a 1 minute wash using RNaseZAP (Ambion, cat. # 9780) followed by a 1 minute rinse using RNase-free water. The chip was placed into the system and samples were resolved and analyzed using the 2100 Expert Software (**Figure 6**). Samples were scored an RNA integrity number from 1-10 where low values indicate high degree of RNA degradation and high values indicate well preserved RNA transcripts. Samples with a score of 7.0 or higher were used for cDNA synthesis.

6. Synthesis of cDNA

Synthesis of cDNA was carried out using the SuperScript III Reverse Transcriptase system (Invitrogen, cat. # 18080-044). Reagents were thawed on ice. 2ug of total RNA, 1uL of 50uM oligo (dT) 12-18 primer (Invitrogen, cat. # 18418-012), 1 uL of 10mM prepared

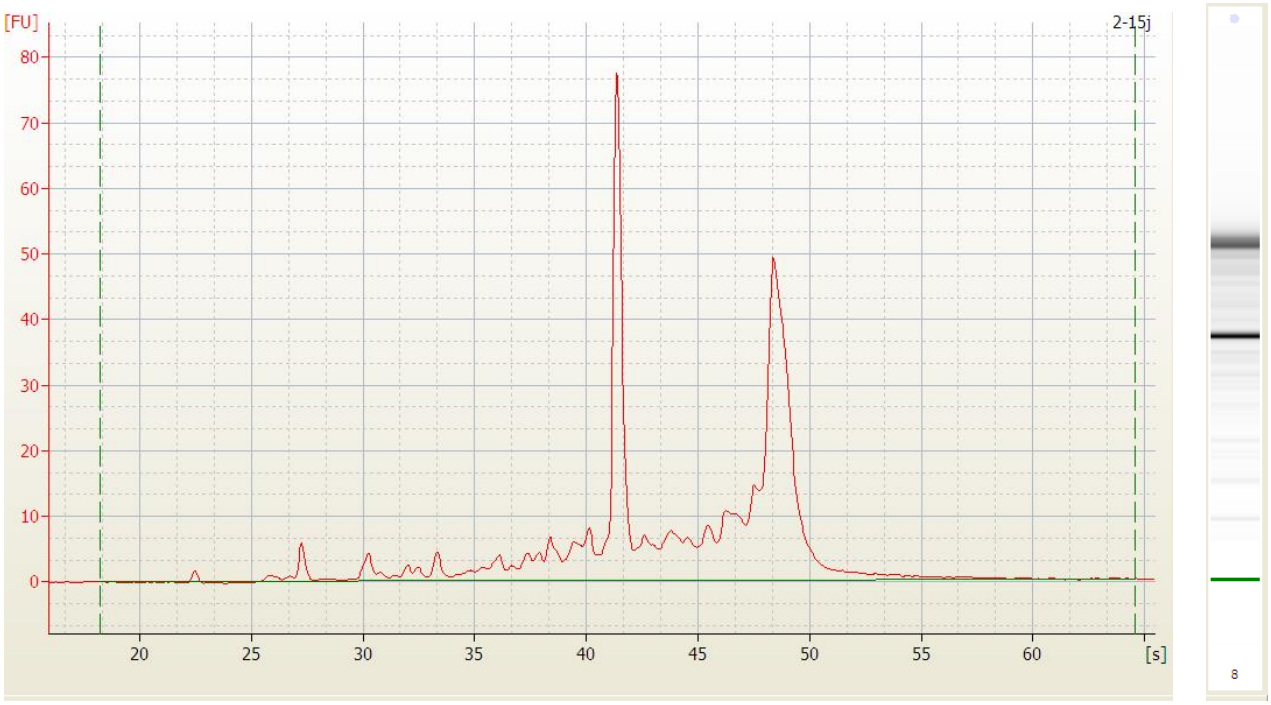

Overall Results for sample 2-15j:	**Infected-Term 1**
RNA Area:	403.8
RNA Concentration:	488ng/uL
rRNA Ratio [28s / 18s]:	1.3
RNA Integrity Number (RIN):	8.1 (B.02.08)

Figure 6: An example of the electropherogram, gel image and overall results obtained by using the Agilent 2100 Bioanalyzer.

dNTP mix (Invitrogen, cat. # 10297-018) and nuclease free water were combined in thin walled 0.5mL PCR tubes (MJ Research, cat. # TBI-0501.18) to total volume 10uL. Contents of the tube were mixed gently and incubated at 65^{o}C for 5 minutes using the Thermo Cycler PCR machine before placing on ice for at least 1 minute. Then, 4uL of 5x First Strand Buffer (250 mM Tris-HCl (pH 8.3 at room temperature), 375 mM KCl, 15 mM $MgCl_2$), 1uL of 0.1M DTT and 1uL of RNase OUT –Recombinant Ribonuclease Inhibitor (40units/uL) (Invitrogen, cat. # 10777-019) was added to the RNA, mixed gently, spun down briefly by centrifugation and placed into the Thermo Cycler PCR machine. Samples were incubated at 50^{o}C for 55 minutes where 1uL of SuperScript III (200units/uL) was added 1 minute into the incubation, followed by a 15 minute incubation at 70^{o}C and a cooling period to 4^{o}C. 1uL of RNase H (2units/uL) (Invitrogen, cat. # 18021-014) was added to the sample, spun down and incubated at 37^{o}C for another 20 minutes. The newly synthesized cDNA was applied to an Amicon Ultra-0.5, Ultracel-30 Membrane, 30 kDa centrifugal filter (Millipore, cat. # UFC503096) in a provided collection tube with 480uL of nuclease free water and centrifuged for 8 minutes at 10000 RCF. The column was transferred to a fresh collection tube and inverted before being centrifuged for an additional 3 minutes at 1000 RCF to recover purified cDNA. Concentration of the cDNA was determined using the NanoDrop as described previously and then stored in the -30^{o}C freezer until further used for real-time PCR analysis.

7. Development of Standard Curve Calibrator for qRT-PCR

i) Generating Target Gene Fragment

Primers were designed for BDKR1 and iNOS mouse genes, flanking an amplicon between 75-150 base pairs, using DNASTAR, PrimerSelect software (**Appendix 1**). Laboratory primers for housekeeping genes GAPDH, HRPT1 and PGK1 were part of our inventory and readily available. Primers were synthesized by DNA Core Services at the Public Health Agency of Canada. Regions of interest were amplified in whole mouse brain by conventional PCR in a 100uL total volume reaction. 10uL of 10x Dream Taq Buffer (20 mM MgCl2 with unspecified volumes of KCl and $(NH_4)_2SO_4$) (Fermentas, cat. # B65), 2uL of 10mM dNTP mix, 2 uL of each forward and reverse primer at 50ng/uL, 3uL of Dream Taq DNA Polymerase (5units/uL) (Fermentas, cat. # EP0701), 2uL of 50ng/uL whole brain homogenate cDNA and nuclease free water (Ambion, cat. # AM9937) were combined into a 0.5mL tube and inserted into a Thermo Cycler PCR machine. Samples were incubated with the following PCR conditions: 95^{o}C for 5 minutes, followed by 4 cycles of 94^{o}C for 30 seconds, 65^{o}C/ 63^{o}C for 30 seconds and 72^{o}C for 30 seconds. This was followed by a touchdown phase with 11 cycles of 94^{o}C for 30 seconds, 65^{o}C/63^{o}C – 0.5^{o}C/cycle for 30 seconds and 72^{o}C for 30 seconds. Then, the remaining 22 cycles were carried out at 95^{o}C for 30 seconds, 55^{o}C/53^{o}C for 30 seconds and 72^{o}C for 30 seconds. A final step of 72^{o}C for 5 minutes was added before cooling to 4^{o}C. Then the amplified cDNA mixed with 6x DNA Loading Dye (Thermo Scientific, cat. # R0611) was run on a 2% UltraPure Agarose 1000 (Invitrogen, cat. # 10975-035) gel with SYBR Safe DNA gel stain

(Invitrogen, cat. # S33102) at 80 volts for 70 minutes. The target band was excised with a scalpel and placed into a weighed 1.5mL tube for further gel extraction processing.

ii) Gel Extraction of Target Gene Fragment

Gel extraction was carried out using the QIAquick Gel Extraction Kit (Qiagen, cat. # 28706). The gel slice was weighed and then 3 volumes of Buffer QG (5.5M guanidine thiocyanate, 20mM Tris HCl pH6.6) was added to 1 volume of gel, where 100mg equals 100uL. The gel was incubated at 50^{o}C for 10 minutes with a heating block to assist solubilisation and periodically mixed every 2-3 minutes. Once completely dissolved, 1 volume of isopropanol was added and mixed. The DNA solution was applied to a QIAquick spin column in a 2mL collection tube and centrifuged at 18000 RCF for 1 minute. All centrifugation steps were carried out at 18000 RCF for 1 minute here forth. The supernatant was discarded and 500uL of Buffer QG was applied to the column. The samples were centrifuged and the supernatant was discarded. Then, 750uL of Buffer PE (80% Ethanol, 10mM Tris-HCl pH7.5) was applied to the column to wash the DNA. Samples were allowed to stand for 5 minutes at room temperature before proceeding to centrifugation. The supernatant was discarded and a final centrifugation was done before transferring the dried column to a new collection tube. For increased DNA concentration, only 30uL of Buffer EB (10mM Tris-HCl, 0.5mM EDTA, pH 9.0) was applied to the center of the QIAquick membrane. The sample stood for 5 minutes at room temperature to solubilize the DNA before recovery by centrifugation. The isolated DNA fragment was then stored at -30^{o}C or immediately used for TA cloning.

iii) The Synthesis and Propagation of Plasmid with Target Gene Fragment

Plasmid construct with my gene of interest was carried out by the TOPO TA Cloning Kit for Subcloning with One Shot TOP10 chemically competent *E. coli* (Invitrogen, cat. # 45-0001). This pCR2.1 vector contains the ampicillin resistance gene and the B-galactosidase gene in the multiple cloning site as strategies for the selection of recombinant bacteria. Kit reagents were all thawed on ice. 2 uL of PCR product (20ng/uL), 1uL of salt solution (1.2 M NaCl, 0.06 M MgCl2), 2uL of water and 10ng/uL of TOPO vector (vector in 50% glycerol, 50 mM Tris-HCl, pH 7.4 (at 25°C), 1 mM EDTA, 2 mM DTT, 0.1% Triton X-100, 100ug/mL BSA, 30 µM phenol red) were combined into a 0.5mL tube, gently mixed by pipet and allowed to sit at room temperature for 5 minutes. The TOP 10 cells were divided into two tubes by transferring 25uL from the thawed vial into a cold 1.5mL tube. Then, 2uL of the TOPO cloning reaction was added to both tubes of TOP10 cells and gently mixed by pipet. These tubes were incubated on ice for 5 minutes followed by a heat shock at 42^{o}C for 30 seconds using a water-filled heating block (Eppendorf Thermomixer). The cells were immediately placed on ice and 250uL of SOC medium (2% Tryptone, 0.5% Yeast Extract, 10 mM NaCl, 2.5 mM KCl, 10 mM MgCl2, 10 mM MgSO4, 20 mM glucose) was added to each tube, mixing by pipet. Then the cells were incubated at 37^{o}C for 1 hour while shaking. After incubation, 50uL of cells was applied and evenly spread across Luria-Bertani Agar Miller (1.5% agar, 1% tryptone, 1% NaCl, 0.5% yeast extract) plates containing 100ug/mL of ampicillin and 80ug/mL of X-gal to screen for ampicillin resistant colonies with disrupted B-galactosidase operons respectively. The plates were incubated at 37^{o}C overnight and

through blue and white selection, positive white colonies were picked the next day and transferred to 13mL snap cap culture tubes containing 3mL of LB Broth-Miller with 50uM Carbenicillin. The cells were then incubated at 37^{o}C shaking, overnight for a maximum of 16 hours with caps set in the semi lock position to provide good aeration.

iv) Plasmid Isolation

Plasmid Isolation was carried out by the QIAprep Spin Miniprep Kit (Qiagen, cat. # 27106). The overnight bacterial culture was pelleted by centrifugation at 7000 RCF for 3 minutes at room temperature. The LB Broth was decanted and the pellet was re-suspended in 250uL of Buffer P1 (50Mm Tris-HCl pH 8.0, 10mM EDTA, 100ug/mL RNase A) where it was transferred to a 1.5mL tube. Next, 250uL of Buffer P2 (200mM NaOH, 1% SDS) was added and the sample was mixed thoroughly by inverting the tube 4-6 times to lyse the cells. Then, 350uL of Buffer N3 (4.2M Gu-HCl, 0.9M potassium acetate, pH 4.8) was added and the sample was immediately mixed by inverting 4-6 times. This was followed by a centrifugation for 10 minutes at 18000 RCF. All centrifugation steps were carried out at 18000 RCF for 1 minute here forth. Carefully, the supernatant was transferred to the QIAprep spin column and centrifuged. Flow through was discarded and the column was washed with 500uL of Buffer PB (5M Gu-HCl, 30% isopropanol). Samples were centrifuged, flow through discarded and washed again with 750uL of Buffer PE (10mM Tris-HCl pH7.5, 80% ethanol). Samples were centrifuged, flow through discarded and a final centrifugation was done before transferring the column to a new 1.5mL tube. DNA was eluted by adding 50uL of Buffer EB (10mM Tris-HCl, 0.5mM EDTA, pH 9.0) to the center of the membrane and allowing it to stand for 5 minutes at

room temperature before centrifugation. The plasmid concentration was determined by NanoDrop as previously described and a 10uL aliquot of 150ng/mL was sent to DNA Core Services at the Public Health Agency of Canada for sequencing to validate the insertion of the target gene fragment. The remaining plasmid volume was stored at -30^{o}C until needed for real-time PCR analysis.

v) Development of the Standard Curve

Real-time PCR was carried out with the LightCycler 480 SYBR Green I Master kit (Roche, cat. # 04887352001). Reagents were all thawed on ice. The pCR2.1 TOPO vector with insert was diluted with nuclease free water to 2.5pg/uL. This was followed by five, ten-fold serial dilutions ultimately yielding 2.5pg/uL, 250fg/uL, 25fg/uL, 2.5fg/uL, 250ag/uL and 25ag/uL of calibrating plasmid for the standard curve. Then, 10uL of SYBR Green I Master, 6uL of PCR Grade water, 1uL each of 50ng/uL target reverse and forward primers and 2uL of either pCR2.1 TOPO vectors + insert or 2ul of nuclease free water blank were combined into a LightCycler 480 96-well plate (Roche, cat. # 04729692001). TOPO vectors were plated in 5-8 replicates and the water blank in triplicate. The plate was sealed with provided transparent foil, mixed using a plate vortex for 1 minute and then gently centrifuged for 2 minutes at 2000 RCF. The plate was inserted into the LightCycler 480 and set to run for the following conditions: 95^{o}C for 5 minutes, followed by 50 cycles of 95^{o}C for 5 seconds, 62^{o}C/58^{o}C/56^{o}C depending on target gene for 5 seconds, and 72^{o}C for 7 seconds. This PCR program was followed by a melting curve program which consisted of 5 seconds of denaturing at 95^{o}C, 30 seconds of annealing at 55^{o}C, and a melting and continuous measuring step up to 95^{o}C at 2.2^{o}C/s.

Measurements were analyzed by the absolute quantification/second derivative maximum method of the LightCycler software. Results were displayed both as crossing points (Cp) and as concentration (pg/ul) relative to the standard curve.

8. Quantitative Real-Time Polymerase Chain Reaction for Genes of Interest

i) Real-time PCR of Whole Brain Homogenate

For sample analysis, 10uL of SYBR Green I Master, 6uL of PCR Grade water, 1uL each of 50ng/uL target reverse and forward primers and 2uL of either 2.5pg/uL of pCR2.1 TOPO vector with corresponding insert, 2ul of 25ng/uL of whole brain cDNA or 2ul of water blank were combined into a LightCycler 480 96-well plate. Samples were plated in triplicate, positive plasmid calibrator and water blank in duplicate. The plate was sealed with provided transparent foil, mixed using a plate vortex for 1 minute and then gently centrifuged for 2 minutes at 2000 RCF. The plate was inserted into the LightCycler 480 and set to run for the following conditions: 95^{o}C for 5 minutes, followed by 50 cycles of 95^{o}C for 5 seconds, 62^{o}C/58^{o}C/56^{o}C depending on target gene for 5 seconds, and 72^{o}C for 7 seconds. This PCR program was followed by a melting curve program which consisted of 5 seconds of denaturing at 95^{o}C, 30 seconds of annealing at 55^{o}C, and a melting and continuous measuring step up to 95^{o}C at 2.2^{o}C/s.

ii) Analysis of Gene Expression

Measurements were analyzed by the advanced relative quantification method of the LightCycler software. Results were displayed both as crossing points and target/reference points relative to each housekeeping gene. GraphPad Software analysis available online was used to carry out a Grubb's test on the data set. A

confidence level of 99% was used to allow room for biological variation. Infected samples were normalized to the control average and graphed as fold change increase. Daniel's XL toolbox, a free, open source add-in for Microsoft Excel was used for statistical analyses.

9. Total Protein Purification

Whole brain homogenate protein aliquots were allowed to thaw on ice. Once thawed, 2% NaDOC was added to a 0.01% final concentration and mixed by vortex before incubating on ice for 30 minutes. Then, 20% TCA was added at 1:20 v/v and immediately mixed by vortex to break up the precipitate. Samples were incubated on ice for 1 hour. After incubation, the samples were centrifuged at 15000 RCF at 4^{o}C for 10 minutes. The supernatant was discarded and 1mL of cold acetone was added to the pelleted protein. Ensuring the protein remains cold during this procedure, a 20 gauge needle and a 3mL syringe was used to crush the protein into "grain of sand" consistency. Then the sample was centrifuged at 15000 RCF at 4^{o}C for 10 minutes. The supernatant was discarded and this acetone wash process was repeated two more times. After the third wash, the protein was air dried on a Biological Safety Cabinet grill for 2 minutes and then rehydrated by adding 150uL of Rehydration buffer (31mM Tris pH 8.0, 2M ThioUrea, 7M Urea, 4% (wt/vol) CHAPS in water). The pellet was mixed with a pipet tip and then incubated for approximately 1 hour at room temperature with periodic mixing using a vortex to aid solubilization. Then the samples were stored in the -20^{o}C freezer overnight. Next day, the protein was thawed at room temperature. Additional rehydration buffer was added to each vial as needed to reach a glycerol-like consistency.

The samples remained at room temperature with periodic mixing by vortex for another hour to fully solubilise as much protein as possible. The aliquots were then combined into one 1.5mL tube and stored in the -80^{o}C freezer until further processed.

10. Protein Quantification

Whole brain homogenate protein samples were thawed at room temperature. Samples were mixed well with a vortex and then centrifuged at 12000 RCF at 4^{o}C for 5 minutes to remove any insoluble protein. The supernatant was transferred to a new 1.5mL tube and placed on ice. To the remaining insoluble pellet, 150uL of rehydration buffer was added to re-suspend more protein. This tube was incubated for 1 hour at room temperature with periodic mixing with a vortex. Then it was centrifuged at 12000 RCF at 4oC for 5 minutes. The supernatant was collected and added to the supernatant collected earlier. The remaining insoluble pellet was discarded. This solubilised protein was quantified with the 2-D Quant Kit (GE Healthcare, cat. # 80-6483-56), a standard curve was prepared by adding increments of 5uL of 2mg/ml Bovine serum albumin (BSA) to five 1.5mL tubes in duplicate. A sixth tube in duplicate containing no BSA was included as the assay blank. 2uL of protein sample was added to 1.5mL tubes in duplicate. Then, 500uL of precipitant was added to all standard and sample tubes. All tubes were mixed briefly by vortex and incubate at room temperature for 3 minutes. Then, 500uL of co-precipitant was added to each tube and mixed briefly by simultaneously inverting all tubes between two racks several times. All tubes were centrifuged at 12000 RCF at 4^{o}C for 5 minutes. The supernatant was decanted and the process was repeated from the precipitant addition again. After decanting the

supernatant for the second time, an additional brief spin for 10 seconds was added to recollect and remove the excess liquid from the tube. Then, 100uL of copper solution and 400uL of distilled water was added to each tube and mixed by vortex. Next, 1mL of working color reagent (consisted of 100 parts of color reagent A and 1 part color reagent B) was quickly added to all tubes followed by immediate and simultaneous mixing by inversion. Samples were incubated at room temperature for 20 minutes and then immediately loaded to a 96-well flat bottomed, clear plate in 200uL volumes. The absorbance was read with a spectrophotometer (Molecular Devices, SpectroMax PLus) at 480nm and a linear standard curve was generated by the SpectroMax PLus software extrapolated protein concentration from the graph.

11. Western Blot Analysis

i) Gel Electrophoresis and Transfer

Protein samples were prepared by combining 50ug of protein in 10uL of nuclease free water and 10uL of 2x sample buffer. Samples were heated for 5 minutes at 95^{o}C and immediately placed on ice. Then, samples were separated by SDS-polyacrylamide gel electrophoresis using 12% Bis-Tris Criterion XT Precast gels (BioRad, cat**. #** 345-0117) with either 20x XT MOPS (BioRad, cat. # 161-0788) or 20x XT MES (BioRad, cat. # 161-0789) running buffers or 5% Tris-HCl Criterion XT Precast gels (BioRad, cat. **#** 345-0001) with 10x Tris/Glycine/SDS running buffer (BioRad, cat. #161-0732) at 200 volts for either 60 or 55 minutes respectively. Then the gels were transferred to iBlot Gel Transfer Nitrocellulose Stacks (Invitrogen, cat. # IB301001) using the 7 minute transfer program with the iBlot (Invitrogen, cat. # IB1001).

ii) Total Protein Quantification

Total protein staining was done for the 5% Tris-HCl membrane and was carried out by the Memcode Reversible Protein Stain Kit for Nitrocellulose Membrane (Thermo Scientific, cat. # 24580). The membrane was washed with ultrapure water for 5 minutes rocking. The water was discarded and MemCode Stain was added for 1 minute rocking to stain total protein blue. Stain was immediately removed and the membrane was rinsed three times followed by a 10 minute wash with MemCode Destain Solution. Then the membrane was rinsed four times followed by a 5 minute was with ultrapure water. The membrane was scanned, saved as a coloured jpeg file and then washed with the MemCode Stain Eraser for 3 minutes rocking. The membrane was further rinsed four times with ultrapure water and a final 5 minute wash. The jpeg file was converted into a gray scale TIFF file in Adobe Photoshop and then quantified with Image Quant TL Software from GE Health Sciences with the rolling ball method for background subtraction.

iii) Target Protein Detection

Nitrocellulose membranes were blocked in 5% BSA in TBST for 1 hour rocking and probed with either KNG HC (A-21) (Santa Cruz, cat. # sc-25887) at a 1:200 dilution, NOS2 (M-19) (Santa Cruz, cat. # sc-650) at a 1:200 dilution or GFAP (Dako, cat. # 20334) at a 1:20000 dilution in TBST 5% BSA rocking overnight at 4^{O}C. Membranes were washed 3 times with TBST for 10 minutes rocking and then incubated with a 1:2000 dilution of horseradish peroxidase (HRP) secondary antibodies rabbit anti-goat (Dako, cat. # PO449) or goat anti-rabbit (Dako, cat. # PO448) for 1 hour rocking. Membranes were washed 3

times with TBST for 10 minutes rocking and rinsed 3 times with TBS. Super Signal West Pico Chemiluminescent Substrate (Thermo Scientific, cat. # 34080) was applied to the membrane in a 1:1 volume ratio. The membrane rocked for 5 minutes to evenly distribute signal and then was immediately imaged with the Bio Rad Versa Doc imaging system.

iv) Re-probing for Loading Control

Probed membranes were stripped with Restore PLUS Western Blot Stripping Buffer (Thermo Scientific, cat. # 46430) for 20 minutes and washed extensively with TBST. Membranes were re-blocked in 5% BSA in TBST for 1 hour and probed with either monoclonal anti-α-Tubulin (Sigma, cat. # T9026) at a 1:3000 a dilution or Vinculin (Sigma, cat. # V4139) at a 1:1000 dilution rocking overnight at 4^{o}C. Membranes were washed 3 times with TBST for 10 minutes rocking and then incubated with a 1:2000 dilution of horseradish peroxidase (HRP) secondary antibodies goat anti-mouse (Dako, catalogue # PO447) or goat anti-rabbit (Dako, catalogue # PO448) for 1 hour rocking. Membranes were washed 3 times with TBST for 10 minutes rocking and rinsed 3 times with TBS. Super Signal West Pico Chemiluminescent Substrate was applied to the membrane in a 1:1 volume ratio. The membrane rocked for 5 minutes to evenly distribute signal and then was immediately imaged with the Bio Rad Versa Doc imaging system.

v) Analysis of Protein Expression

Protein expression was measured with Quantity One 1D Analysis Software from Bio-Rad. Band intensities were measured as density INT/mm^2 and adjusted by background

subtraction. Target protein bands were compared relative to their corresponding loading controls. Any lanes displaying evidence of unequal antibody contact were omitted in the analysis. Infected samples were then normalized to the control average and graphed as fold change increase. Statistical analyses were carried out in Microsoft Excel.

12. 8-OHdG Urine Assay

8-OHdG levels were measured in urine using the DNA Damage EIA kit (Enzo Life Sciences, cat. # ADI-EKS-350). The kit contains the 8-OHdG Immunoassay plate, 20x wash buffer, sample diluents, antibody diluents, HRP conjugate diluents, TMB substrate and stop solution 2 which are all brought to room temperature before use. 8-OHdG standards were generated in duplicate. 3uL of stock solution was added to 500uL of sample diluent and mixed well to generate the first standard. Then, subsequent 1:1 dilutions in sample diluent were carried out until 7 standards were generated. An eighth standard is also prepared containing only sample diluent to serve as the blank. Urine samples were prepared in triplicate and were also diluted 1:20 with the sample diluent. Ten, 50uL of prepared standard or samples were added to 8-OHdG immunoassay plate. The primary antibody was prepared by combining 6.6uL of anti-8-OHdG with 1.666mL of antibody diluent. With a multi-channel, 50uL of the primary antibody was added to all wells except for the blanks. The plate was sealed to prevent contamination and incubated at room temperature for 1 hour. Then the primary antibody was removed and the wells were washed 8 times with 200uL of 1 x Wash Buffer. On the final wash, the plate was gently inverted and patted dry. Next, the secondary antibody was

prepared by combining 7.3uL of anti-mouse IgG HRP conjugate with 3.6mL of HRP conjugate diluent. 100uL of the secondary antibody was added to all wells except for the blanks. The plate was sealed again and incubated at room temperature for 1 hour. The secondary antibody was removed and the wells were washed 8 times with 200uL of 1 x Wash Buffer. On the final wash, the plate was gently inverted and patted dry. Next, 100uL of TMB substrate was added to all wells and was placed aside in the dark for 15 minutes. Then, 100uL of stop solution was added to all wells in the same order as the TMB substrate had been administered to stop the colorimetric reaction. The absorbance was measured at 450nm with a spectrophotometer and an 8-OHdG standard curve was generated to calculate the unknown 8-OHdG sample concentrations.

13. Immunohistochemistry

All histology procedures were carried out in Level 3 containment.

Formalin fixed paraffin embedded brain tissue was sliced into 5 µm thick coronal sections and placed on charged microscope slides (ThermoFisher, cat. # 12-550-15). Sections were incubated overnight at 37°C to deparaffinize. The next day, the tissue was rehydrated with an ethanol series beginning with 3-3 minute washes with agitation in Pro-Par Clearant (Anatech Ltd, cat. # NC9537734), 2-2 minute washes in 100% ethanol, 2-2 minute washes in 90% ethanol, 2-2 minute washes in 70% ethanol and a final rinse in distilled water. Then the tissue was incubated in 3% hydrogen peroxide for 10 minutes to inactivate any endogenous peroxidases. The tissue was rinsed with distilled water 3 times and then an antigen retrieval step was carried out by incubating tissue in 10mM sodium citrate for 20 minutes in a pressurized autoclave, reaching a temperature

of 121°C. Slides were cooled by the addition of distilled water followed by complete submersion in TBST. Slides were arranged in a humidifier chamber and incubated with anti-B1 bradykinin receptor (Alomone Labs, cat. # ABR-011) at a 1:200 dilution or iNOS (Sigma, cat. # ABN26) at a 1:500 dilution over night at 4°C. Antibody diluent was provided by the Polink-2 HRP Plus Rabbit DAB Detection System for IHC kit (GBI Labs, cat. # D39-110). Tissue was washed with TBST 3 times for 2 minutes and then incubated for 10 minutes with rabbit antibody linker/enhancer provided by the kit. Tissue was washed with TBST 3 times for 2 minutes and then incubated for another 10 minutes with the secondary antibody, POLYMER-HRP for rabbit, provided by the kit. Tissue was washed for a final time with TBST 3 times for 2 minutes. DAB (3,3'-diaminobenzidine) stain was prepared by a 1:20 dilution of the DAB chromogen with the supplied diluent agent provided by the Betazoid DAB Chromogen Kit (Inter Medico, cat. # BDB2004 H, L, MM). Tissue was incubated with DAB for 20 seconds on iNOS sections and 1 minute on B1 receptor sections. Slides were immediately submerged in distilled water to stop the reaction and then counterstained with hemotoxylin (Richard Allan Scientific, cat. # 7211) for 3 minutes. Slides were rinsed well under running tap water for 3 minutes and then dunked 10-12 times in acid alcohol (0.5% HCl, 70% ethanol) (EMS, cat. # 26071-01) to remove excess stain and help define nuclei. Slides were rinsed under running tap water for 1 minute and then transferred to Scott's Tap Water (0.17M magnesium sulphate heptahydrate, 0.02M sodium bicarbonate) to soak for 1 minute, until tissue reveals blue color. Slides were rinsed again for 1 minute under running tap water. Finally, the slides were dehydrated with an ethanol series beginning with 2-2 minute washes in 70%

ethanol, 2-2 minute washes in 90% ethanol, 2-2 minute washes in 100% ethanol and 3-3 minute washes with agitation in Pro-Par Clearant. Slides were mounted with Permount (Fisher, cat. # SP15-500) and left to dry overnight in the dark. Slides were imaged using the Mirex Midi Scanner.

i) Histological Analysis

Specimens were examined using Pannoramic Viewer Software, a download readily available through 3DHISTECH Ltd. A maximum of six images were taken per region, three images in the left hemisphere of the brain and three images on the right. Images were taken at 50x or 70x magnification. Colors were adjusted for optimal brightness and contrast for each image, ensuring all images for the same antibody were set to the same level to allow for comparison. Total positive cell count over total cell count was counted manually using the cell counter plugin found in ImageJ, a free application found online. Positive cell counts were defined by nuclear staining of cells for iNOS and membrane bound staining for the B1 receptor. Final counts for each region were summed and then a percentage was determined for each experimental mouse. The average percentage was graphed and statistical analyses were carried out in Microsoft Excel.

C. Results

1. Defining Stages of Disease Relative to Days Post Infection

Changes in locomotor activity and posture have historically been indicators for the onset of clinical prion disease [175, 176]. Cunningham ***et al.*** have observed significant impairment in burrowing and nesting activity as early as 91 days post infection [176]. Conversely, using the same animal model, we find that significant impairment to burrowing and nesting activity occurs consistently closer to 110 days post infection [133, 174]. With these behavioural changes in mind, along with our quantitatively collected data on inflammatory and oxidative stress levels, we have created a schematic diagram indicating the clinical stages of disease with respect to days post infection (DPI). We have defined preclinical stages to be prior to DPI 90, a transitory stage from DPI 90-100 and clinical stages after DPI 100 (**Figure 7**).

2. Quantitative Real-time Polymerase Chain Reaction

Two target genes, NOS2 and BDKRB1 were normalized to three different housekeeping genes, HRPT1, PGK1 and conventional GAPDH [177]. Three housekeeping genes were selected to confirm consistency of each observed mRNA expression profile in addition to a minimum of 4 biological replicates, each tested in triplicate for each time point, DPI 70, 90, 100, 110, 120, 130, terminal. Mice were normalized to the control subset and then individually compared to their respective control average using the one-way ANOVA with the Bonferroni-Holm posthoc test.

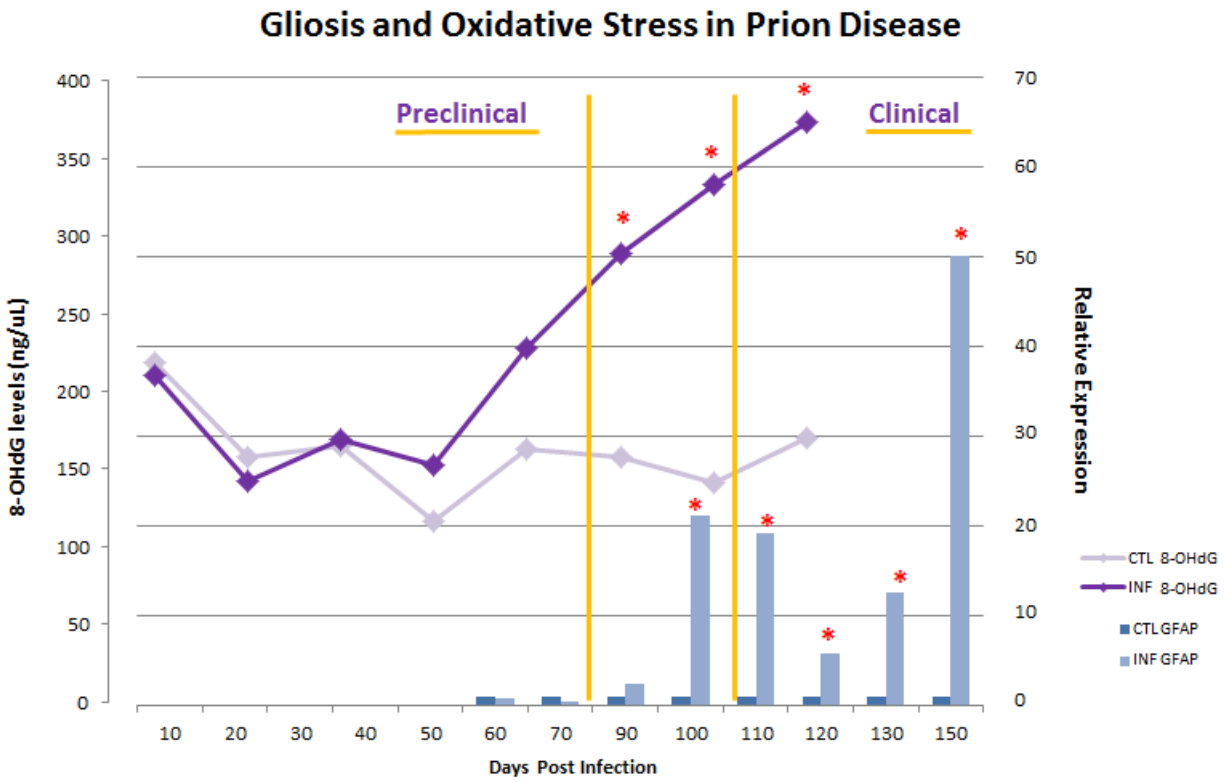

Figure 7: An overlap schematic of 8-OHdG levels versus GFAP levels in scrapie infected and age-matched control mice. Diagram demonstrates the preclinical phase of disease prior DPI 90, the transition phase DPI 90-100 and the clinical phase of disease post DPI 100. A red asterisk indicates statistical significance.

i) Inducible Nitric Oxide Synthase

Overall, iNOS mRNA expression showed no change between control and prion infected whole mouse brain in the preclinical and early clinical stages of disease, DPI 70 - 110 (**Figure 8-10**). The few significant exceptions included DPI 90 where infected mouse 5 demonstrated a lower expression of iNOS when compared to PGK1 only. DPI 100 showed infected mouse 1 and 5 with a lower iNOS expression level across all three housekeeping genes. Infected mouse 4 in DPI 110 demonstrated a lower expression level when compared to PGK1 only and infected mouse 1 showed a lower expression level across all three housekeeping genes. Interestingly, all housekeeping genes agreed on an increasing trend of iNOS mRNA expression from DPI 120-130. We began to see one infected mouse express an average 4.2-fold increase in iNOS expression at DPI 120. At DPI 130, we saw infected mice 2, 4, and 6 display an average 4.0-fold, 3.0-fold and 7.6-fold increase in iNOS levels respectively. At the terminal stage of disease, iNOS mRNA expression returned to control levels with two infected mice that elicited a statistically significant decrease when compared to PGK1 only.

ii) B1 Receptor

B1 receptor mRNA expression followed a similar pattern as the iNOS mRNA expression profile. Overall, there did not appear to be a change between control and prion infected whole mouse brain in the preclinical and early clinical stages of disease, DPI 70-110 (**Figure 11-13**). The few statistically significant exceptions included a minimal decrease in expression at DPI 70 for infected mouse 4 when compared to GAPDH and infected mice 2, 4 and 5 when compared to HRPT1. In addition, DPI 100 revealed infected

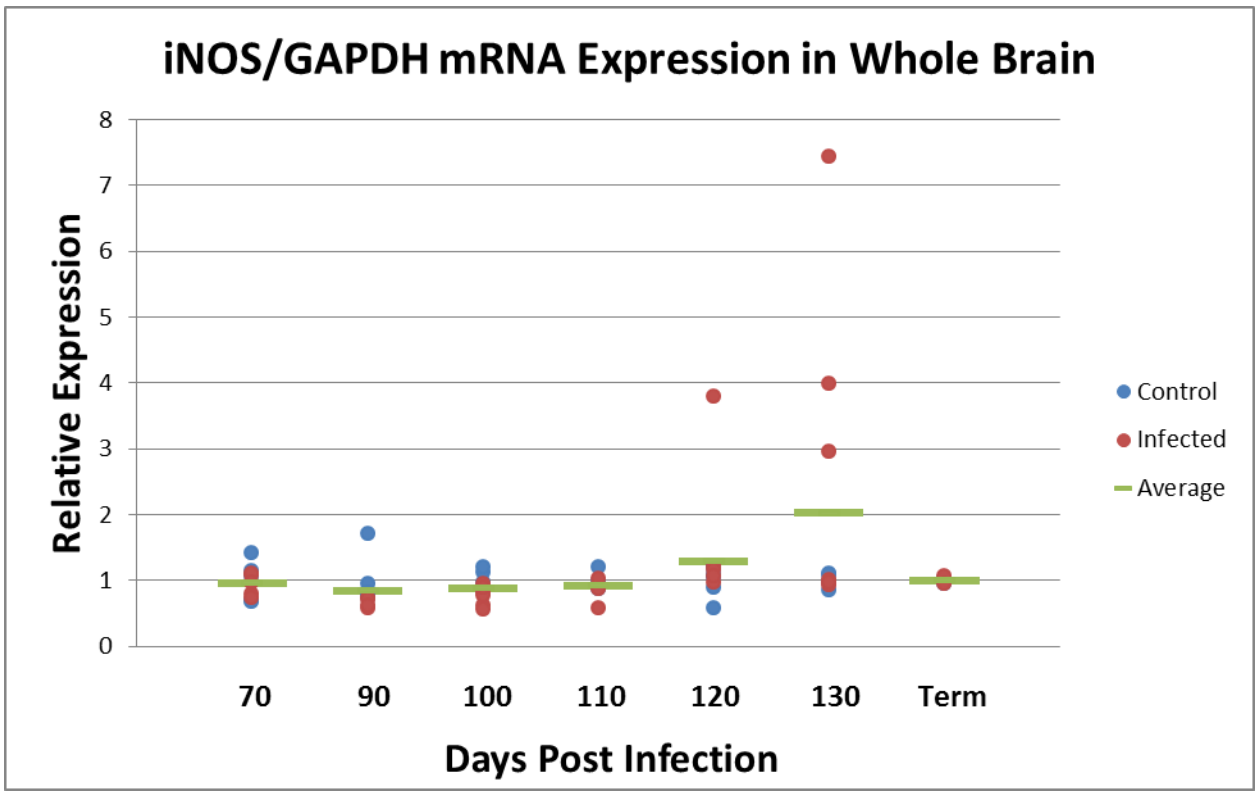

Figure 8: iNOS mRNA levels were measured in whole mouse brain of scrapie infected and age-matched controls by real-time PCR. Each circular marker represents the triplicate average of an individual animal with a minimum of four biological replicates per time point. Target gene was normalized to housekeeping gene GAPDH. One-way ANOVA with Bonferroni-Holm posthoc test was used for multiple comaparisons of data set. There was no significant difference between infected and control mice at DPI 70 and DPI 90. In scrapie infected mice, two mice expressed a statistically significant decrease at DPI 100 (p=2.7E-04, p=6.0E-05) and one mouse significantly decreased at DPI 110 (p=9.4E-04). At DPI 120, one mouse expressed a statistically significant increase (p=9.5E-14) and three mice significantly increased at DPI 130 (p=5.4E-13, p=1.5E-12, p=4.1E-20). Expression levels returned to control levels at term stages of disease.

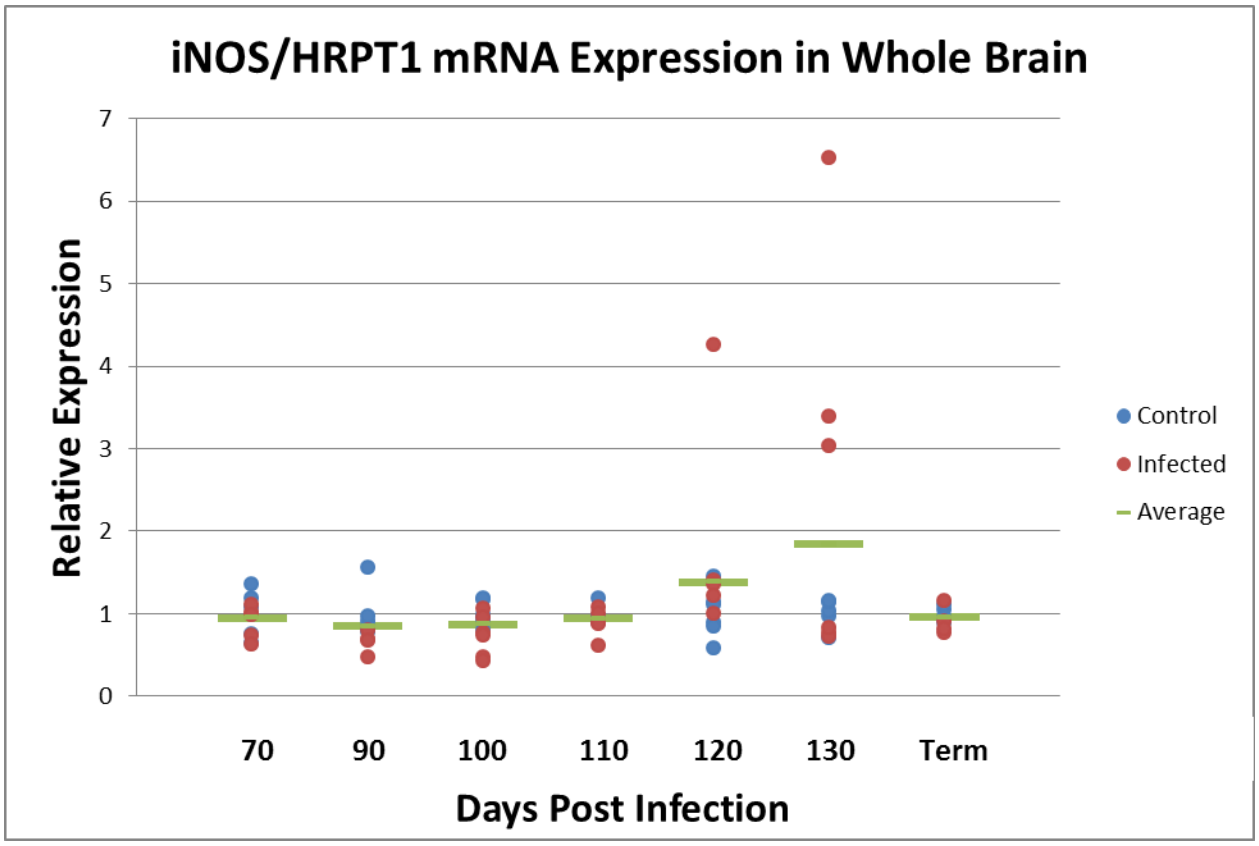

Figure 9: iNOS mRNA levels were measured in whole mouse brain of scrapie infected and age-matched controls by real-time PCR. Each circular marker represents the triplicate average of an individual animal with a minimum of four biological replicates per timepoint. Target gene was normalized to housekeeping gene HRPT1. One-way ANOVA with Bonferroni-Holm posthoc test was used for multiple comaparisons of data set. There was no significant difference between infected and control mice at DPI 70 and DPI 90. In scrapie infected mice, two mice expressed a statistically significant decrease at DPI 100 (p=1.3E-05, p=5.3E-06) and one mouse significantly decreased at DPI 110 (p=9.6E-04). At DPI 120, one mouse expressed a statistically significant increase (p=1.6E-12) and three mice significantly increased at DPI 130 (p=1.6E-12, p=2.2E-13, p=4.8E-19). Expression levels returned to control levels at term stages of disease.

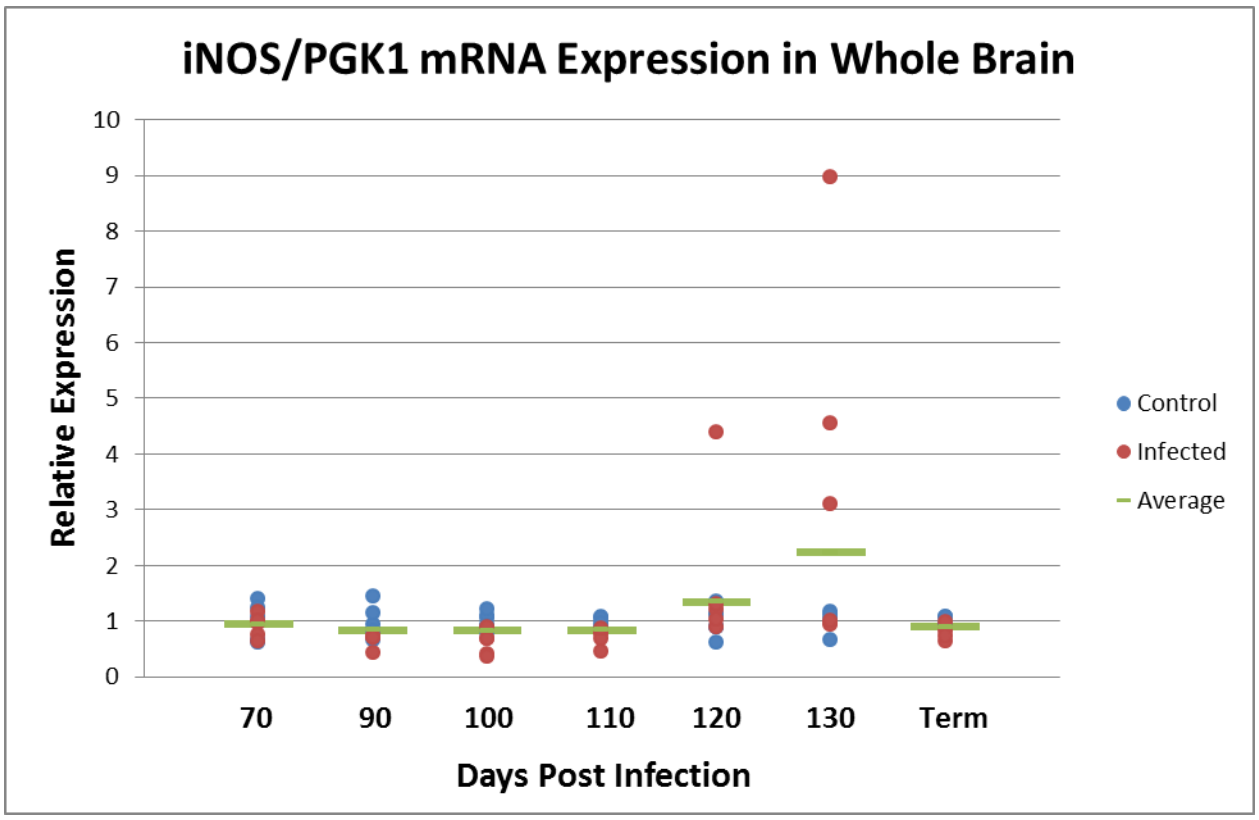

Figure 10: iNOS mRNA levels were measured in whole mouse brain of scrapie infected and age-matched controls by real-time PCR. Each circular marker represents the triplicate average of an individual animal with a minimum of four biological replicates per timepoint. Target gene was normalized to housekeeping gene PGK1. One-way ANOVA with Bonferroni-Holm posthoc test was used for multiple comaparisons of data set. There was no significant difference between infected and control mice at DPI 70. In scrapie infected mice, one mouse expressed a statistically significant decrease at DPI 90 (p= 4.9E-03), two mice had a significant decrease at DPI 100 (p=2.5E-06, p=1.2E-06) and two mice significantly decreased at DPI 110 (p=1.7E-05, 1.6E-03). At DPI 120, one mouse expressed a statistically significant increase (p=1.2E-14) and three mice significantly increased at DPI 130 (p=4.6E-12, p=3.2E-10, p=4.6E-18). Expression levels returned to control levels with two mice expressing a significant decrease at term stages of disease (p=7.3E-04, 5.0E-03).

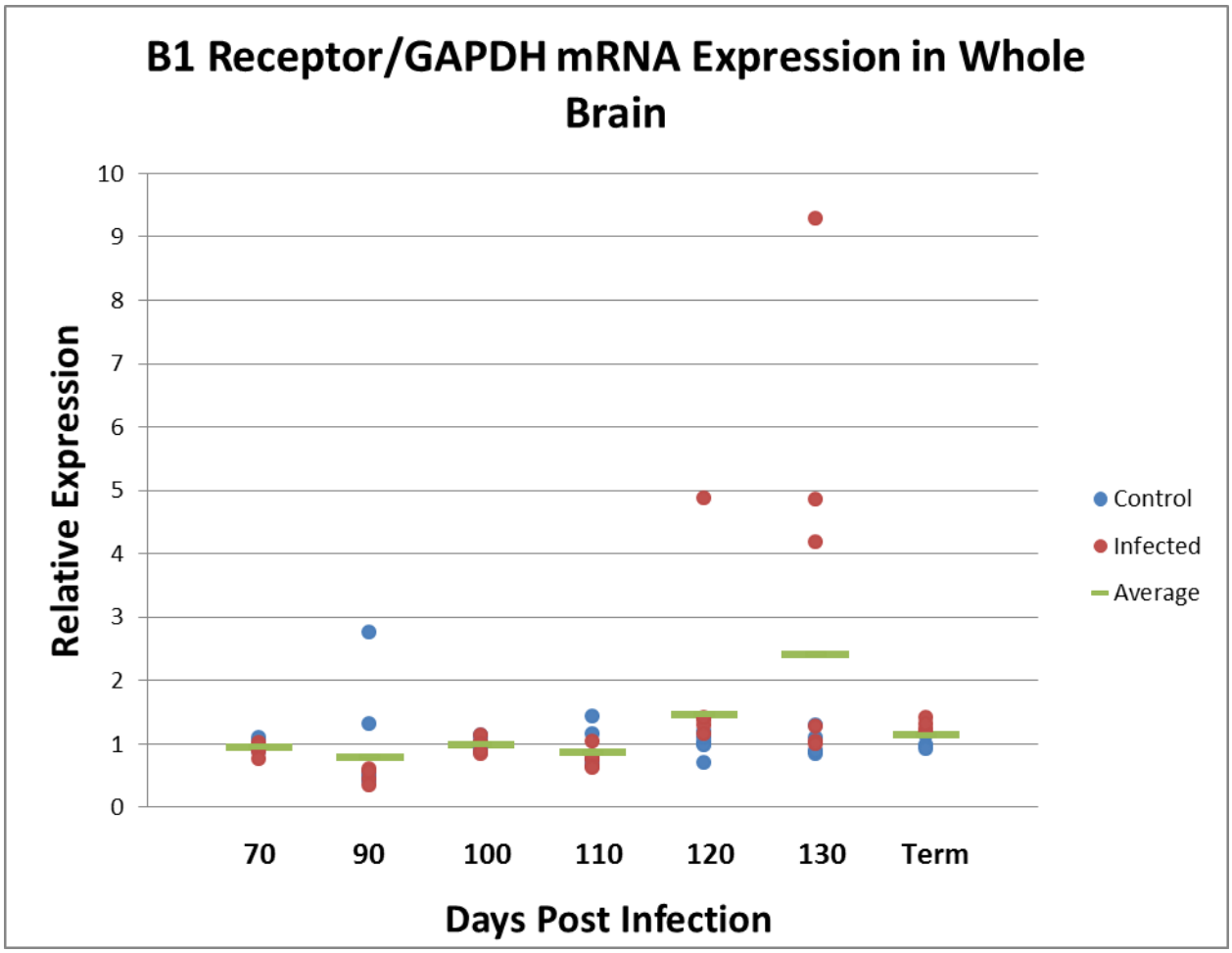

Figure 11: B1 receptor mRNA levels were measured in whole mouse brain of scrapie infected and age-matched controls by real-time PCR. Each circular marker represents the triplicate average of an individual animal with a minimum of four biological replicates per timepoint. Target gene was normalized to housekeeping gene GAPDH. One-way ANOVA with Bonferroni-Holm posthoc test was used for multiple comaparisons of data set. There was no significant difference between infected and control mice at DPI 90, 100 and 110. In scrapie infected mice, one mouse expressed a statistically significant decrease at DPI 70 ($p=3.8E-04$). At DPI 120, one mouse expressed a statistically significant increase ($p=1.5E-16$), three mice significantly increased at DPI 130 ($p=3.1E-15$, $p=3.2E-14$, $p=3.6E-21$) and one mouse significantly increased at term stages of disease ($p=1.1E-03$).

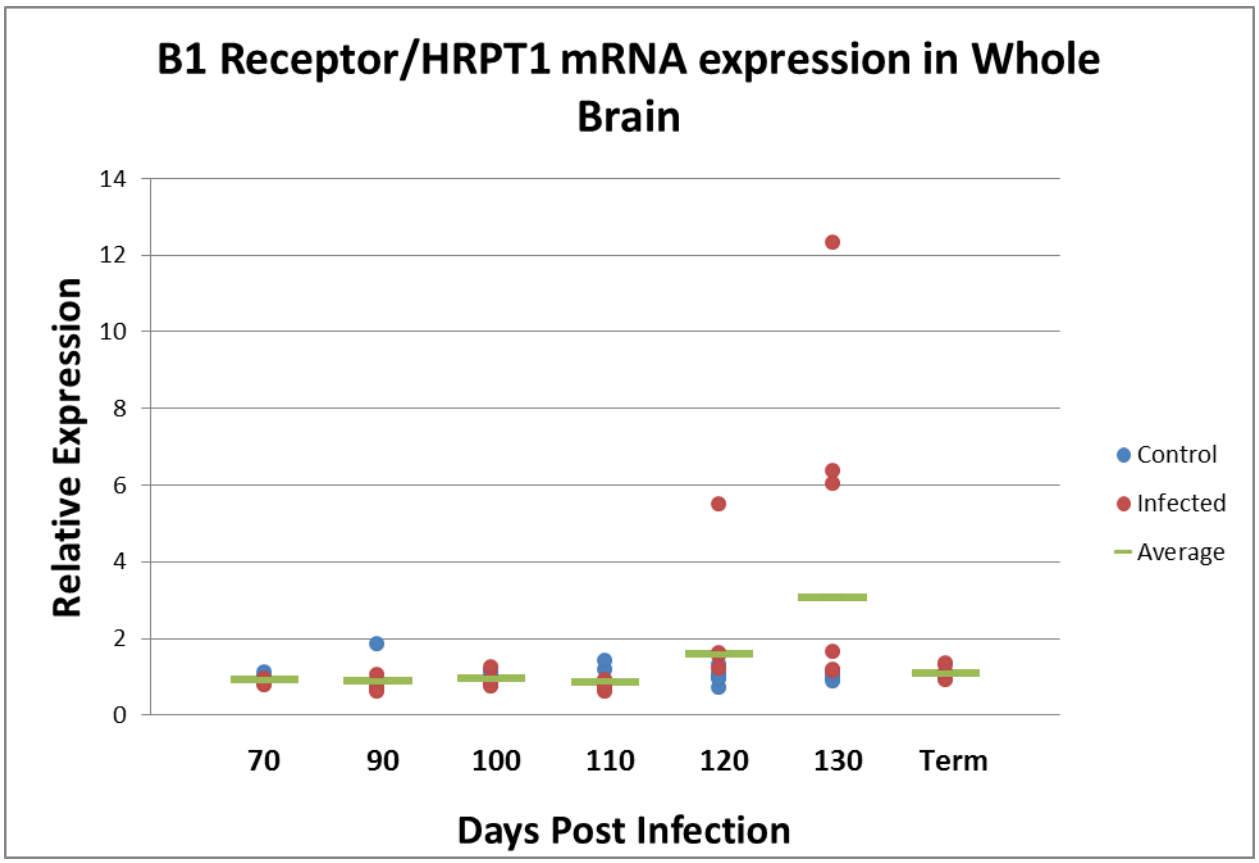

Figure 12: B1 receptor mRNA levels were measured in whole mouse brain of scrapie infected and age-matched controls by real-time PCR. Each circular marker represents the triplicate average of an individual animal with a minimum of four biological replicates per timepoint. Target gene was normalized to housekeeping gene HRPT1. One-way ANOVA with Bonferroni-Holm posthoc test was used for multiple comaparisons of data set. There was no significant difference between infected and control mice at DPI 90, 100, and 110. In scrapie infected mice, three mice expressed a statistically significant decrease at DPI 70 (p=2.8E-03, p=1.6E-04, p=1.7E-03). At DPI 120, four mice expressed a statistically significant increase (p=2.3E-04, p=6.4E-04, p=2.8E-04, p=2.7E-16), five mice significantly increased at DPI 130 (p=1.0E-14, p=1.1E-02, p=7.3E-16, p=1.1E-07, p=2.9E-25) and two mice significantly increased at term stages of disease (p=3.4E-03, p=1.6E-03).

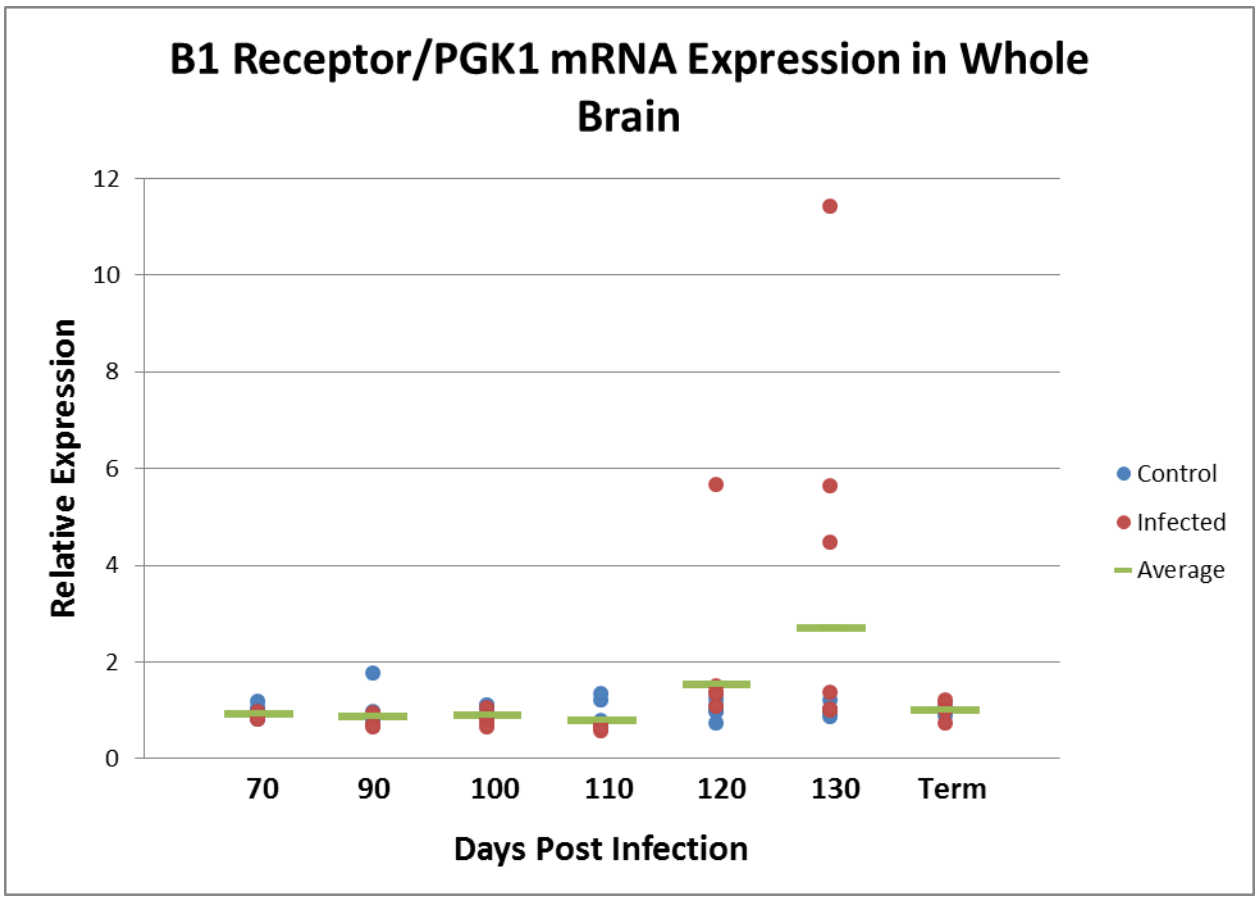

Figure 13: B1 receptor mRNA levels were measured in whole mouse brain of scrapie infected and age-matched controls by real-time PCR. Each circular marker represents the triplicate average of an individual animal with a minimum of four biological replicates per timepoint. Target gene was normalized to housekeeping gene PGK1. One-way ANOVA with Bonferroni-Holm posthoc test was used for multiple comaparisons of data set. There was no significant difference between infected and control mice at DPI 70, 90, 110 and term. In scrapie infected mice, two mice expressed a statistically significant decrease at DPI 100 (p=2.4E-03, p=1.5E-03). At DPI 120, four mice expressed a statistically significant increase (p=3.3E-03, p=3.7E-04, p=5.7E-03, p=5.1E-18) and four mice significantly increased at DPI 130 (p=6.4E-17, p=2.3E-16, p=2.7E-04, p=9.5E-24).

mice 1 and 5 displaying a minimal decrease when compared to PGK1 only. These observations, however, were not consistent with all three housekeeping genes. Excitingly, the same increasing trend observed at DPI 120-130 in the iNOS mRNA expression profile, was observed with the B1 receptor. At DPI 120, infected mice 1, 2, 4 and 6 expressed a statistically significant increase in B1 receptor mRNA expression when compared to HRPT1 and PGK1 housekeeping genes. Although mice 1, 2 and 4 displayed only a minimal increase, mouse 6 expressed an average 5.4-fold increase across all housekeeping genes. This was the same infected mouse that expressed a statistically significant increase in iNOS levels. At DPI 130, 5 out 6 infected mice expressed a statistically significant increase in B1 receptor mRNA when compared to HRPT1. This decreased to 4 out of the 6 mice when compared to PGK1 housekeeping gene and further dropped to 3 out of 6 mice when compared to GAPDH. These three infected mice, 2, 4 and 6, revealed an average 5.5-fold, 5.0-fold and 11.0-fold increase in B1 receptor levels respectively. This increase correlates with the expression of iNOS levels observed in the same infected mice. At the terminal stage of disease, B1 receptor mRNA expression was increased in infected mice 1 and 4 when normalized to HRPT1. When compared to GAPDH, only infected mouse 1 was statistically significant and when compared to PGK1, there did not appear to be any change in levels between control and infected mice.

3. Western Blot Analysis

Four proteins, high molecular weight kininogen, low molecular weight kininogen, iNOS and GFAP, were tested by Western blot analysis for their expression levels through the

course of prion disease. Target proteins were normalized to tubulin or vinculin in combination with total protein to ensure uniform protein concentration. Due to the larger molecular weight of iNOS, 130 kDa, a lower gel percentage was used to better resolve proteins in the 100 kDa or greater range. Thus, an alternative loading control was required to replace alpha tubulin as it is far too small for this type of gel. Vinculin is a loading control used specifically for high molecular weight proteins. However, its use in brain tissue is not well described in literature. To ensure the authenticity of our loading control, we also looked at total protein to compare. A minimum of three biological replicates were used for each time point, DPI 60 and/or 70, 90, 100, 110, 120, 130 and terminal.

i) High Molecular Weight Kininogen

High molecular weight kininogen (HMWK) protein levels between control and infected whole mouse brain remained unchanged right up to DPI 120 (**Figure 14**). However, late into the clinical stages of disease at DPI 130, we saw 5 out 6 infected mice expressing greater levels of HMWK than the average control. In fact, HMWK protein levels significantly increased by a 1.7 fold change in infected whole brain ($P<0.05$) (**Figure 15**). Then, at terminal stages of disease, levels dropped back down similar to the control.

ii) Low Molecular Weight Kininogen

Low molecular weight kininogen (LMWK) demonstrated a reverse effect. No change in LMWK protein levels was observed up until DPI 100 (**Figure 16**). At this stage in disease, protein levels began to decrease and continued to decrease at DPI 110 until statistical significance was observed at DPI 120 in infected whole brain ($P<0.001$) (**Figure 17**).

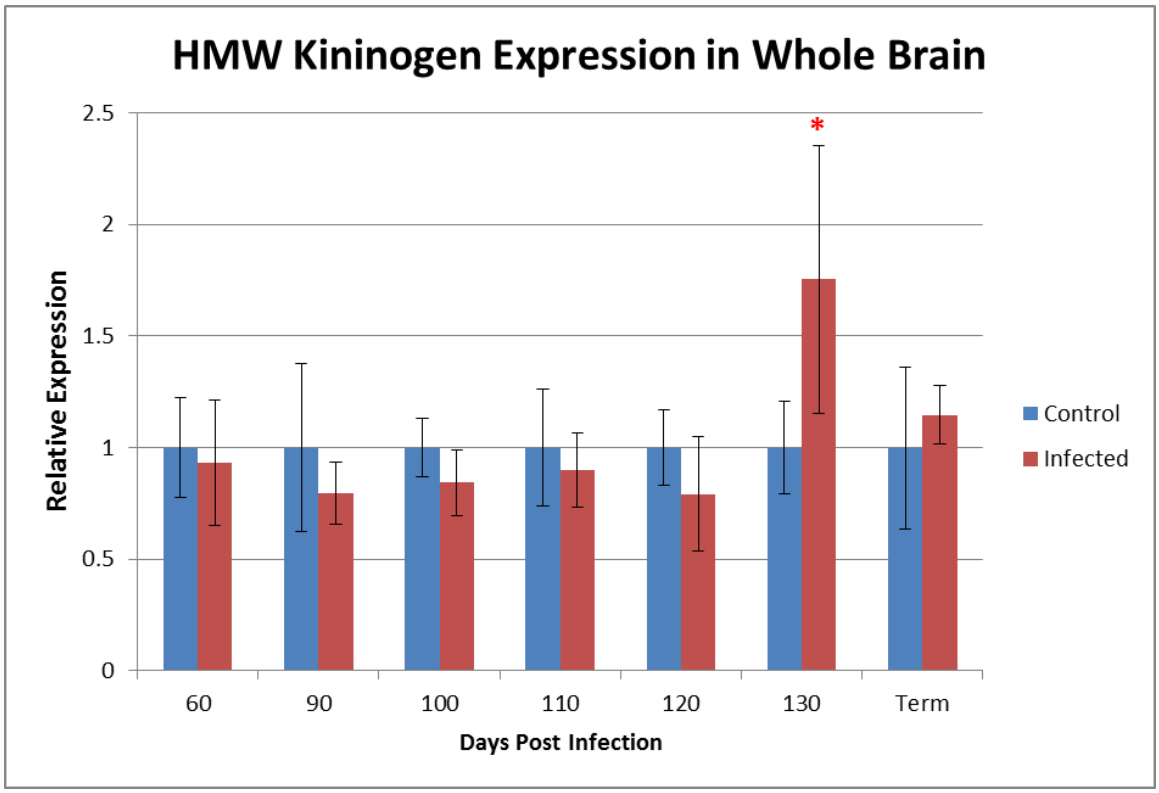

Figure 14: HMWK protein levels were measured in whole mouse brain of scrapie infected and age-matched controls by western blot. The results represent the average of a minimum of four biological replicates. Samples were normalized to α-tubulin loading control. A t-test was used to compare for statistical significance. There was no significant difference between control and infected brains for DPI 60, 90, 100, 110, 120 and Term. In scrapie infected mice, the level of HMWK was significantly increased at DPI 130 ($p = 0.016$) when compared to control mice. A red asterisk indicates statistical significance, error bars represent +/- SD and $N \geq 4$.

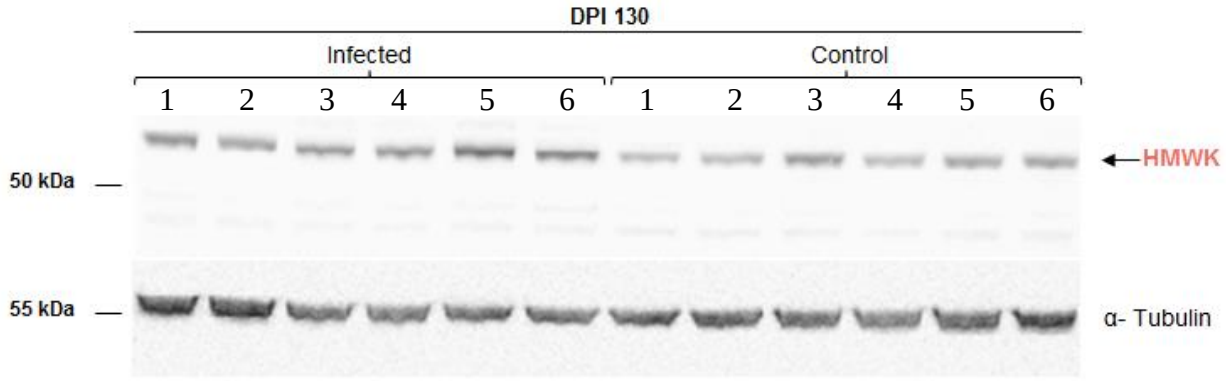

Figure 15: DPI 130 western blot image comparing HMWK protein expression in whole brain of scrapie infected and age-matched control mice. HMWK expression is increased in infected mice 1, 3, 4, 5 and 6. α-Tubulin has been used for the loading control.

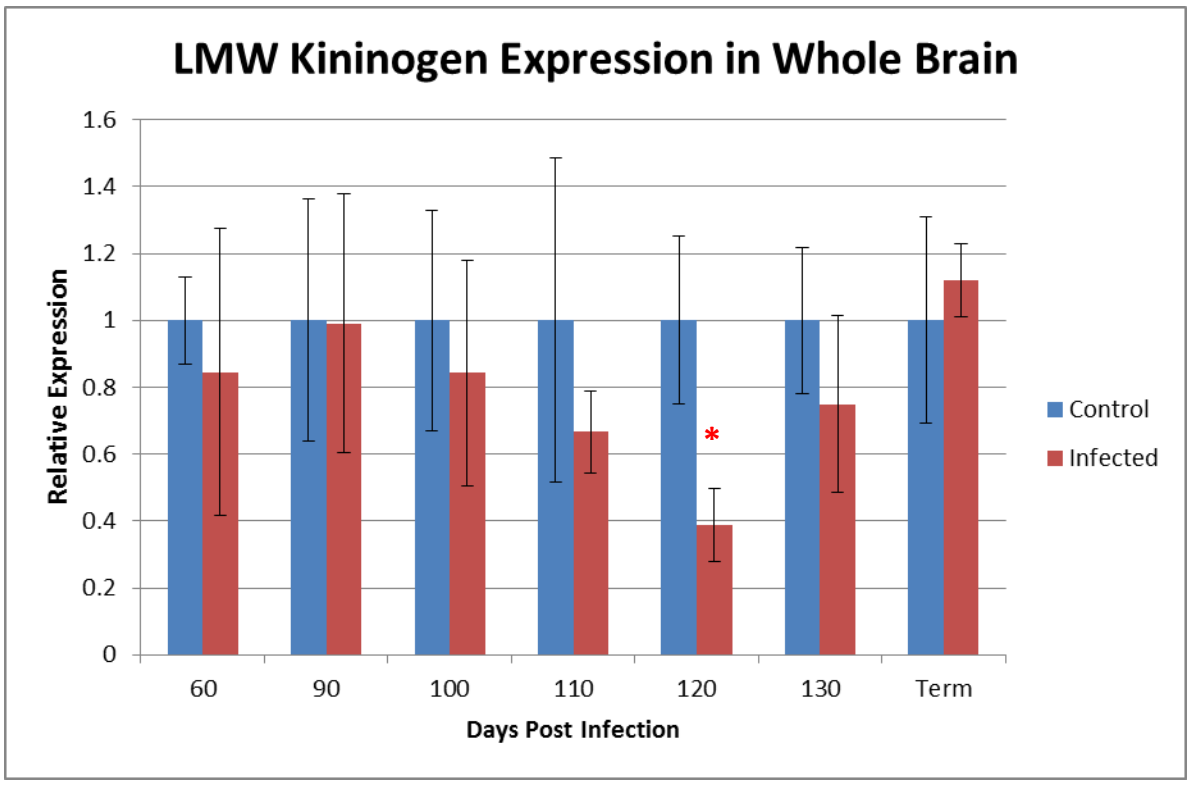

Figure 16: LMWK protein levels were measured in whole mouse brain of scrapie infected and age-matched controls by western blot. The results represent the average of a minimum of four biological replicates. Samples were normalized to α-tubulin loading control. A t-test was used to compare for statistical significance. There was no significant difference between control and infected brains for DPI 60, 90, 100, 110, 130 and Term. In scrapie infected mice, the level of LMWK was significantly decreased at DPI 120 ($p = 0.0003$) when compared to control mice. A red asterisk indicates statistical significance, error bars represent +/- SD and $N \geq 4$.

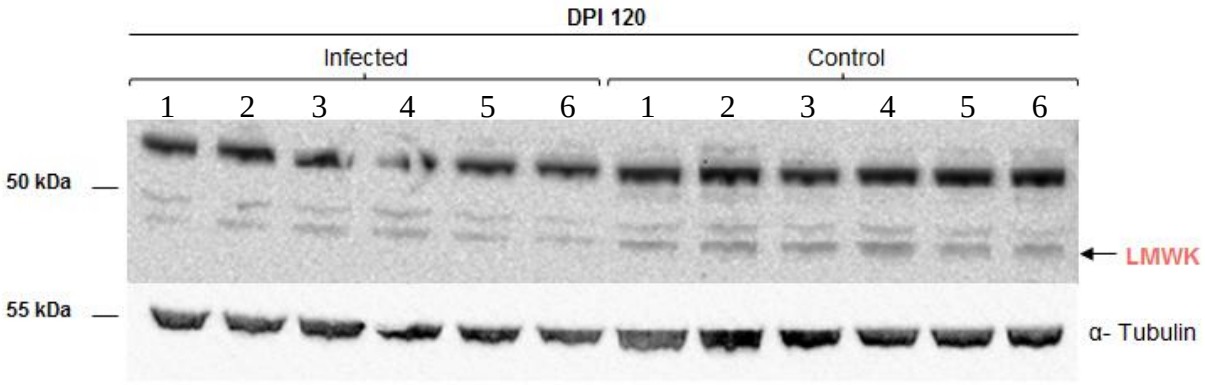

Figure 17: DPI 120 western blot image comparing LMWK protein expression in whole brain of scrapie infected and age-matched control mice. LMWK expression is decreased in infected mice 1-6. α-Tubulin has been used for the loading control.

At this point, 6 out 6 infected mice expressed lower levels of LMWK than the average control. At DPI 130, protein levels began to increase but still remained lower than the control. However, at the terminal stage, LMWK returned to similar expression levels as the control.

iii) Inducible Nitric Oxide Synthase

iNOS protein levels showed no change between control and infected whole brain at preclinical stages of disease (**Figure 18**). At DPI 90, we saw 6 out of 6 infected mice expressing greater levels of iNOS than the average control. This translated to a modest but statistically significant, 1.5 fold increase in infected whole brain ($P<0.01$) (**Figure 19**). This increase was consistent with both vinculin and total protein loading controls, ensuring authenticity. Ten days later, iNOS levels began to drop and then returned to preclinical levels by DPI 110. At DPI 120 we saw a slight elevation in iNOS expression only when normalized to total protein which continued to gradually increase linearly until terminal stages of disease for both vinculin and total protein normalised results (**Figure 20-21**).

iv) Glial Fibrillary Acidic Protein

GFAP protein levels showed no change in total brain between infected and control mice until about DPI 90 (**Figure 22**). At DPI 90, we began to see a 2.4 fold increase in GFAP production in infected mice. At DPI 100, GFAP levels spiked to a significant 20-fold increase in infected mice ($P<0.05$). At 110 days we continued to see a 19-fold increase ($P<0.05$) followed by a drop to a 6-fold increase at DPI 120 ($P<0.05$). Ten days later, we saw a 12-fold increase ($P<0.01$) in GFAP levels which continued to rise to an

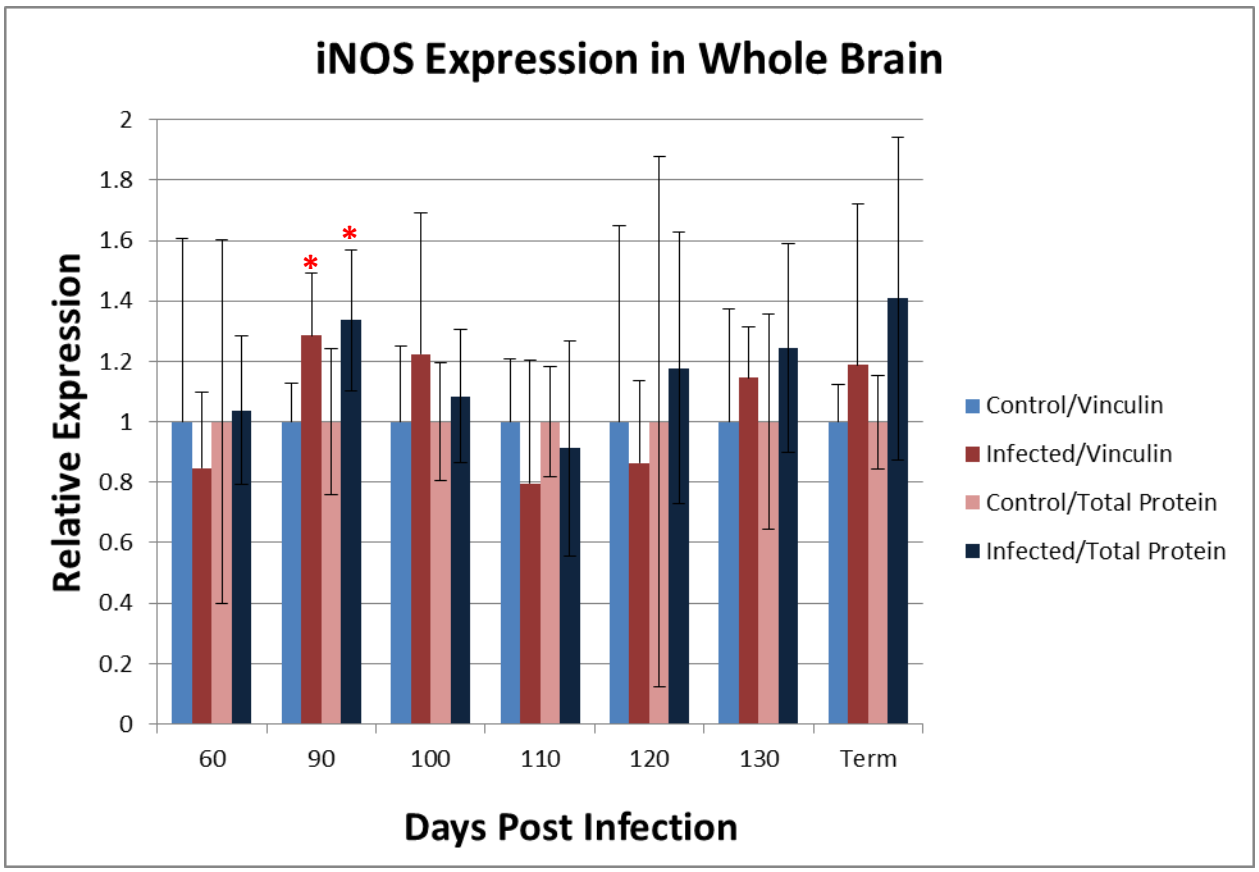

Figure 18: iNOS protein levels were measured in whole mouse brain of scrapie infected and age-matched controls by western blot. The results represent the average of a minimum of four biological replicates. Samples were normalized to vinculin and total protein loading controls. A t-test was used to compare for statistical significance. There was no significant difference between control and infected brains for DPI 60, 100, 110, 120, 130 and Term. In scrapie infected mice, the level of iNOS was significantly increased at DPI 90 ($p = 0.02$ vinculin and $p = 0.045$ total protein) when compared to control mice. An increasing trend in iNOS expression is observed at DPI 130 and Term when compared to both vinculin and total protein. A red asterisk indicates statistical significance, error bars represent +/- SD and $N \geq 4$.

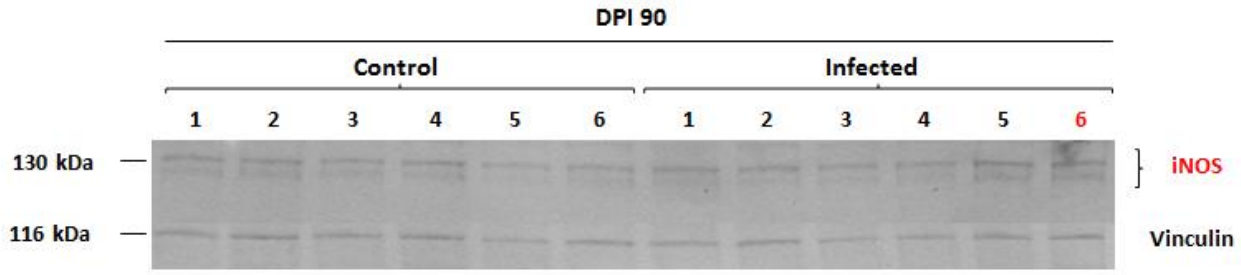

Figure 19: DPI 90 western blot image comparing iNOS protein expression in whole brain of scrapie infected and age-matched control mice. iNOS expression is increased in infected mice 1-6. However, mouse 6 denoted in red was omitted for average calculations due to the aberration on the membrane. Vinculin has been used for the loading control.

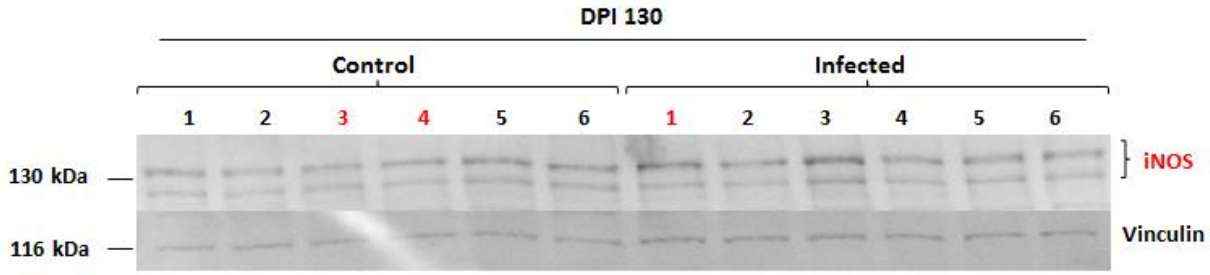

Figure 20: DPI 130 western blot image comparing iNOS protein expression in whole brain of scrapie infected and age-matched control mice. iNOS expression is increased in infected mice 2-6. Mice denoted in red, were omitted for average calculations due to aberrations on the membrane. Vinculin has been used for the loading control.

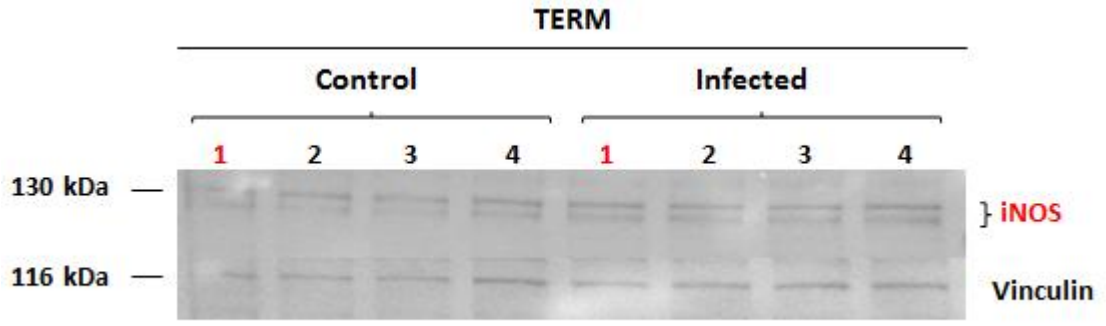

Figure 21: TERM western blot image comparing iNOS protein expression in whole brain of scrapie infected and age-matched control mice. iNOS expression is increased in infected mice 2 and 4. Mice denoted in red, were omitted for average calculations due to aberrations on the membrane. Vinculin has been used for the loading control.

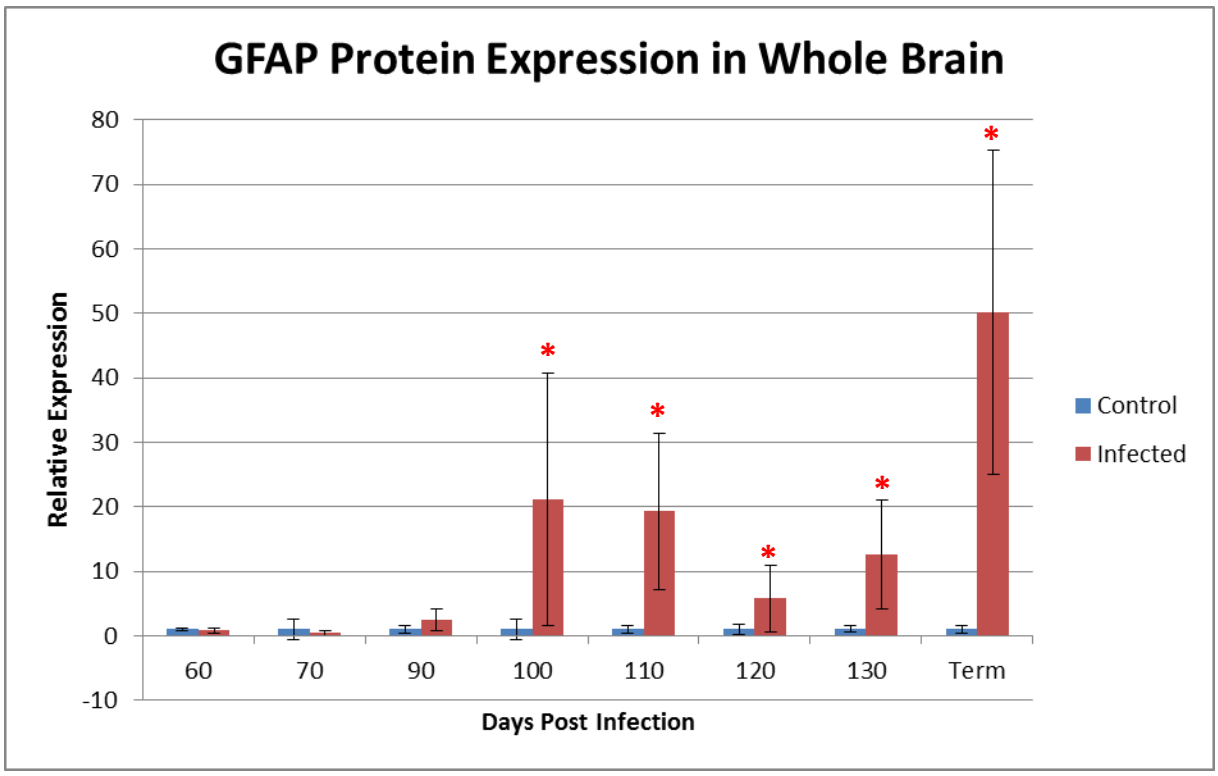

Figure 22: GFAP protein levels were measured in whole mouse brain of scrapie infected and age-matched controls by western blot. The results represent the average of a minimum of three biological replicates. Samples were normalized to α-tubulin loading control. A t-test was used to compare for statistical significance. There was no significant difference between control and infected brains for DPI 60, 70 and 90. In scrapie infected mice, the level of GFAP was significantly increased at DPI 100, 110, 120, 130 and Term ($p = 0.016$, $p = 0.011$, $p = 0.033$, $p = 0.003$ and $p = 0.021$respectively) when compared to control mice. A red asterisk indicates statistical significance, error bars represent +/- SD and $N \geq 3$.

impressive 50-fold increase at terminal stages of disease (P<.05) (**Figure 23**). Our analyses demonstrated a steady GFAP protein increase and therefore, a steady increase in activated astrocytes as prion disease progressed.

4. ELISA

8-OHdG levels showed no change in urine between infected and control mice until about DPI 91 (**Figure 24**). At DPI 91, we began to see a statistically significant increase of 130.7 ng/mL in 8-OHdG levels in infected urine ($p<0.05$). Two weeks later, at DPI 105, levels continued to increase to 192.4 ng/mL ($p<0.01$). After an additional two weeks, at DPI 119, levels continued to project linearly, increasing to 203.7 ng/mL ($p<0.001$). Our analyses indicated a steady increase in oxidative stress as prion disease progressed. When compared to the GFAP time line indicative of the inflammatory response during disease, we saw that both markers began to statistically increase at about the same time, approximately DPI 91-100 (**Figure 7**). This we denoted as the transitory stage separating the preclinical stages prior to DPI 90 and clinical stages of disease post DPI 100 in our prion disease mouse model.

5. Immunohistochemistry

Two inducible protein markers, iNOS and the B1 receptor, were examined by immunohistochemistry in coronal sliced, prion infected brains and their corresponding age-matched controls. Our preliminary data focused on the regions of the brain known to be heavily enriched with the misfolded prion protein [183]. This included the thalamus as well as the CA1, CA3, and dentate gyrus regions of the hippocampus. We looked at 3 time points, DPI 70, 100 and Term, ensuring to encompass the preclinical, transitory and

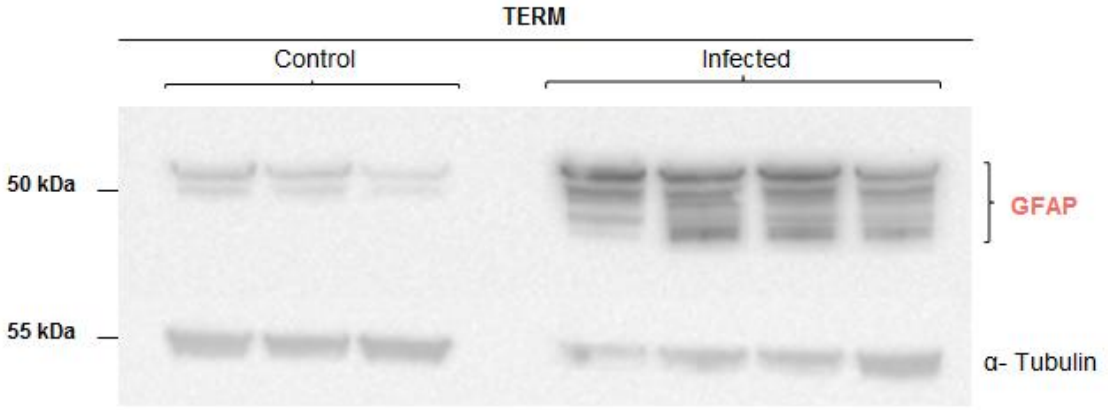

Figure 23: TERM western blot image comparing GFAP protein expression in whole brain of scrapie infected and age-matched control mice. GFAP expression is significantly increased in all infected mice. α-Tubulin has been used for the loading control.

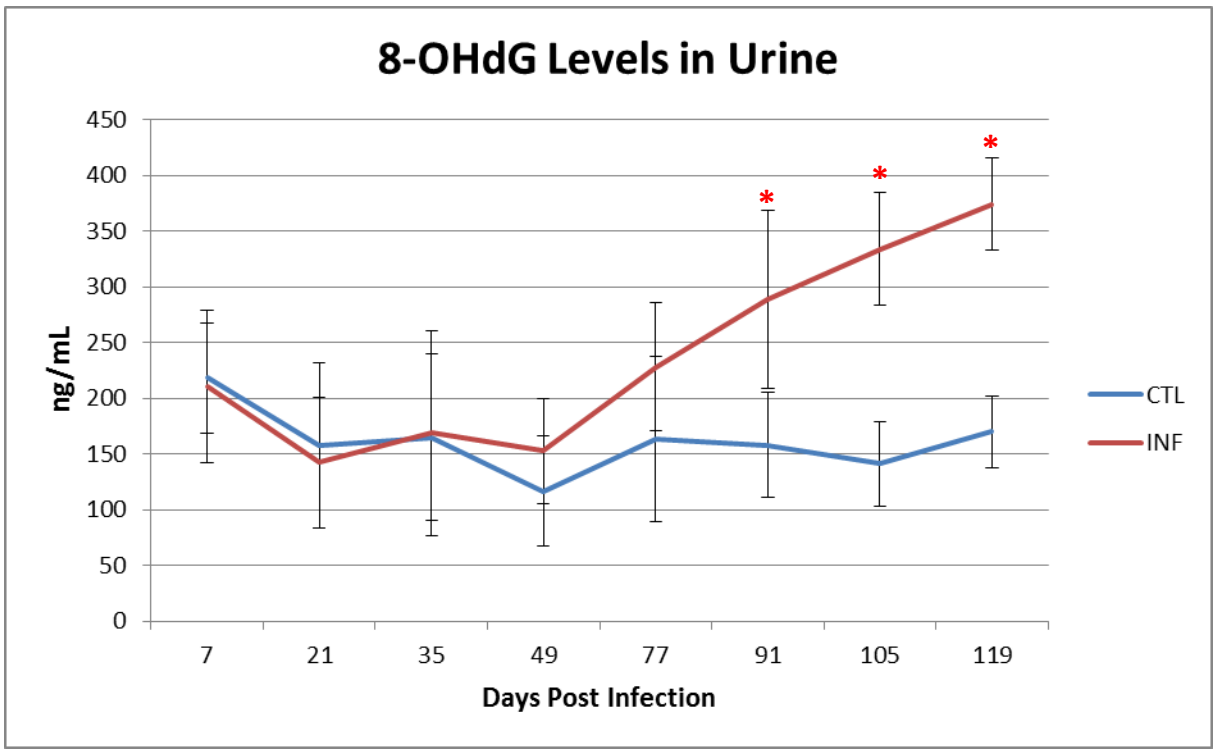

Figure 24: 8-OHdG levels were measured in urine from scrapie infected and age-matched control mice using the Enzo Life Sciences DNA Damage EIA kit. The results represent the average of 3-6 mice per time point. A t-test was used to compare for statistical significance. There was no significant difference between control and infected mice for DPI 7, 21, 35, 49 and 77. In scrapie infected mice, the level of 8-OHdG was significantly increased at DPI 91, 105 and 119 ($p = 0.03$, $p = 0.002$ and $p = 0.0002$ respectively) when compared to the control mice. A red asterisk indicates statistical significance, error bars represent +/- SD and $N \geq 3$.

clinical stages of disease. Total positive cell counts consisted of 4-6 images per region taken at 50x magnification unless otherwise noted. Due to the scarcity and quality of samples, only 1-2 mice were examined per condition (**Appendix 5-6**).

i) iNOS Expression Levels

a) CA1 Region of the Hippocampus

Total iNOS protein levels in the infected CA1 region were increased as early as DPI 70 (**Figure 25**). We saw an increase in expression by 9.7% when compared to the control. At DPI 100, although one control mouse appeared to be expressing an abnormally high quantity of iNOS, there was still an increase of 13.8% observed in the infected brain. At terminal stages of disease, we saw similar levels in both infected and control brains, however, only one infected mouse was analyzed for this region. Upon cross reference with the Allen Mouse Brain Atlas available online, we determined that the CA1 region was not present in our second mouse staining. This particular cross section was taken on the beginning cusp of the hippocampus structure thus, missing the CA1 region. Nevertheless, when we examined the CA1 region across disease progression, we saw that the staining of the positive cells became significantly darker by terminal stages (**Figure 26**). Although total positive cell count may be similar between control and infected brains at terminal stages, our immunohistological staining suggested that significantly more iNOS protein was being produced within cells of infected brains.

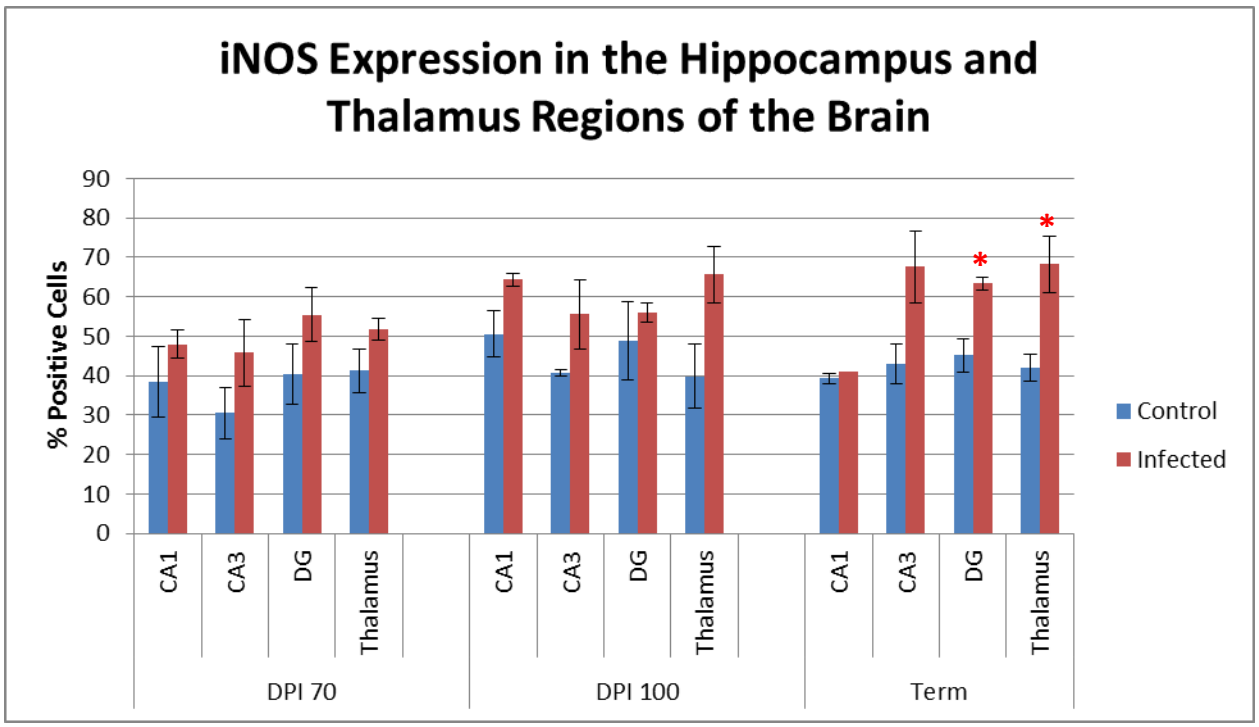

Figure 25: Total iNOS protein expression was measured in the hippocampus and thalamus regions of the brain in control and scrapie infected mice at time points DPI 70, 100 and term. iNOS expression is represented as a positive cell count percentage based on a total of six images taken randomly in each specified region of the brain. The graphed results are an average of two biological replicates with the exception of data point, infected CA1 term. Overall, an increasing trend in iNOS expression is observed as disease progresses with statistically significant increases observed in the dentate gyrus and thalamus at terminal stages of disease ($p<0.05$). A red asterisk indicates statistical significance, error bars represent +/- SD and N=2.

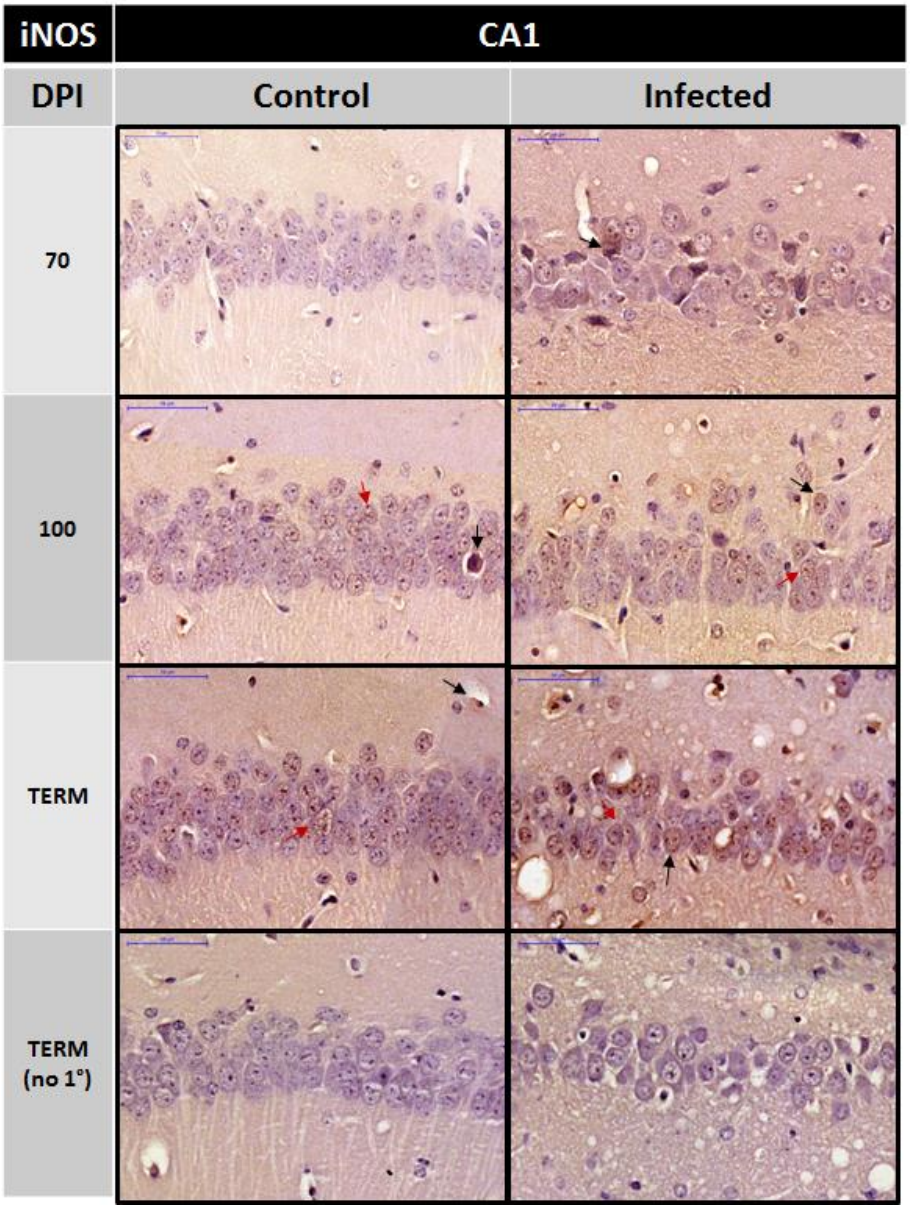

Figure 26: Total iNOS protein expression was measured in the CA1 region of the hippocampus in scrapie and control mice at time points DPI 70, 100 and term. Images are taken at 50x magnification. Black arrows indicate an example of a strong positive signal and red arrows indicate a weaker positive signal. In general, as disease progresses, as evidenced by the increased vacuolation, cells become a darker brown suggesting an increase in signalling intensity within cells. A negative control denoted as "no 1°" is provided in the bottom panels taken at terminal stages of disease.

b) CA3 Region of the Hippocampus

Total iNOS protein levels in the infected CA3 region were increased as early as DPI 70 (**Figure 25**). We saw an increase in expression by 15.3% when compared to the control. At DPI 100, expression was maintained at a 14.9% increase in the infected brain. However, at terminal stages of disease, iNOS expression approached significant levels with an observed 24.6% increase in infected brain. Overall, a gradual increasing trend was observed in this region as prion disease progressed. Additionally, the staining of the positive cells became significantly darker at terminal stages suggesting that significantly more iNOS protein was being produced within cells of infected brains (**Figure 27**).

c) DG Region of the Hippocampus

Total iNOS protein levels in the infected DG region also increased as early as DPI 70 (**Figure 25**). We saw an increase in expression by 14.9% when compared to the control. At DPI 100, the same control mouse as described in the CA1 region, elicited an abnormally high level of iNOS in the DG region, thus only a 7.1% increase in expression was observed in the infected brain. However, at terminal stages of disease, we saw a statistically significant increase by 18.3% of iNOS expression in infected brain ($p<0.05$). Complementing these findings was the significantly darker staining of the positive cells in the infected brains, indicating that more iNOS was being produced within cells as well (**Figure 28**). Overall, a gradual increasing slope in iNOS expression was observed in this region as prion disease progressed.

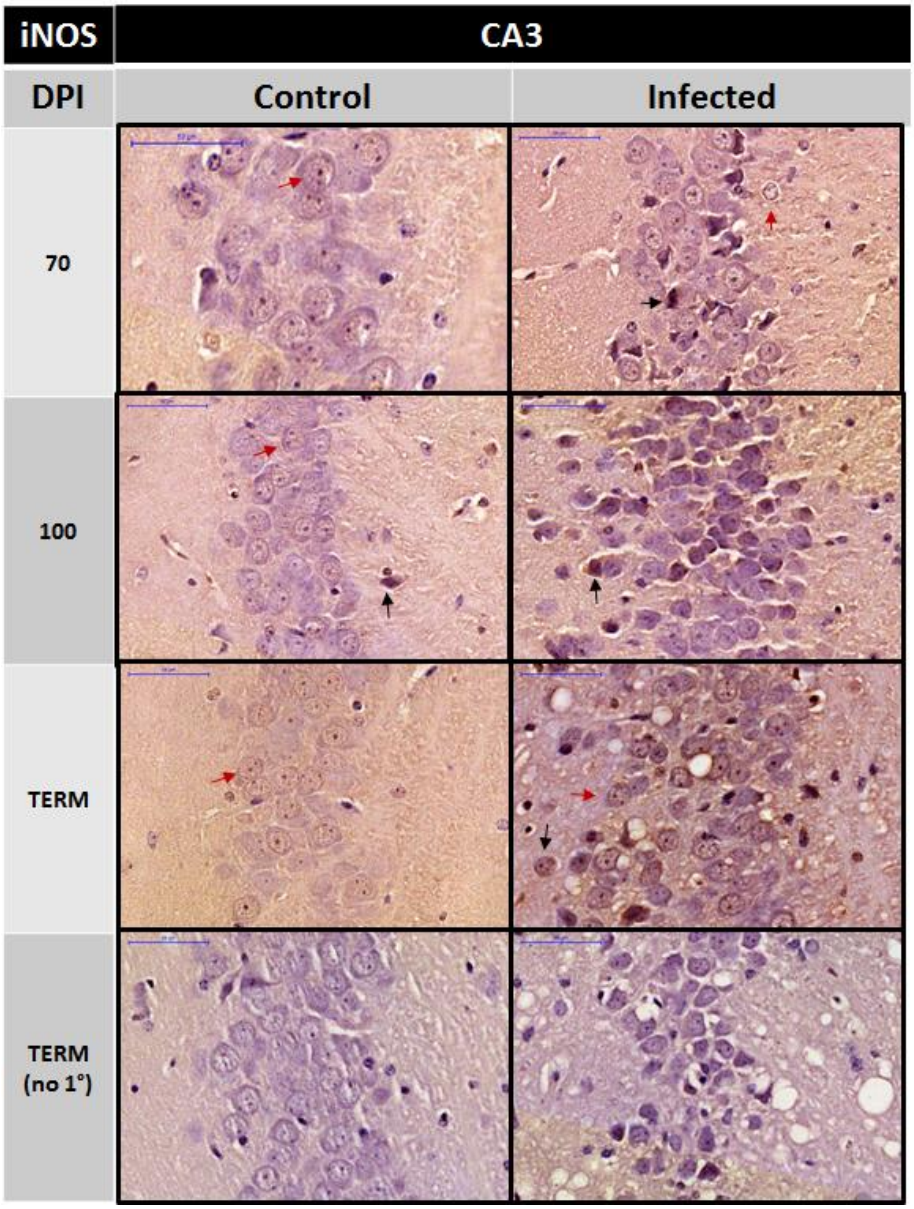

Figure 27: Total iNOS protein expression was measured in the CA3 region of the hippocampus in scrapie and control mice at time points DPI 70, 100 and term. Images are taken at 50x magnification. Black arrows indicate an example of a strong positive signal and red arrows indicate a weaker positive signal. In general, as disease progresses, as evidenced by the increased vacuolation, cells become a darker brown suggesting an increase in signalling intensity within cells. A negative control denoted as "no 1°" is provided in the bottom panels taken at terminal stages of disease.

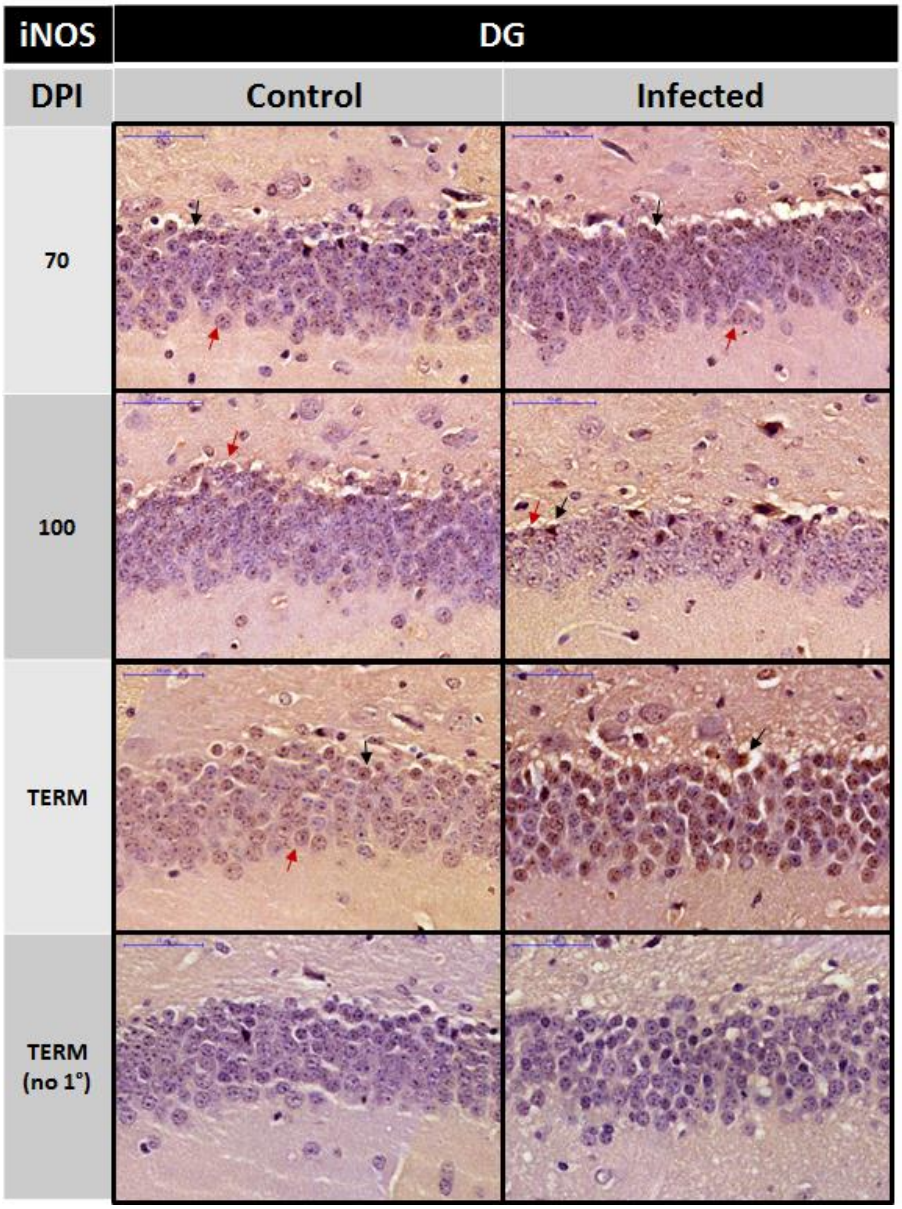

Figure 28: Total iNOS protein expression was measured in the dentate gyrus region of the hippocampus in scrapie and control mice at time points DPI 70, 100 and term. Images are taken at 70x magnification. Black arrows indicate an example of a strong positive signal and red arrows indicate a weaker positive signal. In general, as disease progresses, as evidenced by the increased vacuolation, cells become a darker brown suggesting an increase in signalling intensity within cells. A negative control denoted as "no 1°" is provided in the bottom panels taken at terminal stages of disease.

d) Thalamus Region of the Brain

Total iNOS protein levels in the infected thalamus region were increased as early as DPI 70 (**Figure 25**). We saw an increase in expression by 10.6% when compared to the control. At DPI 100, there was a 25.8% increase in expression in the infected brain. By terminal stages of disease, we saw a statistically significant increase in expression by 26.2% in infected brain ($p<0.05$). Further complementing these findings was the significantly darker staining of the positive cells in the infected brains, suggesting that more iNOS was being produced within cells (**Figure 29**). Overall, a gradual increasing slope in iNOS expression was observed in this region as prion disease progressed.

ii) B1 Receptor Expression Levels

We examined the same time course and brain regions for B1 receptor protein as in the iNOS histology. We did not observe any change in B1 receptor expression in the pre-clinical and early clinical stages of prion disease, DPI 70 and 100 respectively. However, at terminal stages of disease, we saw substantial up regulation of the B1 receptor both in the hippocampus and thalamus regions of the brain (**Figure 30**).

a) CA1 and DG Regions of the Hippocampus

Unfortunately, both infected, coronal brain sections obtained from two different mice did not appear to contain the CA1 region when cross referenced with the Allen Mouse Brain Atlas. This was due to a cross section made on the beginning cusp of the hippocampus structure. Furthermore, due to the smaller section of the hippocampus, the dentate gyrus region was also hindered in the process. Although present, it was

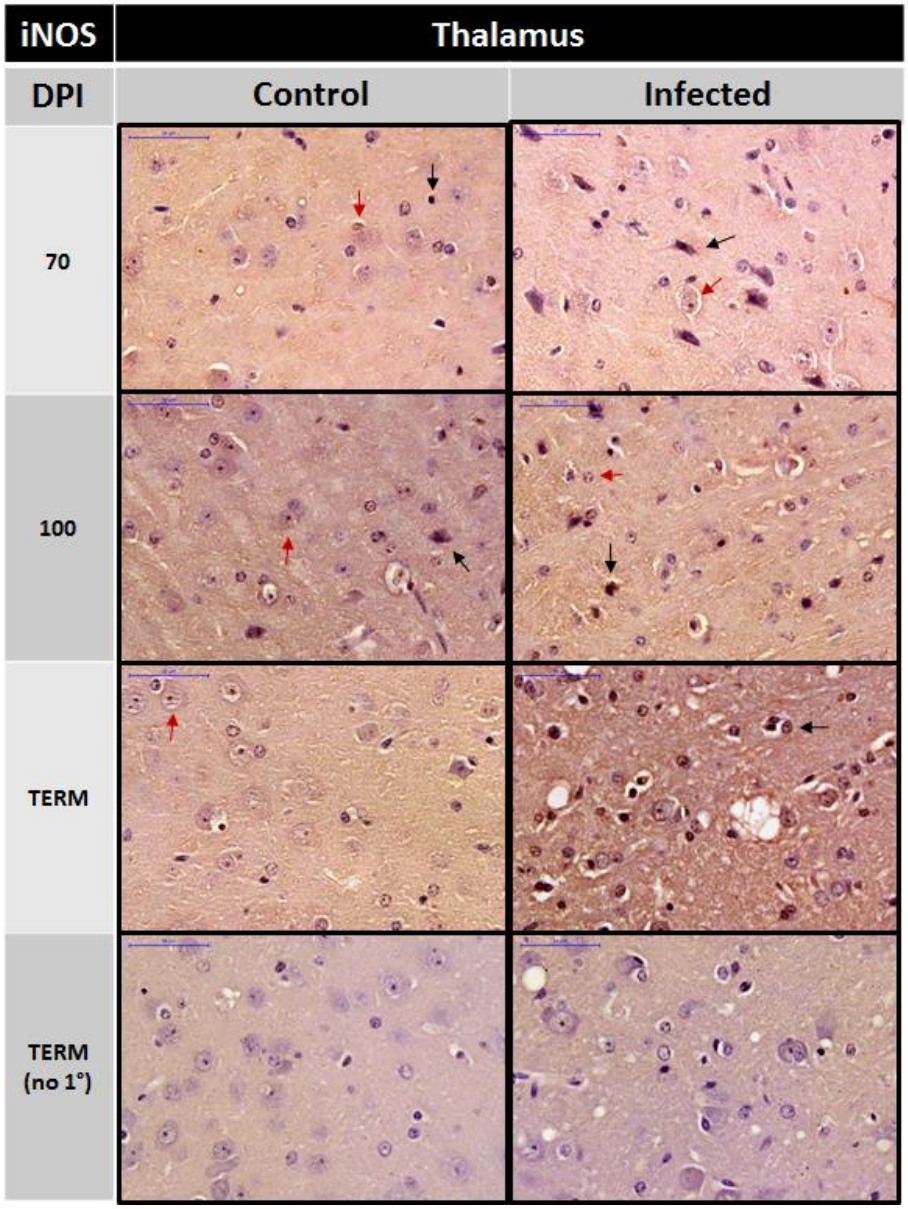

Figure 29: Total iNOS protein expression was measured in the thalamus region of scrapie and control mice at time points DPI 70, 100 and term. Images are taken at 50x magnification. Black arrows indicate an example of a strong positive signal and red arrows indicate a weaker positive signal. In general, as disease progresses, as evidenced by the increased vacuolation, cells become a darker brown suggesting an increase in signalling intensity within cells. A negative control denoted as “no 1°” is provided in the bottom panels taken at terminal stages of disease.

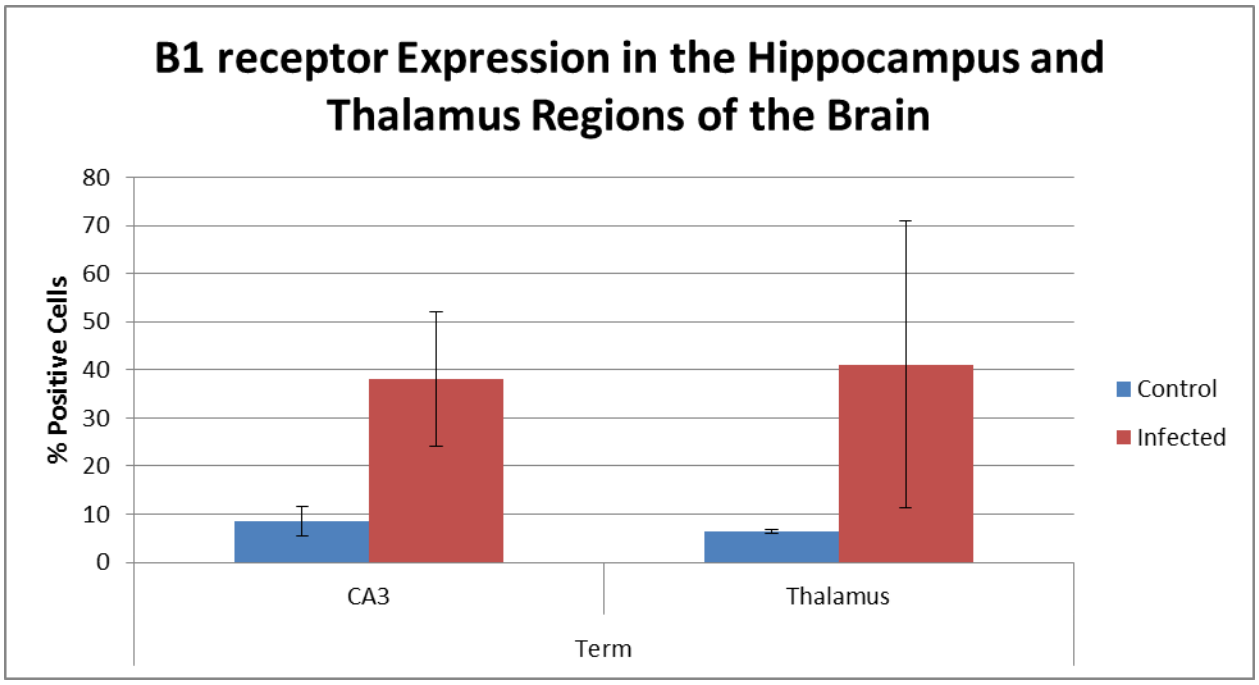

Figure 30: Expression of B1 receptor protein was measured in the hippocampus and thalamus regions of the brain in control and scrapie infected mice at terminal stages of disease. B1 expression is represented as a positive cell count percentage based on a total of six images taken in each specified region of the brain. The graphed results are an average of two biological replicates. Error bars represent +/- SD and N=2.

much smaller when compared to the control sections, making it difficult to accurately compare any changes. One of our control brain sections also tore along the left DG region of the brain resulting in a count based on only the right hemisphere of the brain. However, overall, we could detect upregulation of the B1 receptor in this region although it was only apparent in one mouse (**Figure 31**) (**Appendix 6**).

b) CA3 Region of the Hippocampus and Thalamus

At terminal stages of disease, B1 receptor protein was substantially elevated in the CA3 region of the hippocampus and thalamus region of infected brains (**Figure 32-33**). We saw an average 29.5% increase in expression in the CA3 region and a 34.6% increase in the thalamus when compared to the control (**Figure 30**). A high degree of variability between mice was evident which was similar to what we observed at the transcriptional level.

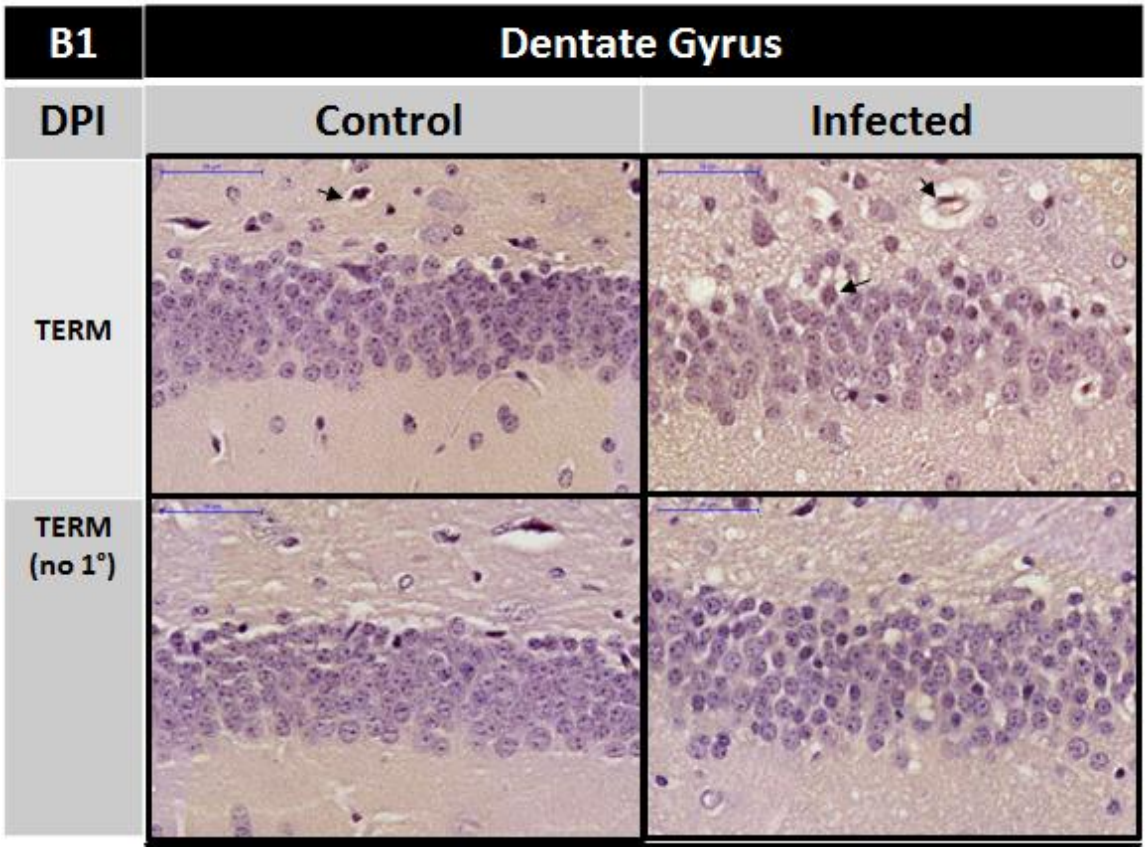

Figure 31: Expression of B1 receptor protein was measured in the DG region of the hippocampus in scrapie and control mice at terminal stages of the disease. Images are taken at 70x magnification. Black arrows indicate an example of a positive signal. A negative control denoted as “no 1°” is provided in the bottom panels taken at terminal stages of disease.

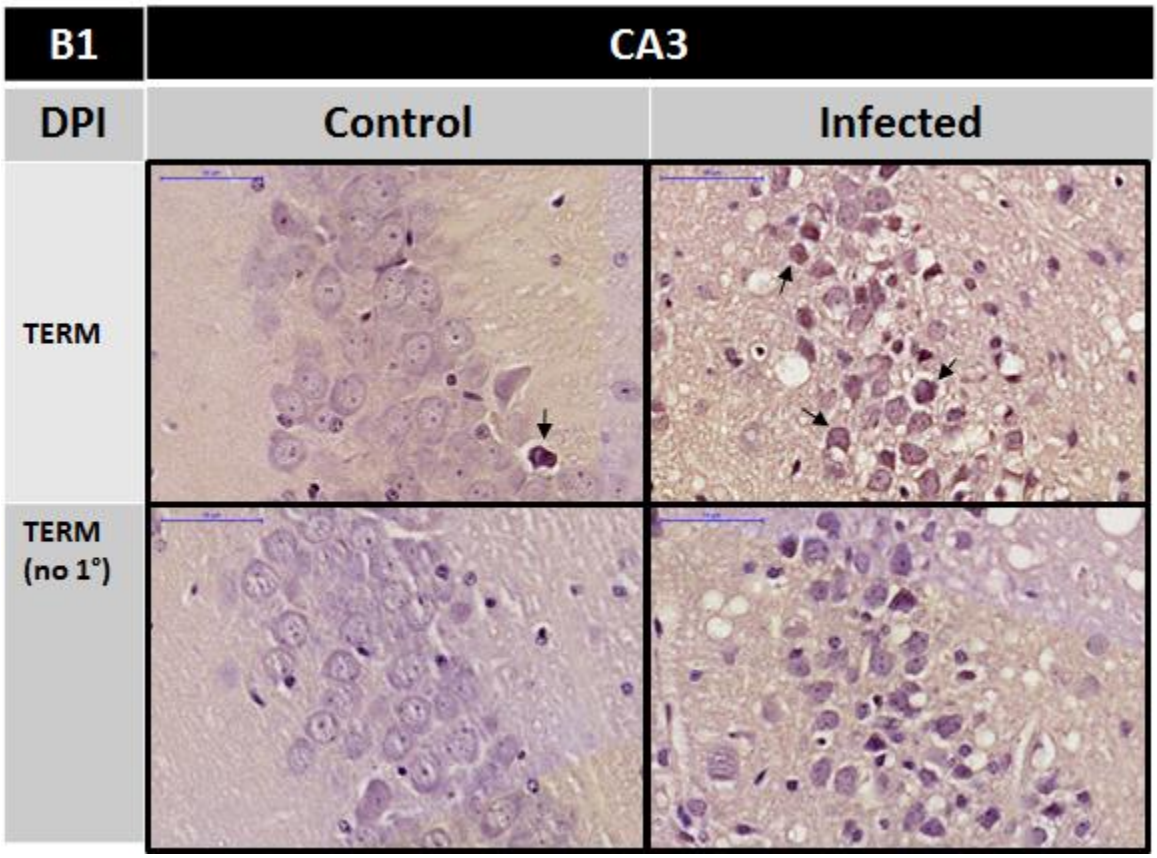

Figure 32: Expression of B1 receptor protein was measured in the CA3 region of the hippocampus of scrapie and control mice at terminal stages of the disease. Images are taken at 50x magnification. Black arrows indicate an example of a positive signal. A negative control denoted as “no 1°” is provided in the bottom panels taken at terminal stages of disease.

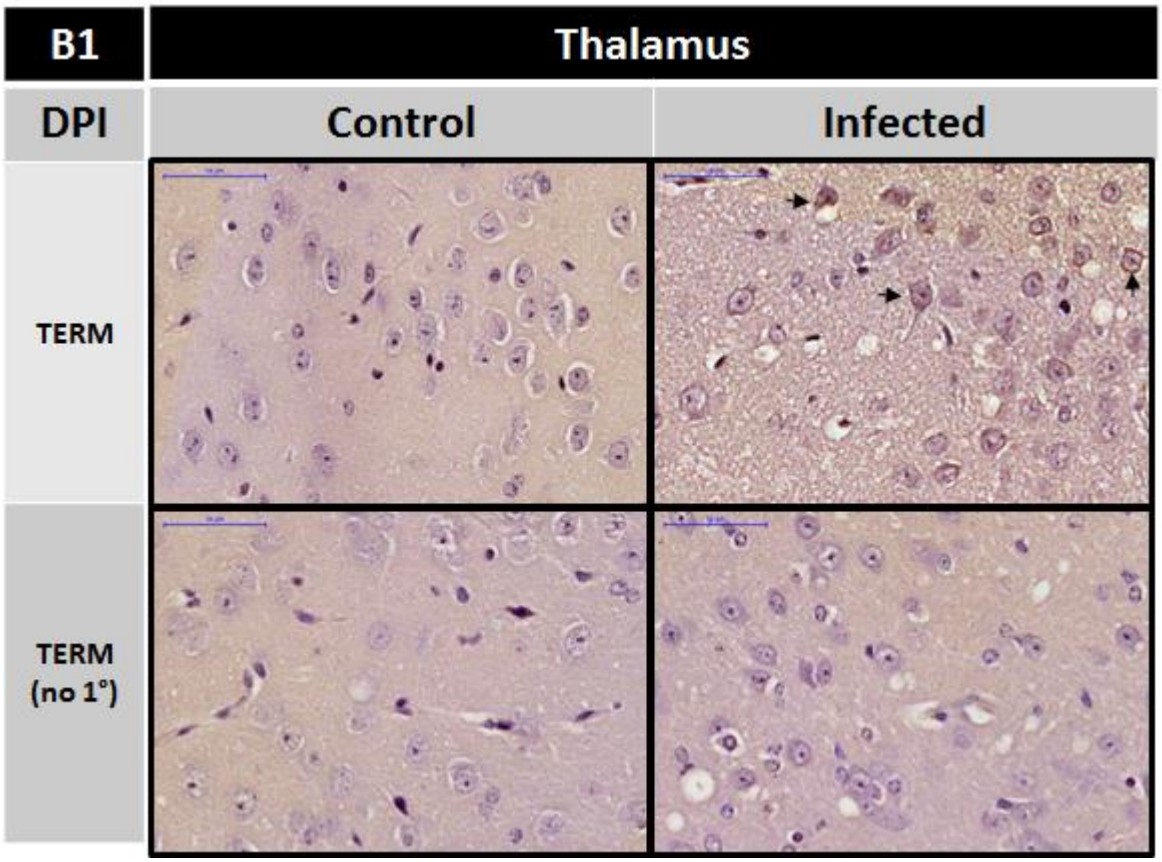

Figure 33: Expression of B1 receptor protein was measured in the thalamus of scrapie and control mice at terminal stages of the disease. Images are taken at 50x magnification. Black arrows indicate an example of a positive signal. A negative control denoted as “no 1°” is provided in the bottom panels taken at terminal stages of disease.

D. Discussion

1. Glial Cell Activation and Oxidative Stress

It has been repeatedly confirmed that prion protein deposition correlates with glial cell activation and oxidative stress [92, 93]. We looked at two markers of these processes to define a timeline of disease in our scrapie mouse model. 8-OHdG levels were measured in the urine to determine the degree of prion-induced oxidative damage. GFAP protein expression was examined to monitor gliosis progression in the brain. Once disease progression is defined in our model, we can begin to look at where the kinin-kallikrein pathway initiates its role in prion disease.

i) Levels of 8-OHdG

8-OHdG is an oxidized and very stable nucleoside produced as a result of ROS damage to nuclear and mitochondrial DNA. It is excised during repair and excreted in urine [178]. Other groups have looked at 8-OHdG staining directly in infected brain tissue, however, our lab has determined 8-OHdG to be a highly sensitive urinary marker of prion-induced oxidative stress [110, 174].

In our study, there was no change in 8-OHdG levels in the early stages of disease as expected. However, at 91 days post infection, we see a statistically significant increase in nucleoside levels which continue to linearly increase until terminal stages of disease. This evidence is supported by our previously published data which revealed significant 8-OHdG levels beginning at 98 days post infection [174]. This is indicative of the consistency that is obtained in our ME7 prion strain mouse model. Furthermore, the

results are also consistent with how we perceive prion pathology. We begin with the incubation phase where misfolded prion protein increases as a proportion of total prion protein. Aggregates continue spreading through various regions of the brain [82]. Microglial cells recognize misfolded prion protein and become activated. As new deposits spread, newly stimulated neurons and glial cells also recruit more microglial cells [168]. Microglial cells are one of the major inducers of oxidative damage, in this case, oxidative damage to cellular DNA. Instinctively, the damaged host cell triggers DNA repair machinery to excise the toxic nucleotide [178]. Our urinary analysis reflects this balance between amplifying damage and corresponding DNA repair.

ii) Levels of Glial Fibrillary Acidic Protein

Our GFAP analysis shows no change in protein levels in total brain between infected and control mice until approximately 100 days post infection. At 100 days post infection, GFAP levels spike to a 20-fold increase in infected mice. This statistically significant increase is maintained until terminal stages of disease, with a final 50-fold increase of GFAP protein in whole brain. There is a visible drop in expression levels at days 120 and 130 when compared to days 100 and 110. This may be explained by natural biological variation. Every time point consists of a different set of mice. Thus, a mouse which may develop disease at a slightly slower/ faster rate than the others may hinder the overall, smooth transition across time points. Nevertheless, the trend evidently increases and is highly significant as disease progresses with time.

An overwhelming amount of evidence is available on the up-regulation of GFAP in prion disease. This phenomenon has been extensively characterized across multiple strains

and animal models [90, 179]. However, our data does complement other studies that have used the same prion strain, animal model and general time points. GFAP staining was carried out in infected mouse brain and was initially detected to be increased by 104 days post infection [180]. Our results are again indicative of the consistency observed in our ME7 mouse model and the consistency observed with prion disease progression. As misfolded prion protein continues to propagate and spread through the brain, more recruitment and stimulation of astrocytes is observed.

iii) The Correlation between Gliosis and Oxidative Stress

Oxidative Stress and astrogliosis are key characteristics of prion disease. 8-OHdG and GFAP appear to provide a measure of disease progression. By overlapping data (**Figure 7**), we can begin to see the progression of disease over the course of a mouse's life span and define the different stages. Oxidative stress increase is observed first at 91 days post infection followed by astrogliosis nine days later. Unfortunately, we were not able to coordinate urine and brain collections at the same time point, but it is fair to say that these changes are occurring at approximately the same time. Mis-folded prion protein is detected as early as 30-40 days post infection [181, 182]. Naturally, time is required for the misfolded prion protein to amplify and spread throughout the brain. Tribouillard-Tanviet and colleagues revealed only 0.1% of PrP^{res} at 40 days post infection when compared to total amounts at terminal stages of disease. These levels only increased to 10% by 100 days post infection. This gradual accumulation of PrP^{sc} at the initial stages of the disease reflects the timing associated with glial cell activation during disease and as a result, our inflammatory and oxidative stress analysis. This particular study confirms that any

detectable changes between control and infected profiles in whole brain will not likely occur before 90-100 days post infection.

Our laboratory has also previously shown that these inflammatory and oxidative stress changes precede the appearance of overt clinical signs [174]. Nonetheless, based upon our molecular markers of disease, we have defined 90-100 days post infection as a transitory period between preclinical and clinical stages of disease (**Figure 7**). Changes observed prior to 90 days post infection fall under the preclinical stages of disease whereas changes observed after 100 days post infection are defined to occur at the clinical stage. Using this as our framework we have examined where changes in our target genes and proteins occur with respect to disease progression.

2. The Detection of Kininogens in Brain Tissue

i) High Molecular Weight Kininogen

Similar to Alzheimer's, we believe the inflammatory molecules evident in prion disease are sufficient to initiate the kinin-kallikrein pathway. Thus, we began our study by looking at the key protein we identified in infected mouse urine in an earlier study, kininogen [133]. Our Western blot analysis reveals that high molecular weight kininogen protein significantly increases in the brain of scrapie infected mice at 130 days post infection. This is followed by a drop to control levels at terminal stages of disease. This observation would suggest that this decline in kininogen levels is probably due to its excretion into the urinary system [133].

Although our data shows only a very modest 2.4 fold increase of high molecular weight kininogen, it is critical to note that we examined protein expression in whole brain.

Prion protein deposition is not equally distributed throughout the brain particularly at the initial amplifying stages of disease [183]. Thus, the areas devoid of prion pathology will dull or mask the highly localized changes in the affected regions and only present as slight overall differences. This 'masking' phenomenon will be referred to on several occasions throughout this discussion.

Despite the caveat for insensitivity to localized changes, the ability to detect significant HMWK differences in the entire brain, suggests an impressive modification to the kinin-kallikrein pathway during prion pathology. By increasing available kinin precursor substrate in tissue, the likelier kallikrein will cleave kininogen to release bradykinin and further promote an inflammatory response. However, to further support the suggested activation of the kinin-kallikrein pathway, we looked for the expression of genes and protein deeper into the pathway to confirm its activation and role.

ii) Low Molecular Weight Kininogen

In addition to HMWK, we also looked at low molecular weight kininogen (LMWK) expression in total brain of prion infected mice and their age matched controls. What we found was a steady decrease in LMWK at the onset of clinical disease that became statistically significant at 120 days post infection. This evidence further complements the increase of HMWK seen 10 days later at 130 days post infection. Since HMWK and LMWK are splice variants of the same gene, it is not surprising for the transcription machinery to slow production of one variant and focus production on the dominant kininogen, in this case, HMWK. At 130 days post infection, LMWK expression was shown

to slightly increase but continues to remain below the expression levels of the control mice.

At this time it is unknown why there may be a selection for HMWK as oppose to LMWK. Plasma kallikrein typically cleaves HMWK and it has been shown to be increased in the brain during Alzheimer's disease [184]. In contrast, tissue kallikrein has been shown to preferentially cleave LMWK but it can also act on HMWK [138]. LMWK releases kallidin which can be further cleaved into bradykinin if membrane-bound or soluble plasma carboxypeptidases are present. However, HMWK directly releases bradykinin and this preferential production of HMWK may promote the observed microglial migration to the site of insult due to bradykinin's chemoattractant capabilities [148].

iii) Literature validity of our kininogen findings

Most studies have solely focused on HMWK and therefore this variant is better defined than the alternatively spliced product, LMWK. One reason for the lack of specific data may be due to its very low abundance in many tissues, including the brain [185]. Our data are supported through this notion as LMWK in whole brain visually expressed a significantly lower abundance than when compared to HMWK (**Appendix 2**). Furthermore, the evidence is consistent with literature findings where both HMWK1 and HMWK2 genes are highly expressed in mouse brain and only LMWK1 gene is found to be weakly expressed by RT-PCR [185].

3. The Detection of the B1 Receptor in Brain Tissue

The B1 receptor has been identified to be an inducible receptor specific to the kinin-kallikrein pathway [136, 140]. If we could detect its presence in prion infected mice, it would

suggest activation and involvement of the kinin-kallikrein pathway in prion disease. Due to its inducible nature a delay in expression relevant to disease progression was expected and indeed that is what we were able to confirm.

i) Transcriptional levels of the B1 receptor

We examined BDKRB1 gene expression in whole mouse brain through the course of prion disease. During the early stages of disease, in general, there is no change between healthy and infected mice. However, there are a few statistically significant decreases in expression apparent according to one-way ANOVA analysis. These changes between control and infected mice are minimal considering the physiological environment and inconsistency between housekeeping genes.

Moving towards the clinical stages of disease, we begin to see statistically significant increases in select mice beginning at 120 days post infection. Ten days later, more mice are eliciting an increase and at much more significant levels. Although there is some biological variation, this observation is consistent with all three housekeeping genes providing strong evidence that changes in B1 receptor expression can be observed in whole brain.

We do observe that at the terminal time point mRNA expression abruptly subsides. This could be explained by a general loss in gene regulation at terminal stages of disease. We would expect a diverse and complex gene expression profile with various signalling pathways firing in a cascading manner, to try and save the organ. Therefore too much noise would be present for any analyses to produce data specifically related to the disease.

Nevertheless, it is clear that a trend of increased B1 receptor mRNA levels is evident during the clinical stages of disease. These data indicate both that the BDKRB1 gene is expressed in the diseased murine brain and possibly, undergoes further induction during prion disease. This suggests a functional role of the kallikrein-kinin system in prion pathology.

ii) Literature validity of our B1 receptor findings

Very little is documented regarding mRNA levels of the B1 receptor over a progressive, neurodegenerative time course. Studies in the Alzheimer's rodent model, are typically carried out at the translational level. However, using our specific mouse model, one study of focal cerebral ischemia demonstrated that transient middle cerebral artery occlusion stimulated increased transcription of the BDKRB1 gene. Interestingly, the mice that do elicit a significant increase in our study reveal levels of B1 receptor mRNA comparable to the expression profile seen in a study carried out by Austinat and collegues [156]. This group, however, examined the basal ganglia area of the brain within 24 hours where as we observed a correspondingly lower signal in whole brain but in a span of 10 days.

It seems that by sampling the entire brain, we dampen the signal for any localized changes that may be occurring in specific areas of the brain. In the case of Alzheimer's, one study saw an increase in B1 receptors only in the ventral hippocampal commissure, fimbria, CA1 and CA3 hippocampal areas as well as the habenular nuclei and optical tract [186]. These are very specific and tiny structures in the center of the brain, making up no more than 20.2% of total whole brain volume [187]. If a similar and specific expression

profile is present during prion disease, than up to 80% of the surrounding brain tissue would be mere background noise. This particular Alzheimer's study, was carried out at the protein level and therefore strongly suggests that we should take a more localized and translational level approach to see if there are indeed changes occurring in the brain with respect to the B1 receptor.

iii) Translational levels of the B1 receptor

The next question we addressed was whether we could detect the B1 receptor at the protein level. To answer this question we initially began with a series of western blots using total, whole brain protein extracts. We tested various conditions with multiple antibodies as well as multiple pre-treatment assays including glycosylation treatment, competition assays and immunoprecipitation protocols to obtain B1 receptor banding (**Appendix 3-4**). Unfortunately we were not successful due to high backgrounds of non–specific binding and what we believe is over saturation of protein from whole brain. Thus, we opted for an alternative, in situ method to determine if the B1 receptor protein is induced during prion disease.

We examined the global cell population of the brain to determine if we could first obtain a positive signal for expression using immunohistochemistry. Our preliminary data for B1 receptor expression reveals that it is induced in prion disease. However, it was not detected until the terminal stages through our immunohistochemistry analysis. These findings are consistent with our real-time PCR data where we noticeably see an increase in BDKR1 gene expression at 130 days post infection. Thus, for protein expression, we would expect to detect protein after 130 days.

We see a positive signal specifically in the hippocampus and thalamus regions of the brain. These regions are known to be enriched with deposition of the misfolded prion protein particularly when infected with the ME7 prion strain [183] and thus have been selected for analysis. Both mice examined displayed increased B1 receptor expression. However, only one mouse showed a substantial increase in both regions. The second mouse showed only moderately increased B1 receptor expression in the CA3 region but similar levels to the controls in the thalamus region. Further obstacles that we encountered were the unequal brain slices that resulted in missing or incomplete representation of brain structures in the prion diseased brains, limiting our analysis to only a third of the hippocampus region. However, during initial examination of the unequal dentate gyrus regions, the histology also reveals one mouse with a substantial increase of 37.3% in receptor expression even though the total cell count was almost half of one of the controls. The second diseased mouse however, was similar to the controls (**Appendix 6**).

Given the wide range in biological variation, it is evident that a larger mouse set would be required to truly confirm our speculations. However, these preliminary data along with our gene analysis reveal that the B1 receptor is expressed later than kininogen protein levels suggesting that the kinin-kallirkein pathway is being propelled primarily through the B2 receptor. Unlike Alzheimer's disease, prion disease consists of a rapid neurodegenerative decline after its quiescent incubation phase, which may in fact be too short of a span for the inducible components of the system to fully carry out their

effects. In which case, it appears more likely for the kinin-kallikrein pathway activation to be a consequence of the disease rather than the cause.

4. Inducible Nitric Oxide Synthase

The second inducible marker of the kinin-kallikrein pathway that we examined over our time course was iNOS. As previously mentioned, iNOS expression is not specific to the kinin-kallikrein pathway. However, the pathway has been shown to be involved in post translational activation of iNOS, phosphorylating the enzyme through its stimulation of the ERK/MAP kinase pathway to generate uncontrolled and prolonged nitric oxide [153]. Excessive NO production is believed to cause cell damage and apoptosis in a variety of disorders [188]. Although iNOS expression has been known to be up regulated in prion disease for some time, we are the first to examine its progression over a time course and its possible correlation to the kinin-kallikrein pathway [97, 189].

i) Transcriptional Levels of iNOS

We examined NOS2 gene expression in whole mouse brain through the course of prion disease. During the early stages of disease, in general, we see no change between healthy and infected mice. However, according to one-way ANOVA analysis, two infected mice show a statistically significant decrease in iNOS mRNA at the 100 and 110 days post infection time points. One mouse also revealed a decrease at 90 days post infection when compared only to the PKG1 housekeeping gene. These anomalies are minimal fluctuations with less than a 0.5 fold change difference and are likely due to biological variation.

Continuing to the clinical stages of disease, we see a similar pattern as the BDKRB1 gene expression profile particularly when normalized to the GAPDH housekeeping gene. Gene expression begins to change during the clinical stages of disease. The same mouse eliciting increased BDKRB1 transcripts is also demonstrating significantly increased expression of NOS2 at 120 days post infection. At 130 days post infection, the same three mice expressing increased BDKRB1 transcripts are also expressing increased iNOS mRNA. There is an obvious trend for increased gene expression evident in the clinical stages of disease. This delay in expression during disease is consistent with its inducible nature and similar to BDKRB1 mRNA expression, any significant change at the terminal time point is largely abolished. This identical pattern with similar increased levels of expression between both genes further supports the direct correlation between B1 receptor stimulation and iNOS production in the kinin-kallikrein pathway.

ii) Literature Validity of our iNOS Findings

Prion disease is known for its atypical inflammatory nature, where fewer cytokines are increased and at much lower levels than in typical CNS infections [95, 97, 182]. This lower threshold for detection, in addition to the various animal models and prion strains available, adds great variability to current evidence available for iNOS mRNA levels in prion disease. Our data are consistent with other studies available in literature in the sense that mRNA levels are increased during the clinical stages of disease. However, precise quantification of the increased levels remains controversial and dependent on many variables [97, 190].

iii) Translational Levels of iNOS

We then proceeded to determine the expression pattern of iNOS at the protein level to see if a significant trend could be established through Western blot ananlysis. To our surprise, there was no large change in iNOS protein expression. There was only a modest, but statistically significant 1.5 fold increase in the infected samples at 90 days post infection. This struck us odd because our real-time PCR analysis did not show an increase in mRNA levels until the late clinical stages of disease. Furthermore, no significant change was apparent at the terminal time point which also does not reflect available literature. Whether Alzheimer's disease or prion disease, at the terminal stage, researchers have shown an up regulation of iNOS protein in the brain typically by immunohistochemistry methods [189, 191]. However, we do see the beginnings of an increasing trend in expression at 120 days post infection when normalized to total protein and at 130 days post infection when compared to vinculin. To confirm these speculations at a more sensitive level, we continued to examine iNOS protein levels through immunohistochemistry methods.

Once again, we examined global cell populations in the brain to determine if we could first obtain a strong signal. We do know that neurons and glial cells express iNOS, including astrocytes [192, 193]. As the number of activated glial cells increase during disease, iNOS expression is expected to increase as well.

As predicted, our preliminary data for iNOS protein levels do reveal an increase in expression during prion disease, specifically in the hippocampus and thalamus regions which we selected to examine for this study. We were able to detect increases in expression as early as 70 days post infection supporting some validation to the

statistically significant increase observed at 90 days post infection in our Western blot analysis.

In almost all cases, infected brain regions display an increased number of cells expressing iNOS. The single exception being the CA1 region of the hippocampus at the terminal time point where only one mouse could be examined due to a missing CA1 region in the second mouse. Nevertheless, we can see that as the disease progresses, expression levels correspondingly increase reaching statistically significant levels in the dentate gyrus of the hippocampus and the thalamus by terminal stages of disease. Furthermore, through examination of our immunohistological images, we can also see that as prion disease progresses, the intensity of the staining strengthens suggesting that not only are more cells producing iNOS protein but the levels within each cell are increasing as well.

These observations are supported by our real-time PCR analysis where we see significantly increased levels of iNOS mRNA, ranging from 3-fold to 9-fold increases just before terminal stages of disease. In addition, they are also consistent to other studies available in literature where iNOS expression has been determined to be increased in scrapie infected mice at terminal stages of disease [189]. However, our in situ analysis of the time course of iNOS expression at a histological level is a novel contribution describing it's progression through the course of prion disease.

As previously mentioned, one control mouse seemed to display an atypical increased level of iNOS protein in the brain. This observation is based on comparing the average protein expression across all control time points. This odd increase may be explained by

a stress induced environment. Prolonged stress has been shown to cause neurodegenerative changes including up regulation of iNOS protein [194]. For example, incompatibility with other residing mice could have induced an aggressive environment and thus an up regulation of iNOS protein through alternative pathways.

With the exception of the one control mouse displaying an odd amount of iNOS protein, it is interesting to note that in all healthy mice regardless of their time point, an average 40% basal expression level of iNOS protein was observed. This is comparable to other iNOS studies in rodent brain where protein levels reached as high as 58 +/- 4% in the cerebral cortex alone [195]. For an inducible marker, its expression seems abnormally high suggesting that post translational regulation plays a significant role for the function of this protein. In which case, the kinin-kallikrein pathway would play a crucial role in the assistance of iNOS functionality through its ERK/MAP kinase pathway. For iNOS to function and emit NO, it must form a homodimer and become phosphorylated [145]. Unfortunately, our antibody was unable to distinguish between the presence or absence of this post translational modification. Nevertheless, the sheer quantity/intensity observed at terminal stages of disease strongly encourages functional activity.

E. Conclusions

It was hypothesized that the kinin-kallikrein pathway may be partially responsible for the atypical inflammation and oxidative stress that is observed in prion pathogenicity. To test this hypothesis we examined several components of the kinin-kallirein pathway at various stages of disease and correlated their expression profiles to our generated and defined time frame describing prion disease progression in our mouse model.

Our Western blot analysis reveals a slight upregulation in iNOS during the transitory stage of disease but this may be due to an alternative pathway given that kininogen levels only begin to fluctuate at clinical stages of disease. In addition, our real-time PCR analysis in combination with our histology has confirmed the expression of our inducible markers at the clinical stages of disease. Although the confirmed expression of the B1 receptor indicates that the pathway is activated, it is not responsible for the stages of gliosis and oxidative stress observed.

The kinin-kallikrein pathway is indeed activated during prion disease and thus a contributor of inflammation and oxidative stress in prion pathogenicity. We successfully detected an increase in all selected targets of this pathway in the brains of infected mice. However, the increase in these selected markers occurred relatively late in disease progression suggesting that the increased activity of the kinin-kallikrein system is a consequence of disease processes initiated at an earlier time point via an alternative pathway.

F. Future Directions

The measuring of mRNA and protein in whole brain proved to be problematic. We now believe that the changes that are occurring during disease are very localized and thus background noise from the remaining areas of the brain dampen our positive signal. This becomes a significant issue when we examine the preclinical stages of disease where the initial changes could be completely masked. In the future, it would be beneficial to isolate the various brain regions of interest, followed by the extraction of total RNA and protein from the tissue. This could be accomplished through laser capture microdissection where select regions of the brain are carved out of the tissue slice and collected for further processing [196]. This would significantly increase the sensitivity for the detection of genes and protein of interest.

To truly confirm the association of the kinin-kallikrein pathway in prion disease, it would be beneficial to incorporate B1 and B2 receptor knockout mice into future experiments. Knockout mice, in combination with B1 and B2 receptor inhibitors that are readily available in mouse models, could easily be tested to determine if inhibiting sections of the pathway can prolong survival of diseased mice [165, 197]. Should the results prove to be promising, particularly through B2 receptor inhibition, an FDA approved drug already on the market would allow for immediate clinical trial testing. Icatibant is a B2 receptor inhibitor on the market for hereditary angiodema patients [198]. Although almost certainly not a cure for prion disease, it could delay disease progression. It would be particularly interesting to see its effects on familial CJD where misfolded prion protein deposition

may be scarce but a strong inflammatory response is evident [47]. According to our data, we believe the kinin kallirien pathway is a contributor for inflammation and oxidative stress. Thus, it is of our opinion that it would be worth to explore this avenue of research which could lead to the very first therapeutic treatment available for prion disease.

Appendix 1

NOS2

Forward Primer – 5’-CTCACTCAGCCAAGCCCTCACCTACT-3’

Reverse Primer – 5’ –GCCTCCAATCTCTGCCTATCCGTCTC-3’

BDKRB1

Forward Primer – 5’-GGGGACCCAAGGACAGCAAGACAATG-3’

Reverse Primer – 5’-CCAGGAAATCCAGGAAGGCAAAGAAG-3’

GAPDH

Forward Primer – 5’-AGCTTGTCATCAACGGGAAG-3’

Reverse Primer – 5’ -TTTGATGTTAGTGGGGTCTCG-3’

HRPT1

Forward Primer – 5’-TCCTCCTCAGACCGCTTTT -3’

Reverse Primer – 5’-CCTGGTTCATCATCGCTAATC -3’

PGK1

Forward Primer – 5’-TACCTGCTGGCTGGATGG -3’

Reverse Primer – 5’-CACAGCCTCGGCATATTTCT-3’

Appendix 2

Comparing protein expression between HMWK and LMWK in mouse brain. HMWK is denoted in blue and is substantially darker (ie. more abundant) in the brain than it`s splice variant LMWK denoted in red. One antibody targeting a shared domain on the heavy chain segment of the protein was used to detect both splice variants.

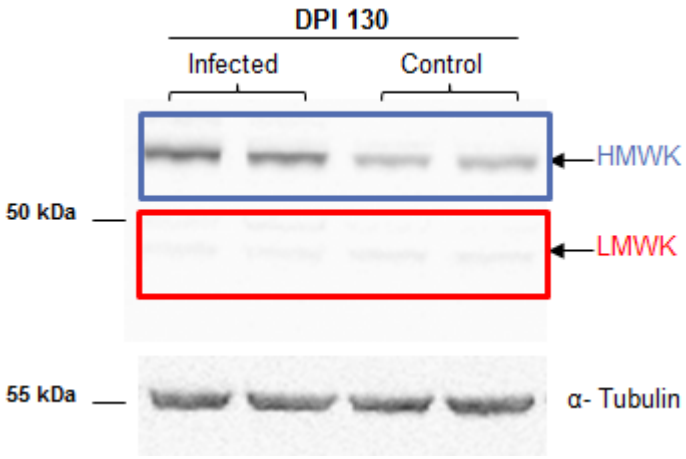

Appendix 3

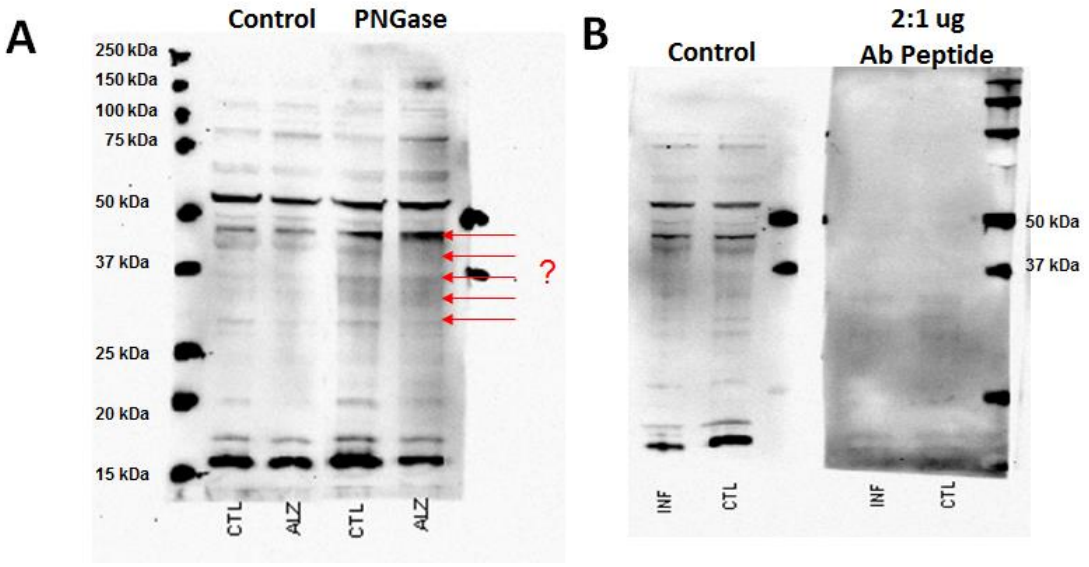

Panel A: PNGase F treatment of samples was performed to remove all N-linked glycans in the efforts to identify the correct B1 receptor band at approximately 40 kDa. Non-specific binding remains evident in the treated samples as indicated by the red arrows. **Panel B:** Peptide competition assay performed at a 2:1 ratio removes presumably non-specific binding with a few faint bands remaining far below the 37 kDa range.

Appendix 4

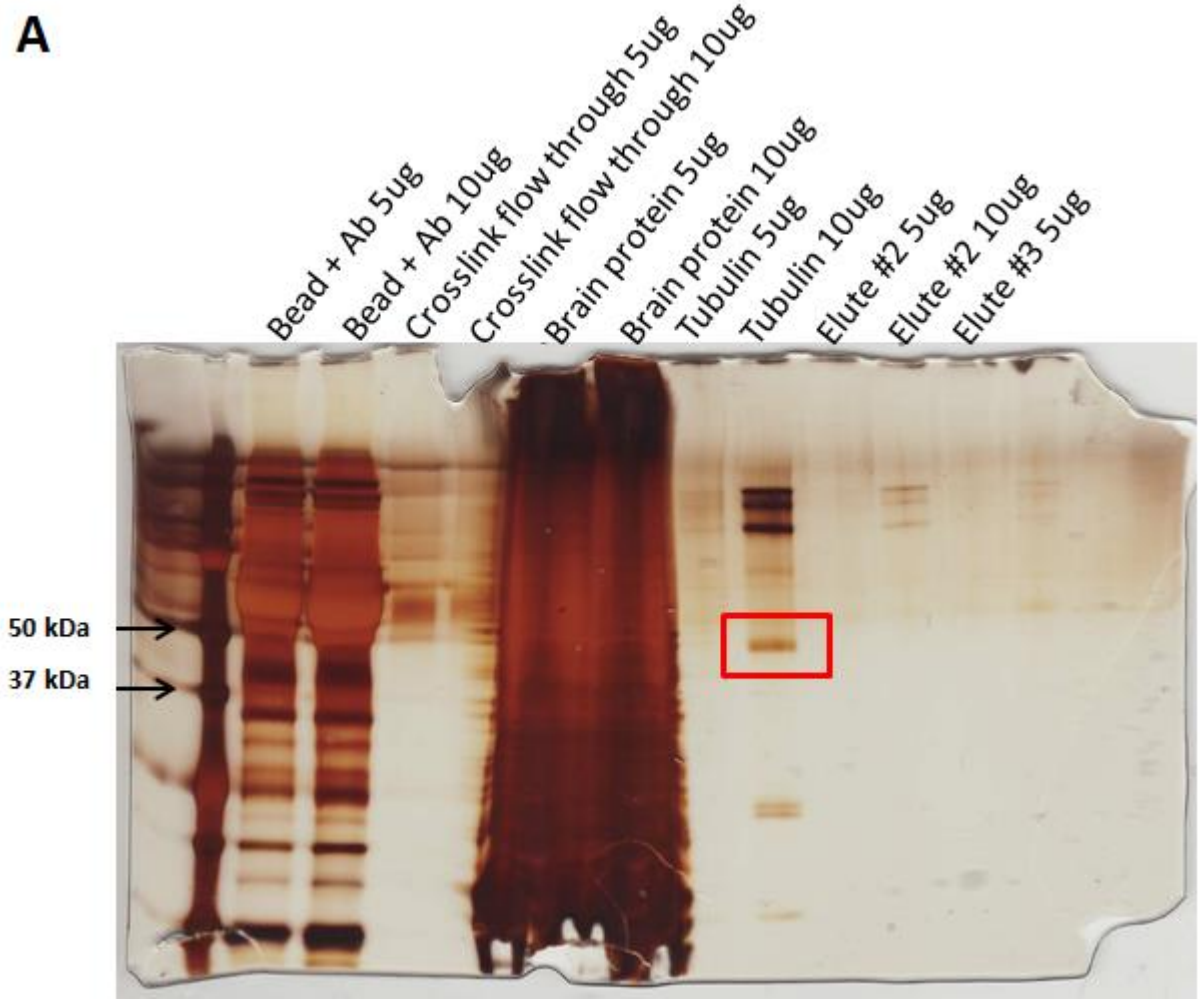

Panel A: Silver stained gel demonstrating the isolation of α-tubulin (denoted by the red box) from 10ug of whole brain protein, through a cross-linking immunoprecipitation assay.

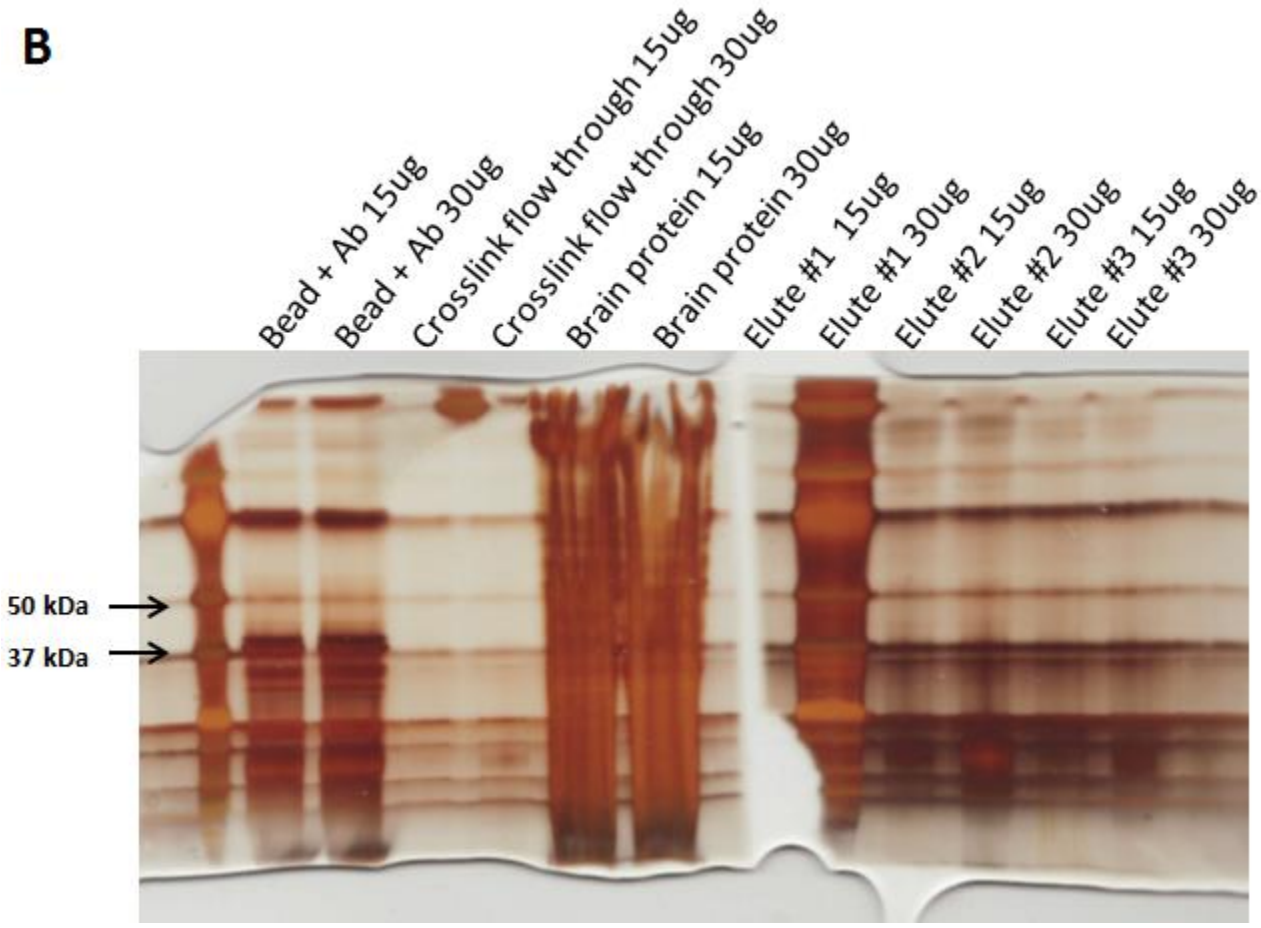

Panel B: Silver stained gel attempting the isolation of B1 receptor protein from 15ug and 30ug of whole brain protein, through a cross-linking immunoprecipitation assay. Multiple banding in elute indicates non-specific binding by antibody.

Appendix 5

Histological counts for iNOS positive cells in various regions of the brain at all tested time points:

iNOS- CA1	***Control***											
	DPI 70											
Mouse #	**1**						**2**					
Region of Brain	**Left CA1**			**Right CA1**			**Left CA1**			**Right CA1**		
Image #	1	2	3	4	5	6	1	2	3	4	5	6
Positive Cell Count	31	10	28	42	37	35	34	47	50	45	39	33
Total Cell Count	92	80	100	94	111	95	80	87	98	95	97	99
Sum Positive Count	183						248					
Sum Cell Count	572						556					
% Increase	32.0%						44.6%					
Avg % Increase	38.3%											

iNOS-CA1	***Infected***											
	DPI 70											
Mouse #	**1**						**2**					
Region of Brain	**Left CA1**			**Right CA1**			**Left CA1**			**Right CA1**		
Image #	1	2	3	4	5	6	1	2	3	4	5	6
Positive Cell Count	31	27	29	61	74	58	38	47	45	52	54	45
Total Cell Count	86	74	76	104	111	102	97	106	113	93	99	110
Sum Positive Count	280						281					
Sum Cell Count	553						618					
% Increase	50.6%						45.5%					
Avg % Increase	48.1%											

iNOS- CA1	*Control*											
	DPI 100											
Mouse #	**1**						**2**					
Region of Brain	**Left CA1**			**Right CA1**			**Left CA1**			**Right CA1**		
Image #	1	2	3	4	5	6	1	2	3	4	5	6
Positive Cell Count	49	65	71	47	39	43	53	64	67	42	40	41
Total Cell Count	95	116	127	84	74	79	119	118	147	88	90	99
Sum Positive Count	314						307					
Sum Cell Count	575						661					
% Increase	54.6%						46.4%					
Avg % Increase	50.5%											

iNOS- CA1	*Infected*											
	DPI 100											
Mouse #	**1**						**2**					
Region of Brain	**Left CA1**			**Right CA1**			**Left CA1**			**Right CA1**		
Image #	1	2	3	4	5	6	1	2	3	4	5	6
Positive Cell Count	62	62	86	53	56	66	94	75	82	63	62	60
Total Cell Count	104	101	126	83	82	92	133	126	136	102	101	93
Sum Positive Count	385						436					
Sum Cell Count	588						691					
% Increase	65.5%						63.1%					
Avg % Increase	64.3%											

iNOS- CA1	*Control*											
	TERM											
Mouse #	**1**						**2**					
Region of Brain	**Left CA1**			**Right CA1**			**Left CA1**			**Right CA1**		
Image #	1	2	3	4	5	6	1	2	3	4	5	6
Positive Cell Count	34	39	43	30	39	43	42	41	56	10	21	22
Total Cell Count	89	99	100	76	94	108	80	83	89	67	66	116
Sum Positive Count	228						192					
Sum Cell Count	566						501					
% Increase	40.3%						38.3%					
Avg % Increase	39.3%											

iNOS- CA1	*Infected*					
	TERM					
Mouse #	**1**					
Region of Brain	**Left CA1**			**Right CA1**		
Image #	1	2	3	4	5	6
Positive Cell Count	35	57	72	21	26	34
Total Cell Count	95	94	105	94	98	111
Sum Positive Count	245					
Sum Cell Count	597					
% Increase	41.0%					

iNOS- CA3	*Control*											
	DPI 70											
Mouse #	**1**						**2**					
Region of Brain	**Left CA3**			**Right CA3**			**Left CA3**			**Right CA3**		
Image #	1	2	3	4	5	6	1	2	3	4	5	6
Positive Cell Count	11	16	21	20	26	29	34	25	25	26	36	31
Total Cell Count	68	86	80	73	84	83	81	91	73	80	92	87
Sum Positive Count			123						177			
Sum Cell Count			474						504			
% Increase			25.9%						35.1%			
Avg % Increase						30.5%						

iNOS- CA3	*Infected*											
	DPI 70											
Mouse #	**1**						**2**					
Region of Brain	**Left CA3**			**Right CA3**			**Left CA3**			**Right CA3**		
Image #	1	2	3	4	5	6	1	2	3	4	5	6
Positive Cell Count	32	35	56	64	74	64	40	39	34	36	37	41
Total Cell Count	102	106	103	95	122	100	94	103	104	101	92	77
Sum Positive Count			325						227			
Sum Cell Count			628						571			
% Increase			51.8%						39.8%			
Avg % Increase						45.8%						

iNOS- CA3	*Control*											
	DPI 100											
Mouse #	**1**						**2**					
Region of Brain	**Left CA3**			**Right CA3**			**Left CA3**			**Right CA3**		
Image #	1	2	3	4	5	6	1	2	3	4	5	6
Positive Cell Count	44	51	43	25	28		27	39	46	17	25	29
Total Cell Count	125	91	105	74	68		73	88	107	53	74	63
Sum Positive Count			191						183			
Sum Cell Count			463						458			
% Increase			41.3%						40.0%			
Avg % Increase						40.6%						

iNOS- CA3	*Infected*											
	DPI 100											
Mouse #	**1**						**2**					
Region of Brain	**Left CA3**			**Right CA3**			**Left CA3**			**Right CA3**		
Image #	1	2	3	4	5	6	1	2	3	4	5	6
Positive Cell Count	38	75	42	30	38	36	63	67	41	44	38	
Total Cell Count	67	110	81	49	53	59	125	155	91	79	65	
Sum Positive Count			259						253			
Sum Cell Count			419						515			
% Increase			61.8%						49.1%			
Avg % Increase						55.5%						

iNOS-CA3	*Control*											
	TERM											
Mouse #	**1**						**2**					
Region of Brain	**Left CA3**			**Right CA3**			**Left CA3**			**Right CA3**		
Image #	1	2	3	4	5	6	1	2	3	4	5	6
Positive Cell Count	32	48	36	38			29	26	25	30		
Total Cell Count	68	94	75	93			57	72	54	96		
Sum Positive Count	154						110					
Sum Cell Count	330						279					
% Increase	46.7%						39.4%					
Avg % Increase	43.0%											

iNOS-CA3	*Infected*											
	TERM											
Mouse #	**1**						**2**					
Region of Brain	**Left CA3**			**Right CA3**			**Left CA3**			**Right CA3**		
Image #	1	2	3	4	5	6	1	2	3	4	5	6
Positive Cell Count	43	66	67	62			62	90	68			
Total Cell Count	61	107	93	128			90	123	84			
Sum Positive Count	238						220					
Sum Cell Count	389						297					
% Increase	61.2%						74.1%					
Avg % Increase	67.6%											

iNOS-DG	*Control*											
	DPI 70											
Mouse #	**1**						**2**					
Region of Brain	**Left DG**			**Right DG**			**Left DG**			**Right DG**		
Image #	1	2	3	4	5	6	1	2	3	4	5	6
Positive Cell Count	65	74	61	58	48	101	76	141	83	79	110	
Total Cell Count	163	201	159	182	179	275	168	327	177	177	220	
Sum Positive Count	407						489					
Sum Cell Count	1159						1069					
% Increase	35.1%						45.7%					
Avg % Increase	40.4%											

iNOS-DG	*Infected*											
Treatment	**DPI 70**											
Mouse #	**1**						**2**					
Region of Brain	**Left DG**			**Right DG**			**Left DG**			**Right DG**		
Image #	1	2	3	4	5	6	1	2	3	4	5	6
Positive Cell Count	111	117	75	123	117	154	104	91	67	112	115	161
Total Cell Count	192	216	116	180	183	272	207	219	190	177	211	281
Sum Positive Count	697						650					
Sum Cell Count	1159						1285					
% Increase	60.1%						50.6%					
Avg % Increase	55.4%											

iNOS-DG	*Control*											
	DPI 100											
Mouse #	**1**						**2**					
Region of Brain	**Left DG**			**Right DG**			**Left DG**			**Right DG**		
Image #	1	2	3	4	5	6	1	2	3	4	5	6
Positive Cell Count	58	52	97	49	53	91	93	83	102	67	65	84
Total Cell Count	100	101	155	87	89	186	209	165	231	203	157	215
Sum Positive Count	400						494					
Sum Cell Count	718						1180					
% Increase	55.7%						41.9%					
Avg % Increase	48.8%											

iNOS-DG	*Infected*											
	DPI 100											
Mouse #	**1**						**2**					
Region of Brain	**Left DG**			**Right DG**			**Left DG**			**Right DG**		
Image #	1	2	3	4	5	6	1	2	3	4	5	6
Positive Cell Count	79	68	76	74	68	81	60	49	93	52	58	98
Total Cell Count	141	117	124	126	119	145	122	83	171	109	103	168
Sum Positive Count	446						410					
Sum Cell Count	772						756					
% Increase	57.8%						54.2%					
Avg % Increase	56.0%											

iNOS-DG	*Control*											
	TERM											
Mouse #	**1**						**2**					
Region of Brain	**Left DG**			**Right DG**			**Left DG**			**Right DG**		
Image #	1	2	3	4	5	6	1	2	3	4	5	6
Positive Cell Count	99	84	105	68	78	111	72	78	118	61	66	110
Total Cell Count	233	181	253	163	174	286	159	140	251	131	147	221
Sum Positive Count	545						505					
Sum Cell Count	1290						1049					
% Increase	42.2%						48.1%					
Avg % Increase	45.2%											

iNOS-DG	*Infected*											
	TERM											
Mouse #	**1**						**2**					
Region of Brain	**Left DG**			**Right DG**			**Left DG**			**Right DG**		
Image #	1	2	3	4	5	6	1	2	3	4	5	6
Positive Cell Count	108	99	163	90	78		110	121	197	75	98	118
Total Cell Count	166	158	157	130	129		168	168	262	149	176	232
Sum Positive Count	538						719					
Sum Cell Count	740						1155					
% Increase	72.7%						62.3%					
Avg % Increase	67.5%											

iNOS-Thalamus	*Control*											
	DPI 70											
Mouse #	**1**						**2**					
Region of Brain	**Left TH**			**Right TH**			**Left TH**			**Right TH**		
Image #	1	2	3	4	5	6	1	2	3	4	5	6
Positive Cell Count	21	35	25	47	28	25	29	36	30	37	32	25
Total Cell Count	80	79	78	107	77	64	69	89	72	85	65	60
Sum Positive Count	181						189					
Sum Cell Count	485						440					
% Increase	37.3%						43.0%					
Avg % Increase	40.1%											

iNOS-Thalamus	*Infected*											
	DPI 70											
Mouse #	**1**						**2**					
Region of Brain	**Left TH**			**Right TH**			**Left TH**			**Right TH**		
Image #	1	2	3	4	5	6	1	2	3	4	5	6
Positive Cell Count	44	43	42	52	53	48	40	48	41	42	44	36
Total Cell Count	99	92	78	97	83	75	77	99	75	92	78	82
Sum Positive Count	282						251					
Sum Cell Count	524						503					
% Increase	53.8%						49.9%					
Avg % Increase	51.9%											

iNOS-Thalamus	*Control*											
	DPI 100											
Mouse #	**1**						**2**					
Region of Brain	**Left TH**			**Right TH**			**Left TH**			**Right TH**		
Image #	1	2	3	4	5	6	1	2	3	4	5	6
Positive Cell Count	27	23	29	25	29	23	18	15		17	16	27
Total Cell Count	55	51	63	53	71	50	53	53		51	41	74
Sum Positive Count	156						93					
Sum Cell Count	343						272					
% Increase	45.5%						34.2%					
Avg % Increase	39.8%											

iNOS-Thalamus	*Infected*											
	DPI 100											
Mouse #	**1**						**2**					
Region of Brain	**Left TH**			**Right TH**			**Left TH**			**Right TH**		
Image #	1	2	3	4	5	6	1	2	3	4	5	6
Positive Cell Count	27	22	35	35	27	35	61	39	35	42	40	33
Total Cell Count	39	32	47	45	36	57	95	62	53	72	72	59
Sum Positive Count	181						250					
Sum Cell Count	256						413					
% Increase	70.7%						60.5%					
Avg % Increase	65.6%											

iNOS-Thalamus	*Control*											
	TERM											
Mouse #	**1**						**2**					
Region of Brain	**Left TH**			**Right TH**			**Left TH**			**Right TH**		
Image #	1	2	3	4	5	6	1	2	3	4	5	6
Positive Cell Count	29	27	26	32	27	30	24	27	12	20	16	12
Total Cell Count	66	64	59	66	55	76	51	58	40	49	42	40
Sum Positive Count	171						111					
Sum Cell Count	386						280					
% Increase	44.3%						39.6%					
Avg % Increase	42.0%											

iNOS-Thalamus	*Infected*											
	TERM											
Mouse #	**1**						**2**					
Region of Brain	**Left TH**			**Right TH**			**Left TH**			**Right TH**		
Image #	1	2	3	4	5	6	1	2	3	4	5	6
Positive Cell Count	44	85	65	56	66	50	74	96	89	96	113	95
Total Cell Count	71	125	97	94	114	78	87	114	131	141	150	146
Sum Positive Count	366						563					
Sum Cell Count	579						769					
% Increase	63.2%						73.2%					
Avg % Increase	68.2%											

Appendix 6

Histological counts for B1 receptor positive cells in various regions of the brain at the terminal time point:

B1-CA3	***Control***											
	TERM											
Mouse #	**1**						**2**					
Region of Brain	**Left CA3**			**Right CA3**			**Left CA3**			**Right CA3**		
Image #	1	2	3	4	5	6	1	2	3	4	5	6
Positive Cell Count	4	4	10	4	4	2	5	5	3	0	3	6
Total Cell Count	40	40	47	35	50	47	36	58	59	56	68	64
Sum Positive Count	28						22					
Sum Cell Count	259						341					
% Increase	10.8%						6.5%					
Avg % Increase	8.6%											

B1-CA3	***Infected***											
	TERM											
Mouse #	**1**						**2**					
Region of Brain	**Left CA3**			**Right CA3**			**Left TH**			**Right CA3**		
Image #	1	2	3	4	5	6	1	2	3	4	5	6
Positive Cell Count	30	20	26	48	26	29	16	16	15	11	16	15
Total Cell Count	81	50	57	61	47	77	43	44	45	55	61	66
Sum Positive Count	179						89					
Sum Cell Count	373						314					
% Increase	48.0%						28.3%					
Avg % Increase	38.2%											

B1-DG	*Control*											
	TERM											
Mouse #	**1**						**2**					
Region of Brain	**Left DG**			**Right DG**			**Left DG**			**Right DG**		
Image #	1	2	3	4	5	6	1	2	3	4	5	6
Positive Cell Count	4	13	4				2	5	6	4	3	23
Total Cell Count	117	98	63				117	117	178	113	165	170
Sum Positive Count	21						43					
Sum Cell Count	278						860					
% Increase	7.6%						5.0%					
Avg % Increase	6.3%											

B1-DG	*Infected*											
	TERM											
Mouse #	**1**						**2**					
Region of Brain	**Left DG**			**Right DG**			**Left TH**			**Right DG**		
Image #	1	2	3	4	5	6	1	2	3	4	5	6
Positive Cell Count	7	4	6	14	5	5	30	43	32	36	36	27
Total Cell Count	99	108	91	103	91	88	76	95	99	74	73	73
Sum Positive Count	41						204					
Sum Cell Count	580						490					
% Increase	7.1%						41.6%					
Avg % Increase	24.4%											

B1-Thalamus	*Control*											
	TERM											
Mouse #	**1**						**2**					
Region of Brain	**Left TH**			**Right TH**			**Left TH**			**Right TH**		
Image #	1	2	3	4	5	6	1	2	3	4	5	6
Positive Cell Count	2	0	4	4	0	4	0	0	5	3	5	5
Total Cell Count	43	40	37	40	25	40	34	38	53	68	31	45
Sum Positive Count	14						18					
Sum Cell Count	225						269					
% Increase	6.2%						6.7%					
Avg % Increase	6.5%											

B1-Thalamus	*Infected*											
	TERM											
Mouse #	**1**						**2**					
Region of Brain	**Left TH**			**Right TH**			**Left TH**			**Right TH**		
Image #	1	2	3	4	5	6	1	2	3	4	5	6
Positive Cell Count	17	22	30	26	21	17	7	12	7	8	5	6
Total Cell Count	35	38	40	37	34	30	39	35	41	28	31	51
Sum Positive Count	133						45					
Sum Cell Count	214						225					
% Increase	62.1%						20.0%					
Avg % Increase	41.1%											

References

1. Takemura, K., Kahdre, M., Joseph, D., Yousef, A. and Sreevatsan, S. (2004). An overview of transmissible spongiform encephalopathies. Animal Health Research Reviews. 5(2): 103–124.

2. Johnson, R.T. (2005) Prion diseases. Lancet Neurol. 4: 635–42.

3. Schneider, K., Fangerau, H., Michaelsen, B. and Raab, W.H.M. (2008). The early history of the transmissible spongiform encephalopathies exemplified by scrapie. Brain Research Bulletin. 77 (6): 343–355.

4. Pattison, I.H. (1972). Scrapie--a personal view. J Clin Pathol Suppl (R Coll Pathol). 6: 110-4.

5. Gajdusek, D.C. and Zigas, V. (1957). Degenerative disease of the central nervous system in New Guinea: the endemic occurrence of 'kuru' in the native population. N. Engl. J. Med. 257: 974–978.

6. Imran, M. and Mahmood, S. (2011). An overview of animal prion diseases. Virol J. 8: 559.

7. Liberski, P.P. (2013). Kuru: A Journey Back in Time from Papua New Guinea to the Neanderthals' Extinction. Pathogens. 2(3): 472–505.

8. Gajdusek, D.C., Gibbs, C.J. and Alpers, M.P. (1966). Experimental transmission of a kuru-like syndrome to chimpanzees. Nature. 209: 794–796.

9. Hadlow, W.J. (1959). Scrapie and kuru. Lancet. 2: 289–290.

10. Holman, R.C., Belay, E.D., Christensen, K.Y., Maddox, R.A., Minino, A.M., Folkema, A.M., Haberling, D.L., Hammett, T.A., Kochanek, K.D., Sejvar, J.J. and Schonberger, L.B. (2010). Human Prion Diseases in the United States. PLoS ONE. 5(1): e8521.

11. Ironside, J.W. (2006). Variant Creutzfeldt–Jakob disease: risk of transmission by blood transfusion and blood therapies. Haemophilia. 12(Suppl. 1): 8–15.

12. Palmer, M.S., Dryden, A.J., Hughes, J.T. and Collinge, J. (1991). Homozygous prion protein genotype predisposes to sporadic Creutzfeldt-Jakob disease. Nature. 352(6333): 340-2.

13. Mastrianni, J.A. (2010). The genetics of prion diseases. Genet Med. 12(4): 187-195.

14. Minikel, E.V., Vallabh, S.M., Lek, M., Estrada, K., Samocha, K.E., et al. (2016). Quantifying prion disease penetrance using large population control cohorts. Sci Transl Med. 8(322): 322ra9.

15. Lee, H.S., Sambuughin, N., Cervenakova, L., Chapman, J., Pocchiari, M., Litvak, S., Qi, H.Y., Budka, H., del Ser, T., Furukawa, H., Brown, P., Gajdusek, D.C., Long, J.C., Korczyn, A.D. and Goldfarb, L.G. (1999). Ancestral origins and worldwide distribution of the PRNP 200K mutation causing familial Creutzfeldt–Jakob disease. American Journal of Human Genetics 64: 1063–1070.

16. Goldfarb, L.G., Petersen, R.B., Tabaton, M., Brown, P., LeBlanc, A.C., Montagna, P., Cortelli, P., Julien, J., Vital, C. and Pendelbury, W.W. (1992). Fatal familial insomnia and familial Creutzfeldt–Jakob disease: disease phenotype determined by a DNA polymorphism. Science 258: 806–808.

17. Goldgaber, D., Goldfarb, L.G., Brown, P., Asher, D.M., Brown, W.T., Lin, S., Teener, J.W., Feinstone, S.M., Rubenstein, R. and Kascsak, R.J. (1989). Mutations in familial Creutzfeldt– Jakob disease and Gerstmann–Straussler–Scheinker's syndrome. Experimental Neurology. 106: 204–206.

18. Lasmezas, C.I., Deslys, J.P., Demaimay, R., Adjou, K.T., Lamoury, F., Dormont, D., Robain, O., Ironside, J. and Hauw, J.J. (1996). BSE transmission to macaques. Nature. 381: 743–744.

19. The National Creutzfeldt-Jakob Surveillance Unit. (2016). Variant CJD Cases Worldwide. Online at http://www.cjd.ed.ac.uk/sites/default/files/worldfigs.pdf

20. Bishop, M.T., Hart, P., Aitchison, L., Baybutt, H.N., Plinston, C., Thomson, V., Tuzi, N.L., Head, M.W., Ironside, J.W., Will, R.G. and Manson, J.C. (2006). Predicting susceptibility and incubation time of human-to-human transmission of vCJD. Lancet Neurol. 5: 393-8.

21. Wells, G.A., Dawson, M., Hawkins, S.A., Green, R.B., Dexter, I., Francis, M.E., Simmons, M.M., Austin, A.R. and Horigan, M.W. (1994). Infectivity in the ileum of cattle challenged orally with bovine spongiform encephalopathy. Veterinary Record. 135: 40–41.

22. Hilton, D.A., Ghani, A.C., Conyers, L., Edwards, P., McCardle, L., Ritchie, D., Penney, M., Hegazy, D. and Ironside, J.W. (2004). Prevalence of lymphoreticular prion protein accumulation in UK tissue samples. J Pathol. 203: 733–9.

23. MRC Prion Unit. (2016). Acquired prion disease. Online at http://www.prion.ucl.ac.uk/clinic-services/information/acquired-prion-disease/

24. Hewitt, P.E., Llewelyn, C.A., Mackenzie, J. and Will, R.G. (2006). Creutzfeldt-Jakob disease and blood transfusion: results of the UK Transfusion Medicine Epidemiological Review study. Vox Sang. 91(3): 221-30.

25. JPAC. (2013). 3.2: Tests on blood donations. In Handbook of Transfusion Medicine. (Ed. D. Norfolk). Published by TSO, United Kingdom. Online at http://www.transfusionguidelines.org/transfusion-handbook/3-providing-safe-blood/3-2-tests-on-blood-donations

26. Alper, T., Haig, D.A. and Clarke, M.C. (1966). The exceptionally small size of the scrapie agent. Biochem Biophys Res Commun. 22(3): 278-84.

27. Silveira, J.R., Raymond, G.J., Hughson, A.G., Race, R.E., Sim, V.L., Hayes, S.F. and Caughey, B. (2005). The most infectious prion protein particles. Nature. 437(7056): 257-61.

28. Soto, C. (2011). Prion Hypothesis: The end of the Controversy? Trends Biochem Sci. 36(3): 151–158.

29. Pattison, I.H. and Jones, K.M. (1967). The possible nature of the transmissible agent of scrapie. Vet Rec. 80(1): 2-9.

30. Griffith, J.S. (1967). Self-replication and scrapie. Nature. 215(5105): 1043-4.

31. Prusiner, S.B. (1982). Novel proteinaceous infectious particles cause scrapie. Science. 216: 136–144.

32. Büeler, H., Aguzzi, A., Sailer, A., Greiner, R.A., Autenried, P., Aguet, M. and Weissmann, C. (1993). Mice devoid of PrP are resistant to scrapie. Cell. 73(7): 1339-47.

33. Saborio, G.P., Permanne, B. and Soto, C. (2001). Sensitive detection of pathological prion protein by cyclic amplification of protein misfolding. Nature. 411(6839): 810-3.

34. Wang, F., Wang, X., Yuan, C.G. and Ma, J. (2010). Generating a prion with bacterially expressed recombinant prion protein. Science. 327(5969): 1132-5.

35. Prusiner, S.B. (1998). Prions. Proceedings of the National Academy of Sciences of the United States of America. 95: 13363–13383.

36. Stahl, N., Borchelt, D.R., Hsiao, K. and Prusiner, S.B. (1987). Scrapie prion protein contains a phosphatidylinositol glycolipid. Cell 51: 229–240.

37. Harris, D.A., Lele, P. and Snider, W.D. (1993). Localization of the mRNA for a chicken prion protein by in situ hybridization. Proc Natl Acad Sci U S A. 90(9): 4309-13.

38. Barmada, S., Piccardo, P., Yamaguchi, K., Ghetti, B. and Harris, D.A. (2004). GFP-tagged prion protein is correctly localized and functionally active in the brains of transgenic mice. Neurobiol Dis. 16(3): 527-37.

39. Moser, M., Colello, R.J., Pott, U. and Oesch, B. (1995). Developmental expression of the prion protein gene in glial cells. Neuron. 14(3): 509-17.

40. Ford, M.J., Burton, L.J., Morris, R.J. and Hall, S.M. (2002). Selective expression of prion protein in peripheral tissues of the adult mouse. Neuroscience. 113(1): 177-92.

41. Claudia, Y., Morantes, A. and Wille, H. (2014). The Structure of Human Prions: From Biology to Structural Models — Considerations and Pitfalls. Viruses. 6(10): 3875-3892.

42. Harris, D.A., Peters, P.J., Taraboulos, A., Lingappa, V.R., DeArmond, S.J. and Prusiner, S.B. (2004). Cell biology of prions. In: Prusiner SB, editor. Prion Biology and Diseases. Cold Spring Harbor Laboratory Press; Cold Spring Harbor, New York: pp. 483–544.

43. Yedidia, Y., Horonchik, L., Tzaban, S., Yanai, A. and Taraboulos, A. (2001). Proteasomes and ubiquitin are involved in the turnover of the wild-type prion protein. EMBO Journal 20: 5383–5391.

44. Bolton, D.C., McKinley, M.P. and Prusiner, S.B. (1982). Identification of a protein that purifies with the scrapie prion. Science 218: 1309–1311.

45. Prusiner, S.B., Groth, D.F., Bolton, D.C., Kent, S.B. and Hood, L.E. (1984). Purification and structural studies of a major scrapie prion protein. Cell 38: 127–134.

46. Pan, K.M., Baldwin, M., Nguyen, J., Gasset, M., Serban, A., Groth, D., Mehlhorn, I., Huang, Z., Fletterick, R.J. and Cohen, F.E. (1993). Conversion of alpha-helices into beta-sheets features in the formation of the scrapie prion proteins. Proceedings of the National Academy of Sciences of the United States of America 90: 10962–10966.

47. Unterberger, U., Voigtlander, T. and Budka, H. (2005). Pathogenesis of Prion Disease. Acta Neuropathol. 109: 32-48.

48. Hornshaw, M.P., McDermott, J.R. and Candy, J.M. (1995). Copper binding to the N-terminal tandem repeat regions of mammalian and avian prion protein. Biochem Biophys Res Commun. 207(2): 621-9.

49. Hartter, D.A. and Barnea, A. (1988). Evidence for release of copper in the brain: depolarization-induced release of newly taken-up 67copper. Synapse, 2: 412–415.

50. Schlief, M.L., Craig, A.M. and Gitlin, J.D. (2005). NMDA receptor activation mediates copper homeostasis in hippocampal neurons. J Neurosci. 25(1): 239-46.

51. Brown, D.R., Qin, K., Herms, J.W., Madlung, A., Manson, J., Strome, R., Fraser, P.E., Kruck, T., von Bohlen, A., Schulz-Schaeffer, W., Giese, A., Westaway, D. and Kretzschmar, H. (1997). The cellular prion protein binds copper in vivo. Nature. 390(6661): 684-7.

52. Kretzschmar, H.A., Tings, T., Madlung, A., Giese, A. and Herms, J. (2000). Function of PrP(C) as a copper-binding protein at the synapse. Arch Virol Suppl. 16: 239-49.

53. Westergard, L., Christensen, H.M. and Harris, D.A. (2007). The Cellular Prion Protein (PrP^{C}): Its Physiological Function and Role in Disease. Biochim Biophys Acta. 1772(6): 629–644.

54. Kanaani, J., Prusiner, S.B., Diacovo, J., Baekkeskov, S. and Legname, G. (2005). Recombinant prion protein induces rapid polarization and development of synapses in embryonic rat hippocampal neurons in vitro. J Neurochem. 95(5):1373-86.

55. Collinge, J., Whittington, M.A., Sidle, K.C., Smith, C.J., Palmer, M.S,, Clarke, A.R. and Jefferys, J.G. (1994). Prion protein is necessary for normal synaptic function. Nature. 370:295-7.

56. Tobler, I., Gaus, S.E., Deboer, T., Achermann, P., Fischer, M., Rülicke, T., Moser, M., Oesch, B., McBride, P.A. and Manson, J.C. (1996). Altered circadian activity rhythms and sleep in mice devoid of prion protein. Nature. 380(6575): 639-42.

57. Carleton, A., Tremblay, P., Vincent, J.D. and Lledo, P.M. (2001). Dose-dependent, prion protein (PrP)-mediated facilitation of excitatory synaptic transmission in the mouse hippocampus. Pflugers Arch. 442(2): 223-9.

58. Rial, D., Pamplona, F.A., Moreira, E.L., Moreira, K.M., Hipolide, D., Rodrigues, D.I., Dombrowski, P.A., Da Cunha, C., Agostinho, P., Takahashi, R.N., Walz, R., Cunha, R.A. and Prediger, R.D. (2014). Cellular prion protein is present in dopaminergic neurons and modulates the dopaminergic system. Eur J Neurosci. 40(3): 2479-86.

59. Khosravani, H., Zhang, Y., Tsutsui, S., Hameed, S., Altier, C., Hamid, J., Chen, L., Villemaire, M., Ali, Z., Jirik, F.R. and Zamponi, G.W. (2008). Prion protein attenuates excitotoxicity by inhibiting NMDA receptors. J Cell Biol. 181(3): 551-65.

60. Nishida, N., Tremblay, P., Sugimoto, T., Shigematsu, K., Shirabe, S., Petromilli, C., Erpel, S.P., Nakaoke, R., Atarashi, R., Houtani, T., Torchia, M., Sakaguchi, S., DeArmond, S.J., Prusiner, S.B. and Katamine, S. (1999). A mouse prion protein transgene rescues

mice deficient for the prion protein gene from purkinje cell degeneration and demyelination. Lab Invest. 79(6): 689-97.

61. Bremer, J., Baumann, F., Tiberi, C., Wessig, C., Fischer, H., Schwarz, P., Steele, A.D., Toyka, K.V., Nave, K.A., Weis, J. and Aguzzi, A. (2010). Axonal prion protein is required for peripheral myelin maintenance. Nat Neurosci. 13(3): 310-8.

62. Santuccione, A., Sytnyk, V., Leshchyns'ka, I. and Schachner, M. (2005). Prion protein recruits its neuronal receptor NCAM to lipid rafts to activate p59fyn and to enhance neurite outgrowth. J Cell Biol. 169(2): 341-54.

63. Graner, E., Mercadante, A.F., Zanata, S.M., Forlenza, O.V., Cabral, A.L., Veiga, S.S., Juliano, M.A., Roesler, R., Walz, R., Minetti, A., Izquierdo, I., Martins, V.R. and Brentani, R.R. (2000). Cellular prion protein binds laminin and mediates neuritogenesis. Brain Res Mol Brain Res. 76(1): 85-92.

64. Graner, E., Mercadante, A.F., Zanata, S.M., Martins, V.R., Jay, D.G. and Brentani R.R. (2000). Laminin-induced PC-12 cell differentiation is inhibited following laser inactivation of cellular prion protein. FEBS Lett. 482(3): 257-60.

65. Bounhar, Y., Zhang, Y., Goodyer, C.G. and LeBlanc, A. (2001). Prion protein protects human neurons against Bax-mediated apoptosis, J. Biol. Chem. 276: 39145-39149.

66. Kuwahara, C., Takeuchi, A.M., Nishimura, T., Haraguchi, K., Kubosaki, A., Matsumoto, Y., Saeki, K., Matsumoto, Y., Yokoyama, T., Itohara, S. and Onodera, T. (1999). Prions prevent neuronal cell-line death. Nature. 400(6741): 225-6.

67. Brown, D.R., Schulz-Schaeffer, W.J., Schmidt, B. and Kretzschmar, H.A. (1997). Prion protein-deficient cells show altered response to oxidative stress due to decreased SOD-1 activity. Exp Neurol. 146(1): 104-12.

68. Brown, D.R., Nicholas, R.S. and Canevari, L. (2002). Lack of prion protein expression results in a neuronal phenotype sensitive to stress. J Neurosci Res. 67(2): 211-24.

69. Wong, B.S., Liu, T., Li, R., Pan, T., Petersen, R.B., Smith, M.A., Gambetti, P., Perry, G., Manson, J.C., Brown, D.R. and Sy, M.S. (2001). Increased levels of oxidative stress markers detected in the brains of mice devoid of prion protein. J Neurochem. 76(2): 565-72.

70. Brown, D.R., Wong, B.S., Hafiz, F., Clive, C., Haswell, S.J. and Jones, I.M. (1999). Normal prion protein has an activity like that of superoxide dismutase. Biochem J. 344 (Pt 1): 1-5.

71. Brown, D.R., Clive, C. and Haswell, S.J. (2001). Antioxidant activity related to copper binding of native prion protein. J Neurochem. 76(1):69-76.

72. Circu, M.L. and Aw, T.Y. (2010). REACTIVE OXYGEN SPECIES, CELLULAR REDOX SYSTEMS AND APOPTOSIS. Free Radic Biol Med. 48(6): 749–762.

73. Brown, D.R. and Besinger, A. (1998). Prion protein expression and superoxide dismutase activity, Biochem. J. 334: 423-429.

74. Halliwell, B. (2006). Oxidative stress and neurodegeneration: where are we now? J Neurochem. 97(6): 1634-58.

75. Mouillet-Richard, S., Ermonval, M., Chebassier, C., Laplanche, J.L., Lehmann, S., Launay, J.M. and Kellermann, O. (2000). Signal transduction through prion protein. Science. 289(5486): 1925-8.

76. Meggio, F., Negro, A., Sarno, S., Ruzzene, M., Bertoli, A., Sorgato, M.C. and Pinna, L.A. (2000). Bovine prion protein as a modulator of protein kinase CK2. Biochemical Journal 352: 191–196.

77. Spielhaupter, C. and Schatzl, H.M. (2001). PrPC directly interacts with proteins involved in signaling pathways. Journal of Biological Chemistry 276: 44604–44612.

78. Aguzzi, A. and Heppner, F.L. (2000). Pathogenesis of prion diseases: a progress report. Cell Death and Differentiation. 7(10): 889-902.

79. Kimberlin, R.H. and Walker, C.A. (1989) The role of the spleen in the neuroinvasion of scrapie in mice. Virus. Res. 12: 201-211.

80. Kimberlain, R.H., Field, H.J. and Walker, C.A. (1983) Pathogenesis of mouse scrapie: evidence for spread of infection from central to peripheral nervous system. J. Gen. Virol. 64: 713716.

81. Budka, H. (2003). Neuropathology of prion diseases. Br Med Bull. 66(1): 121-130.

82. Budka, H. (1997). Transmissible spongiform encephalopathies (prion diseases). In: Garcia, J.H. (ed) Neuropathology. The Diagnostic Approach. St Louis, MO: Mosby, 449–74.

83. Parchi, P., Giese, A., Capellari, S., Brown, P., Schulz-Schaeffer, W., Windl, O., Zerr, I., Budka, H., Kopp, N., Piccardo, P., Poser, S., Rojiani, A., Streichemberger, N., Julien, J., Vital, C., Ghetti, B., Gambetti, P. and Kretzschmar, H. (1999). Classification of sporadic Creutzfeldt-Jakob disease based on molecular and phenotypic analysis of 300 subjects. Ann Neurol. 46(2): 224-33.

84. Will, R.G., Alperovitch, A., Poser, S., Pocchiari, M., Hofman, A., Mitrova, E., de Silva, R., D'Alessandro, M., Delasnerie-Laupretre, N., Zerr, I. and van Duijn, C. (1998). Descriptive epidemiology of Creutzfeldt–Jakob disease in six European countries, 1993–1995. EU Collaborative Study Group for CJD. Annals of Neurology 43: 763–767.

85. Ironside, J.W. (1998). Neuropathological findings in new variant CJD and experimental transmission of BSE. FEMS Immunology and Medical Microbiology. 21: 91–95.

86. Almer, G., Hainfellner, J.A., Brucke, T., Jellinger, K., Kleinert, R., Bayer, G., Windl, O., Kretzschmar, H.A., Hill, A., Sidle, K., Collinge, J. and Budka, H. (1999) Fatal familial insomnia: a new Austrian family. Brain 122: 5-16.

87. Dorandeu, A., Wingertsmann, L., Chrétien, F., Delisle, M.B., Vital, C., Parchi, P., Montagna, P., Lugaresi, E., Ironside, J.W., Budka, H., Gambetti, P. and Gray, F. (1998). Neuronal apoptosis in fatal familial insomnia. Brain Pathol. 8(3): 531-7.

88. Hegde, R.S., Mastrianni, J.A., Scott, M,R., DeFea, K.A., Tremblay, P., Torchia, M., DeArmond, S.J., Prusiner, S.B. and Lingappa, V.R. (1998). A transmembrane form of the prion protein in neurodegenerative disease. Science. 279(5352): 827-34.

89. Kordek, R., Hainfellner, J.A., Liberski, P.P. and Budka, H. (1999). Deposition of the prion protein (PrP) during the evolution of experimental Creutzfeldt-Jakob disease. Acta Neuropathol. 98(6): 597-602.

90. Giese, A., Brown, D.R., Groschup, M.H., Feldmann, C., Haist, I. and Kretzschmar, H.A. (1998) Role of microglia in neuronal cell death in prion disease. Brain Pathol. 8: 449□457.

91. Burda, J.E. and Sofroniew, M.V. (2014). Reactive gliosis and the multicellular response to CNS damage and disease. Neuron. 81(2): 229-48.

92. Guiroy, D.C., Wakayama, I., Liberski, P.P. and Gajdusek, D.C. (1994) Relationship of microglia and scrapie amyloid-immunoreactive plaques in kuru, Creutzfeldt-Jakob disease and Gerstmann-Straussler syndrome. Acta Neuropathol (Berl). 87: 526-530.

93. Williams, A., Lucassen, P.J., Ritchie, D. and Bruce, M. (1997). PrP deposition, microglial activation, and neuronal apoptosis in murine scrapie. Exp Neurol. 144(2): 433-8.

94. Lull, M.E. and Block, M.L. (2010). Microglial activation and chronic neurodegeneration. Neurotherapeutics. 7(4): 354–365.

95. Tribouillard-Tanvier, D., Striebel, J.F., Peterson, K.E. and Chesebro, B. (2009). Analysis of protein levels of 24 cytokines in scrapie agent-infected brain and glial cell cultures from mice differing in prion protein expression levels. J Virol. 83(21): 11244-53.

96. Brown, A.R., Webb, J., Rebus, S., Walker, R., Williams, A. and Fazakerley, J.K. (2003). Inducible cytokine gene expression in the brain in the ME7/CV mouse model of scrapie is highly restricted, is at a strikingly low level relative to the degree of gliosis and occurs only late in disease. J Gen Virol. 84(Pt 9): 2605-11.

97. Carroll, J.A., Striebel, J.F., Race, B., Phillips, K. and Chesebro, B. (2015). Prion infection of mouse brain reveals multiple new upregulated genes involved in neuroinflammation or signal transduction. J Virol. 89(4): 2388-404.

98. Kielian, T. (2004). Microglia and chemokines in infectious diseases of the nervous system: views and reviews. Front Biosci. 9: 732-50.

99. Jian, T., Baian, C., Lifeng, Y., Kezong, Q., Jing, L. and Deming, Z. (2015). Amyloid-β Activates Microglia and Regulates Protein Expression in a Manner Similar to Prions. Journal of Molecular Neuroscience. 56(2): 509–518.

100. Hafiz, F.B. and Brown, D.R. (2000). A Model for the Mechanism of Astrogliosis in Prion Disease. Molecular and Cellular Neuroscience. 16: 221–232.

101. Victoria, G.S., Arkhipenko, A., Zhu, S., Syan, S. and Zurzolo, C. (2016). Astrocyte-to-neuron intercellular prion transfer is mediated by cell-cell contact. Sci Rep. 6: 20762.

102. Marella, M. and Chabry, J. (2004). Neurons and Astrocytes Respond to Prion Infection by Inducing Microglia Recruitment. The Journal of Neuroscience. 24(3): 620-627.

103. Block, M.L., Zecca, L. and Hong, J.S. (2007). Microglia-mediated neurotoxicity: uncovering the molecular mechanisms. Nature Reviews Neuroscience. 8: 57-69.

104. Rojo, A.I., McBean, G., Cindric, M., Egea, J., López, M.G., Rada, P., Zarkovic, N. and Cuadrado, A. (2014). Redox Control of Microglial Function: Molecular Mechanisms and Functional Significance. Antioxid Redox Signal. 21(12): 1766–1801.

105. Hopt, A., Korte, S., Fink, H., Panne, U., Niessner, R., Jahn, R., Kretzschmar, H. and Herms J. (2003). Methods for studying synaptosomal copper release. J. Neurosci. Methods, 128: 159–172.

106. Viles, J.H., Klewpatinond, M. and Nadal. R.C. (2008). Copper and the structural biology of the prion protein. Biochem. Soc. Trans. 36: 1288–1292.

107. Pauly, P.C. and Harris, D.A. (1998). Copper stimulates endocytosis of the prion protein. J Biol Chem. 273(50): 33107-10.

108. Freixes, M., Rodríguez, A., Dalfó, E. and Ferrer, I. (2006). Oxidation, glycoxidation, lipoxidation, nitration, and responses to oxidative stress in the cerebral cortex in Creutzfeldt-Jakob disease. Neurobiol Aging. 27(12): 1807-15.

109. Guentchev, M., Voigtlander, T., Haberler, C., Groschup M. H. and Budka, H. (2000). Evidence for Oxidative Stress in Experimental Prion Disease. Neurobiol. Dis. 7: 270–273.

110. Guentchev, M., Siedlak, S.L., Jarius, C., Tagliavini, F., Castellani, R.J., Perry, G., Smith, M.A. and Budka, H. (2002). Oxidative damage to nucleic acids in human prion disease. Neurobiol Dis. 9(3): 275-81.

111. Yun, S.W., Gerlach, M., Riederer, P. and Klein, M.A. (2006). Oxidative stress in the brain at early preclinical stages of mouse scrapie. Exp Neurol. 201(1): 90-8.

112. MRC Prion Unit. (2016). Drug Treatment. Online at http://www.prion.ucl.ac.uk/clinic-services/research/drug-treatments/

113. Geschwind, M.D., Kuo, A.L., Wong, K.S., Haman, A., Devereux, G., Raudabaugh, B.J., Johnson, D.Y., Torres-Chae, C.C., Finley, R., Garcia, P., Thai, J.N., Cheng, H.Q., Neuhaus, J.M., Forner, S.A., Duncan, J.L., Possin, K.L., Dearmond, S.J., Prusiner, S.B. and Miller, B.L. (2013). Quinacrine treatment trial for sporadic Creutzfeldt-Jakob disease. Neurology. 81(23): 2015-23.

114. Haïk, S., Marcon, G., Mallet, A., Tettamanti, M., Welaratne, A., Giaccone, G., Azimi, S., Pietrini, V., Fabreguettes, J.R., Imperiale, D., Cesaro, P., Buffa, C., Aucan, C., Lucca, U., Peckeu, L., Suardi, S., Tranchant, C., Zerr, I., Houillier, C., Redaelli, V., Vespignani, H., Campanella, A., Sellal, F., Krasnianski, A., Seilhean, D., Heinemann, U., Sedel, F., Canovi, M., Gobbi, M., Di Fede, G., Laplanche, J.L., Pocchiari, M., Salmona, M., Forloni, G., Brandel, J.P. and Tagliavini, F. (2014). Doxycycline in Creutzfeldt-Jakob disease: a phase 2, randomised, double-blind, placebo-controlled trial. Lancet Neurol. 13(2): 150-8.

115. Silber, B.M., Gever, J.R., Rao, S., Li, Z., Renslo, A.R., Widjaja, K., Wong, C., Giles, K., Freyman, Y., Elepano, M., Irwin, J.J., Jacobson, M.P. and Prusiner, S.B. (2014). Novel compounds lowering the cellular isoform of the human prion protein in cultured human cells. Bioorg Med Chem. 22(6): 1960-72.

116. Karapetyan, Y.E., Sferrazza, G.F., Zhou, M., Ottenberg, G., Spicer, T., Chase, P., Fallahi, M., Hodder, P., Weissmann, C. and Lasmézas, C.I. (2013). Unique drug screening approach for prion diseases identifies tacrolimus and astemizole as antiprion agents. Proc Natl Acad Sci U S A. 110(17): 7044–7049.

117. Kawasaki, Y., Kawagoe, K., Chen, C.J., Teruya, K., Sakasegawa, Y. and Doh-ura, K. (2007). Orally administered amyloidophilic compound is effective in prolonging the incubation periods of animals cerebrally infected with prion diseases in a prion strain-dependent manner. J Virol. 81(23): 12889-98.

118. Lu, D., Giles, K., Li, Z., Rao, S., Dolghih, E., Gever, J.R., Geva, M., Elepano, M.L., Oehler, A., Bryant, C., Renslo, A.R., Jacobson, M.P., Dearmond, S.J., Silber, B.M. and Prusiner, S.B. (2013). Biaryl amides and hydrazones as therapeutics for prion disease in transgenic mice. J Pharmacol Exp Ther. 347(2): 325-38.

119. Berry, D.B., Lu, D., Geva, M., Watts, J.C., Bhardwaj, S., Oehler, A., Renslo, A.R., DeArmond, S.J., Prusiner, S.B. and Giles, K. (2013). Drug resistance confounding prion therapeutics. Proc Natl Acad Sci U S A. 110(44): E4160-9.

120. Wagner, J., Ryazanov, S., Leonov, A., Levin, J., Shi, S., Schmidt, F., Prix, C., Pan-Montojo, F., Bertsch, U., Mitteregger-Kretzschmar, G., Geissen, M., Eiden, M., Leidel, F., Hirschberger, T., Deeg, A.A., Krauth, J.J., Zinth, W., Tavan, P., Pilger, J., Zweckstetter, M., Frank, T., Bähr, M., Weishaupt, J.H., Uhr, M., Urlaub, H., Teichmann, U., Samwer, M., Bötzel, K., Groschup, M., Kretzschmar, H., Griesinger, C. and Giese, A. (2013). Anle138b: a novel oligomer modulator for disease-modifying therapy of neurodegenerative diseases such as prion and Parkinson's disease. Acta Neuropathol. 125(6): 795-813.

121. Peretz, D., Williamson, R.A., Kaneko, K., Vergara, J., Leclerc, E., Schmitt-Ulms, G., Mehlhorn, I.R., Legname, G., Wormald, M.R., Rudd, P.M., Dwek, R.A., Burton, D.R. and Prusiner, S.B. (2001). Antibodies inhibit prion propagation and clear cell cultures of prion infectivity. Nature. 412(6848): 739-43.

122. White, A.R., Enever, P., Tayebi, M., Mushens, R., Linehan, J., Brandner, S., Anstee, D., Collinge, J. and Hawke, S. (2003). Monoclonal antibodies inhibit prion replication and delay the development of prion disease. Nature. 422(6927): 80-3.

123. Chung, E., Ji, J., Sun, Y., Kascsak, R.J., Kascsak, R.B., Mehta, P.D., Strittmatter, S.M. and Wisniewski, T. (2010). Anti-PrP^{C} monoclonal antibody infusion as a novel treatment for cognitive deficits in an alzheimer's disease model mouse. BMC Neurosci. 11: 130.

124. Brandner, S., Isenmann, S., Kühne, G. and Aguzzi, A. (1998). Identification of the end stage of scrapie using infected neural grafts. Brain Pathol. 8(1):19-27.

125. Kübler, E., Oesch, B. and Raeber A.J. (2003). Diagnosis of prion diseases. Br Med Bull. 66 (1): 267-279.

126. Zanusso, G., Fiorini, M., Ferrari, S., Gajofatto, A., Cagnin, A., Galassi, A., Richelli, S. and Monaco, S. (2011). Cerebrospinal fluid markers in sporadic Creutzfeldt–Jakob disease. Int. J. Mol. Sci. 12: 6281–6292.

127. Zanusso, G., Monaco, S., Pocchiari, M. and Caughey, B. (2016). Advanced tests for early and accurate diagnosis of Creutzfeldt–Jakob disease Nature Reviews Neurology. 12: 325–333.

128. UCSF Memory and Aging Center. (2016). Tests for Prion Disease. Online at http://memory.ucsf.edu/cjd/overview/tests

129. Jackson, G.S., Burk-Rafel, J., Edgeworth, J.A., Sicilia, A., Abdilahi, S., Korteweg, J., Mackey, J., Thomas, C., Wang, G., Mead, S. and Collinge, J. (2014). A highly specific blood test for vCJD. Blood. 123: 452–453.

130. Mallucci, G., Dickinson, A., Linehan, J., Klöhn, P.C., Brandner, S. and Collinge, J. (2003). Depleting neuronal PrP in prion infection prevents disease and reverses spongiosis. Science. 302(5646): 871-4.

131. Orrú, C.D., Bongianni, M., Tonoli, G., Ferrari, S., Hughson, A.G., Groveman, B.R., Fiorini, M., Pocchiari, M., Monaco, S., Caughey, B. and Zanusso, G. (2014). A test for Creutzfeldt–Jakob disease using nasal brushings. N. Engl. J. Med. 371: 519–529.

132. Orrú, C.D., Groveman, B.R., Raymond, L.D., Hughson, A.G., Nonno, R., Zou, W., Ghetti, B., Gambetti, P. and Caughey, B. (2015). Bank vole prion protein as an apparently universal substrate for RT-QuIC-based detection and discrimination of prion strains. PLoS Pathog. 11: e1004983.

133. Lamoureux, L., Simon, S.L.R., Plews, M., Ruddat, V., Brunet, S., Graham, C., Czub, S. and Knox J.D. (2013). Urine Proteins Identified by Two-Dimensional Differential Gel Electrophoresis Facilitate the Differential Diagnoses of Scrapie. PLoS ONE 8(5): e64044.

134. Negraes, P.D., Trujillo, C.A., Pillat, M.M., Teng, Y.D. and Ulrich, H. (2015). Roles of Kinins in the Nervous System. Cell Transplantation. 24: 613-623.

135. Bader, M. (2012). Kinins: History and outlook. In Kinins (Ed. M. Bader), Walter de Gruyter, Berlin, Germany, pp. 1-5.

136. Alhenc-Gelas, F. and Girolami, J.P. (2012). Molecular and genetic aspects of the kallikrein-kinin system. In Kinins. (Ed. M. Bader). Walter de Gruyter, Berlin, Germany, pp. 7-31.

137. Bhoola, K.D., Figueroa, C.D. and Worthy, K. (1992). Brioregulation of kinins: Kallikreins, kininogens, and kininases. Pharmacol.Rev. 44: 1-80.

138. Campbell, D.J. (2001). The kallikrein-kinin system in humans. Clin Exp Pharmacol Physiol. 28(12): 1060-5.

139. Lerner, U.H. and Lundberg, P. (2002). Chapter 44: Kinins and Neuro-osteogenic Factors. In Principles of Bone Biology, Two-Volume Set. (Eds. J.P. Bilezikian, L.G. Raisz, G.A. Rodan), Academic Press, United States, pp. 773-799.

140. Ehrenfeld, P., Figueroa, C.D., Bhoola, K.D. and Matus C.E. (2012). Signaling Pathways Coupled to Activation of the Kinin B1 Receptor. In Biochemistry, Genetics and Molecular Biology: Advances in Protein Kinases. (Ed. G.D.S. Xavier), InTech, DOI: 10.5772/48058. Online at http://www.intechopen.com/books/advances-in-protein-kinases/signaling-pathways-coupled-to-activation-of-the-kinin-b1-receptor

141. Colman, R.W., Jameson, B.A., Lin, Y., Johnson, D. and Mousa, S.A. (2000). Domain 5 of high molecular weight kininogen (kininostatin) down-regulates endothelial cell proliferation and migration and inhibits angiogenesis. Blood. 95(2): 543-550.

142. Cao, D.J., Lin, Y. and Colman, R.W. (2004). Urokinase-Type Plasminogen Activator Receptor Is Involved in Mediating the Apoptotic Effect of Cleaved High Molecular Weight Kininogen in Human Endothelial Cells. Circulation Research. 94: 1227-1234.

143. Raidoo, D.M. and Bhoola, K.D. (1998). Pathophysiology of the Kallirein-Kinin System in Mammalian Nervous Tissue. Pharmacol. Ther. 79(2): 105-127.

144. Rhaleb, N.E., Yang, X.P. and Carretero, O.A. (2011). The Kallirkrein-Kinin System as a Regulator of Cardiovascular and Renal Function. Compr Physiol. 1(2):971-93.

145. Kuhr, F., Lowry, J., Zhang, Y., Brovkovych, V. and Skidgel, R.A. (2010). Differential regulation of inducible and endothelial nitric oxide synthase by kinin B1 and B2 receptors. Neuropeptides. 44: 145-154.

146. Thornton, E., Ziebell, J.M., Leonard, A.V. and Vink, R. (2010). Kinin Receptor Antagonists as Potential Neuroprotective Agents in Central Nervous System Injury. Molecules, 15: 6598-6618.

147. Enquist, J., Skröder, C., Whistler, J.L. and Leeb-Lundberg, L.M. (2007). Kinins promote B2 receptor endocytosis and delay constitutive B1 receptor endocytosis. Molecular Pharmacology. 71(2): 494-507.

148. Ifuku, M., Färber, K., Okuno, Y., Yamakawa, Y., Miyamoto, T., Nolte, C., Merrino, V.F., Kita, S., Iwamoto, T., Komuro, I., Wang, B., Cheung, G., Ishikawa, E., Ooboshi, H., Bader, M., Wada, K., Kettenmann, H. and Noda, M. (2007). Bradykinin-induced microglial migration mediated by B1-bradykinin receptors depends on Ca2+ influx via reverse-mode activity of the Na+/Ca2+ exchanger. J Neurosci. 27(48): 13065-73.

149. Voyno-Yasenetskaya, T.A., Tkachuk, V.A., Cheknyova, E.G., Panchenko, M.P., Grigorian, G.Y., Vavrek, R.J., Stewart, J.M. and Ryan, U.S. (1989). Guanine nucleotide-

dependent, pertussis toxin-insensitive regulation of phosphoinositide turnover by bradykinin in bovine pulmonary artery endothelial cells. FASEB J. 3(1): 44-51.

150. Liao, J.K. and Homcy, C.J. (1993). The G proteins of the G alpha I and G alpha q family couple the bradykinin receptor to the release of endothelium-derived relaxing factor. J Clin Invest. 92: 2168-2172.

151. Yang, X., Taylor, L. and Polgar, P. (1999). Effect of the G-protein, G alpha(i2), and G alpha(i3) subunit knockdown on bradykinin-induced signal transduction in rat-1 cells. Mol Cell Biol Res Commun. 1(3): 227-36.

152. Velarde, V., Ullian, M.E., Morinelli, T.A., Mayfield, R.K. and Jaffa, A.A. (1999). Mechanisms of MAPK activation by bradykinin in vascular smooth muscle cells. Am J Physiol. 277(2 Pt 1): C253-61.

153. Brovkovych, V., Zhang, Y., Brovkovych, S., Minshall, R.D. and Skidgel, R.A. (2011). A novel pathway for receptor-mediated post-translational activation of inducible nitric oxide synthase. J Cell Mol Med. 15(2): 258-69.

154. Papapetropoulos, A., Rudic, R.D. and Sessa, W.C. (1999). Molecular control of nitric oxide synthases in the cardiovascular system. Cardiovasc Res. 43: 509-520.

155. Raslan, F., Schwarz, T., Meuth, S.G., Austinat, M., Bader, M., Renné, T., Roosen, K., Stoll, G., Sirén, A.L. and Kleinschnitz, C. (2010). Inhibition of bradykinin receptor B1 protects mice from focal brain injury by reducing blood-brain barrier leakage and inflammation. J Cereb Blood Flow Metab. 30(8): 1477-86.

156. Austinat, M., Braeuninger, S., Pesquero, J.B., Brede, M., Bader, M., Stoll, G., Renne, T. and Kleinschnitz, C. (2009). Blockade of bradykinin receptor B1 but not bradykinin receptor B2 provides protection from cerebral infarction and brain edema. Stroke. 40: 285–293.

157. Göbel, K., Pankratz, S., Schneider-Hohendorf, T., Bittner, S., Schuhmann, M.K., Langer, H.F., Stoll, G., Wiendl, H., Kleinschnitz, C. and Meuth, S.G. (2011). Blockade of the kinin receptor B1 protects from autoimmune CNS disease by reducing leukocyte trafficking. J Autoimmun. 36(2): 106-14.

158. Passos, G.F., Medeiros, R., Cheng, D., Vasilevko, V., Laferla, F.M. and Cribbs, D.H. (2013). The bradykinin B1 receptor regulates Aβ deposition and neuroinflammation in Tg-SwDI mice. Am J Pathol. 182(5): 1740-9.

159. Xia, C.F., Smith, R.S.Jr., Shen, B., Yang, Z.R., Borlongan, C.V., Chao, L. and Chao, J. (2006). Postischemic brain injury is exacerbated in mice lacking the kinin B2 receptor. Hypertension. 47(4) :752-61.

160. Hellal, F., Pruneau, D., Palmier, B., Faye, P., Croci, N., Plotkine, M. and Marchand-Verrecchia, C. (2003). Detrimental role of bradykinin B2 receptor in a murine model of diffuse brain injury. J Neurotrauma. 20(9): 841-51.

161. Trabold, R., Erös, C., Zweckberger, K., Relton, J., Beck, H., Nussberger J., Muller-Esterl, W., Bader, M., Whalley, E. and Plesnila, N. (2010). The role of bradykinin B(1) and B(2) receptors for secondary brain damage after traumatic brain injury in mice. J. Cereb. Blood Flow Metab. 30: 130–139.

162. Albert-Weissenberger, C., Stetter, C., Meuth, S.G., Gobel, K., Bader, M., Siren, AL. and Kleinschnitz, C. (2012). Blocking of bradykinin receptor B1 protects from focal closed head injury in mice by reducing axonal damage and astroglia activation. Journal of Cerebral Blood Flow & Metabolism. 32: 1747–1756.

163. Bergamaschini, L., Parnetti, L., Pareyson, D., Canziani, S., Cugno, M. and Agostoni, A. (1998). Activation of the contact system in cerebrospinal fluid of patients with Alzheimer disease. Alzheimer Dis Assoc Disord. 12(2): 102-8.

164. Wu, Y. (2015). Contact pathway of coagulation and inflammation. Thromb J. 13: 17.

165. Prediger, R.D., Medeiros, R., Pandolfo, P., Duarte, F.S., Passos, G.F., Pesquero, J.B., Campos, M.M., Calixto, J.B. Takahashi, R.N. (2008). Genetic deletion or antagonism of kinin B(1) and B(2) receptors improves cognitive deficits in a mouse model of Alzheimer's disease. Neuroscience. 151(3): 631-43.

166. Bicca, M.A., Costa, R., Loch-Neckel, G., Figueiredo, C.P., Medeiros, R. and Calixto, J.B. (2015). B_2 receptor blockage prevents Aβ-induced cognitive impairment by neuroinflammation inhibition. Behav Brain Res. 278: 482-91.

167. Herring, A., Münster, Y., Akkaya, T., Moghaddam, S., Deinsberger, K., Meyer, J., Zahel, J., Sanchez-Mendoza, E., Wang, Y., Hermann, D.M., Arzberger, T., Teuber-Hanselmann, S. and Keyvani, K. (2016). Kallikrein-8 inhibition attenuates Alzheimer's pathology in mice. Alzheimers Dement. 12(12):1273-1287.

168. Eikelenboom, P., Bate, C., Van Gool, W.A., Hoozemans, J.J., Rozemuller, J.M., Veerhuis, R. and Williams, A. (2002). Neuroinflammation in Alzheimer's disease and prion disease. Glia. 40(2): 232-9.

169. Watts, J.C. and Prusiner, S.B. (2014). Mouse Models for Studying the Formation and Propagation of Prions. The Journal of Biological Chemistry. 289: 19841-19849.

170. Kimberlin, R.H. and Walker, C. (1977). Characteristics of a short incubation model of scrapie in the golden hamster. J Gen Virol. 34: 295–304.

171. Brandner, S. and Jaunmuktane, Z. (2017). Prion disease: experimental models and reality. Acta Neuropathologica. 133(2): 197-222.

172. Bryant, C.D. (2011). The blessings and curses of C57BL/6 substrains in mouse genetic studies. Annals of the New York Academy of Sciences. 1245: 31-33.

173. Di Bari, M.A., Nonno, R. and Agrimi, U. (2012). The mouse model for scrapie: inoculation, clinical scoring, and histopathological techniques. Methods Mol Biol. 849: 453-71.

174. Plews, M., Simon, S.L., Boreham, D.R., Parchaliuk, D., Wyatt, H., Mantha, R., Frost, K., Lamoureux, L., Stobart, M., Czub, S., Mitchel, R.E. and Knox, J.D. (2010). A radiation-induced adaptive response prolongs the survival of prion-infected mice. Free Radic Biol Med. 49(9): 1417-21.

175. Hunter, A.J., Caulfield, M.P. and Kimberlin, R.H. (1986). Learning ability of mice infected with different strains of scrapie. Physiol. Behav. 36: 1089–1092.

176. Cunningham, C., Deacon, R., Wells, H., Boche, D., Waters, S., Diniz, C.P., Scott, H., Rawlins, J.N.P. and Perry V.H. (2003). Synaptic changes characterize early behavioural signs in the ME7 model of murine prion disease. Eur. J. Neurosci. 17: 2147-2155.

177. Boda, E., Pini, A., Hoxha, E., Parolisi, R. and Tempia, F. (2009). Selection of reference genes for quantitative real-time RT-PCR studies in mouse brain. J Mol Neurosci. 37(3): 238-53.

178. Shi, M., Takeshita, H., Komatsu, M., Xu, B., Aoyama, K. and Takeuchi, T. (2005). Generation of 8-hydroxydeoxyguanosine from DNA using rat liver homogenates. Cancer Sci. 96: 13–19.

179. Masters, C.L., Rohwer, R.G., Franko, M.C., Brown, P. and Gajdusek, D.C. (1984). The sequential development of spongiform change and gliosis of scrapie in the golden Syrian hamster. J Neuropathol Exp Neurol. 43(3): 242-52.

180. Kim, H.O., Snyder, G.P., Blazey, T.M., Race, R.E., Chesebro, B. and Skinner, P.J. (2008). Prion disease induced alterations in gene expression in spleen and brain prior to clinical symptoms. Advances and applications in bioinformatics and chemistry. 1: 29-50.

181. Muramoto, T., Kitamoto, T., Tateishi, J. and Goto, I. (1992). The sequential development of abnormal prion protein accumulation in mice with Creutzfeldt-Jakob disease. Am J Pathol. 140(6): 1411-20.

182. Tribouillard-Tanvier, D., Race, B., Striebel, J.F., Carroll, J.A., Phillips, K. and Chesebro, B. (2012). Early Cytokine Elevation, PrPres Deposition, and Gliosis in Mouse Scrapie: No Effect on Disease by Deletion of Cytokine Genes IL-12p40 and IL-12p35. Journal of Virology. 86(19): 10377-10383.

183. Wenborn, A., Terry, C., Gros, N., Joiner, S., D'Castro, L., Panico, S., Sells, J., Cronier, S., Linehan, J.M., Brandner, S., Saibil, H.R., Collinge, J. and Wadsworth, J.D.F. (2015). A novel and rapid method for obtaining high titre intact prion strains from mammalian brain. Sci Rep. 5: 10062.

184. Ashby, E.L., Love, S. and Kehoe, P.G. (2012). Assessment of activation of the plasma kallikrein-kinin system in frontal and temporal cortex in Alzheimer's disease and vascular dementia. Neurobiol Aging. 33(7): 1345-55.

185. Shesely, E.G., Hu, C.B., Alhenc-Gelas, F., Meneton, P. and Carretero, O.A. (2006). A second expressed kininogen gene in mice. Physiol Genomics. 26(2): 152-7.

186. Viel, T.A., Lima-Caetano, A., Nasello, A.G., Lancelotti, C.L., Nunes, V.A., Araujo, M.S. and Buck, H.S. (2008). Increases of kinin B1 and B2 receptors binding sites after brain infusion of amyloid-beta 1-40 peptide in rats. Neurobiol Aging. 29(12): 1805-14.

187. Oh, S.W., Harris, J.A., Ng, L., Winslow, B., Cain, N., Mihalas, S., Wang, Q., Lau, C., Kuan, L., Henry, A.M., et al. (2014). A mesoscale connectome of the mouse brain. Nature. 508(7495): 207-214.

188. Brüne, B., von Knethen, A. and Sandau, K.B. (1998). Nitric oxide and its role in apoptosis. Eur J Pharmacol. 351(3): 261-72.

189. Ju, W.K., Park, K.J., Choi, E.K., Kim, J., Carp, R.I., Wisniewski, H.M. and Kim, Y.S. (1998). Expression of inducible nitric oxide synthase in the brains of scrapie-infected mice. J Neurovirol. 4(4): 445-50.

190. Walsh, D.T., Betmouni, S. and Perry, V.H. (2001). Absence of detectable IL-1beta production in murine prion disease: a model of chronic neurodegeneration. J Neuropathol Exp Neurol. 60(2): 173-82.

191. Lüth, H.J., Holzer, M., Gärtner, U., Staufenbiel, M. and Arendt, T. (2001). Expression of endothelial and inducible NOS-isoforms is increased in Alzheimer's disease, in APP23 transgenic mice and after experimental brain lesion in rat: evidence for an induction by amyloid pathology. Brain Res. 913(1): 57-67.

192. Lee, S.C. and Brosnan, C.F. (1996). Cytokine Regulation of iNOS Expression in Human Glial Cells. Methods. 10(1): 31-7.

193. Akama, K.T. and Van Eldik, L.J. (2000). Beta-amyloid stimulation of inducible nitric-oxide synthase in astrocytes is interleukin-1beta- and tumor necrosis factor-alpha (TNFalpha)-dependent, and involves a TNFalpha receptor-associated factor- and NFkappaB-inducing kinase-dependent signaling mechanism. J Biol Chem. 275(11): 7918-24.

194. Madrigal, J.L.M., Moro, M.A., Lizasoain, I., Lorenzo, P., Castrillo, A., Bosca, L. and Leza, J.C. (2001). Inducible nitric oxide synthase expression in brain cortex after acute restraint stress is regulated by nuclear factor kB-mediated mechanisms. Journal of Neurochemistry. 76: 532-538.

195. Xu, J., Xu, Q., Chen, X., Zou, C. and Zhao, Z. (2010). Neuronal expression of inducible nitric oxide synthase in hypothyroid rat. Neuro Endocrinol Lett. 31(6): 848-51.

196. Emmert-Buck, M.R., Bonner, R.F., Smith, P.D., Chuaqui, R.F., Zhuang, Z., Goldstein, S.R., Weiss, R.A. and Liotta, L.A. (1996). "Laser capture microdissection". Science. 274 (5289): 998–1001.

197. Nsa Allogho, S., Gobeil, F., Pheng, L.H., Nguyen-Le, X.K., Neugebauer, W. and Regoli, D. (1997). Antagonists for kinin B1 and B2 receptors in the mouse. Can J Physiol Pharmacol. 75(6): 558-62.

198. Cicardi, M., Banerji, A., Bracho, F., Malbrán, A., Rosenkranz, B., Riedl, M., Bork, K., Lumry, W., Aberer, W., Bier, H., Bas, M., Greve, J., Hoffmann, T.K., Farkas, H. et al. (2010). Icatibant, a new bradykinin-receptor antagonist, in hereditary angioedema. N Engl J Med. 363(6): 532-541.